AFRL-PR-WP-TR-2006-2212

MUILTIFUNCTIONAL FUEL ADDITIVES FOR REDUCED JET PARTICULATE EMISSIONS

Christopher J. Montgomery, Adel F. Sarofim, and Bradley R. Adams

Reaction Engineering International
77 West 200 South, Suite 210
Salt Lake City, UT 84101

Eric Eddings

University of Utah

Joseph Bozzelli

New Jersey Institute of Technology

Viswanath Katta

ISSI

JUNE 2006

Final Report for 04 August 2003 – 03 December 2005

THIS IS A SMALL BUSINESS INNOVATION RESEARCH (SBIR) PHASE II REPORT.

PROPULSION DIRECTORATE
AIR FORCE MATERIEL COMMAND
AIR FORCE RESEARCH LABORATORY
WRIGHT-PATTERSON AIR FORCE BASE, OH 45433-7251

NOTICE AND SIGNATURE PAGE

Using Government drawings, specifications, or other data included in this document for any purpose other than Government procurement does not in any way obligate the U.S. Government. The fact that the Government formulated or supplied the drawings, specifications, or other data does not license the holder or any other person or corporation; or convey any rights or permission to manufacture, use, or sell any patented invention that may relate to them.

This report was cleared for public release by the Air Force Research Laboratory Wright Site (AFRL/WS) Public Affairs Office and is available to the general public, including foreign nationals. Copies may be obtained from the Defense Technical Information Center (DTIC) (http://www.dtic.mil).

AFRL-PR-WP-TR-2006-2212 HAS BEEN REVIEWED AND IS APPROVED FOR PUBLICATION IN ACCORDANCE WITH ASSIGNED DISTRIBUTION STATEMENT.

//Signature//

EDWIN CORPORAN
Fuels Branch
Turbine Engine Division
Propulsion Directorate

//Signature//

WILLIAM E. HARRISON III
Chief, Fuels Branch
Turbine Engine Division
Propulsion Directorate

//Signature//

JEFFREY M. STRICKER
Chief Engineer
Turbine Engine Division
Propulsion Directorate

This report is published in the interest of scientific and technical information exchange, and its publication does not constitute the Government's approval or disapproval of its ideas or findings.

REPORT DOCUMENTATION PAGE

Form Approved
OMB No. 0704-0188

1. REPORT DATE *(DD-MM-YY)*	2. REPORT TYPE	3. DATES COVERED *(From - To)*
June 2006	Final	08/04/2003 – 12/03/2005

4. TITLE AND SUBTITLE
MUILTIFUNCTIONAL FUEL ADDITIVES FOR REDUCED JET PARTICULATE EMISSIONS

5a. CONTRACT NUMBER
F33615-03-C-2338

5b. GRANT NUMBER

5c. PROGRAM ELEMENT NUMBER
65502F

6. AUTHOR(S)
Christopher J. Montgomery, Adel F. Sarofim, and Bradley R. Adams (Reaction Engineering International)
Eric Eddings (University of Utah)
Joseph Bozzelli (New Jersey Institute of Technology)
Viswanath Katta (ISSI)

5d. PROJECT NUMBER
3005

5e. TASK NUMBER
PO

5f. WORK UNIT NUMBER
FA

7. PERFORMING ORGANIZATION NAME(S) AND ADDRESS(ES)
Reaction Engineering International
77 West 200 South, Suite 210
Salt Lake City, UT 84101

8. PERFORMING ORGANIZATION REPORT NUMBER

9. SPONSORING/MONITORING AGENCY NAME(S) AND ADDRESS(ES)
Propulsion Directorate
Air Force Research Laboratory
Air Force Materiel Command
Wright-Patterson AFB, OH 45433-7251

10. SPONSORING/MONITORING AGENCY ACRONYM(S)
AFRL-PR-WP

11. SPONSORING/MONITORING AGENCY REPORT NUMBER(S)
AFRL-PR-WP-TR-2006-2212

12. DISTRIBUTION/AVAILABILITY STATEMENT
Approved for public release; distribution is unlimited.

13. SUPPLEMENTARY NOTES
This is a Small Business Innovation Research (SBIR) Phase II Report. Report contains color.
PAO case number: AFRL-WS 06-2314; Date cleared: 29 Sep 2006.

14. ABSTRACT
This report was developed under SBIR contract. A study on fuel additives to suppress soot emissions from gas turbines burning JP-8 was completed. The program consisted of a multifaceted approach involving experimental and computational screening tools to assess the effectiveness of multifunctional additives. The experimental program demonstrated that a laminar drop tube furnace at the University of Utah could effectively screen a large number of additives relatively rapidly and inexpensively as a function of furnace temperature, injection orifice size, injection pressure, and oxygen concentration. Additives were found to be most effective under highly oxidizing conditions. Soot reductions of over 90% were observed for metal-containing additives, know ignition enhancers, and a range of proprietary additives. Modeling capabilities for assessing the effectiveness of additives were developed. Soot models using the method of moments and sectional methods were combined with detailed kinetics models for surrogates of JP-8. the models were validated with experimental data in the literature for a number of simple fuels. Detailed Kinetic mechanisms were developed for two ignition enhancers in the study, di-tertiary butyl peroxide and 2-ethyl-hexyl-nitrate. The kinetic models were incorporated in a CFD code to evaluate diffusion flames representative of the drop tube and swirl stabilized combustor.

15. SUBJECT TERMS
SBIR Report, soot, additives, turbine engine emissions, particulates, chemical kinetics, combustion, JP-8 chemistry

16. SECURITY CLASSIFICATION OF:			17. LIMITATION OF ABSTRACT:	18. NUMBER OF PAGES	19a. NAME OF RESPONSIBLE PERSON (Monitor)
a. REPORT	b. ABSTRACT	c. THIS PAGE			Edwin Corporan
Unclassified	Unclassified	Unclassified	SAR	156	19b. TELEPHONE NUMBER *(Include Area Code)* N/A

REACTION
ENGINEERING
INTERNATIONAL

August 23, 2006

Edwin Corporan
Program Manager
Propulsion Directorate
AFRL/PRTG Bldg 490
1790 Loop Rd North
Wright-Patterson AFB OH 45433-7103

Subject: Public Release of Final Report for Contract F33615-03-C-2338

Mr. Corporan:

Reaction Engineering International hereby certifies that the information in the final report for AFRL/PRKA Contract F33615-03-C-2338, "Multifunctional Fuel Additives for Reduced Jet Particulate Emissions" is approved for the public domain and that the information is not proprietary.

Sincerely,

Bradley R. Adams

Bradley R. Adams, Ph.D.
President

77 West 200 South #210 • Salt Lake City, Utah 84101
Telephone (801) 364-6925 • Fax (801) 364-6977

Table of Contents

Table of Contents (Concluded)

List of Figures

List of Figures (Continued)

List of Figures (Continued)

List of Figures (Continued)

List of Figures (Concluded)

List of Tables

1. Executive Summary

Reaction Engineering headed up a team to study additives to suppress soot emission from gas turbines burning JP-8. The program consisted of a multifaceted approach involving experimental and computational screening tools to evaluate the effectiveness of multifunctional additives.

The experimental program demonstrated that a laminar drop tube furnace at the University of Utah (the U) could effectively screen a large number of additives relatively rapidly and inexpensively as a function of furnace temperature, injection orifice size, injection pressure, and oxygen concentration. Additives were found to be most effective under highly oxidizing conditions. Soot reductions of over 90 percent were observed for metal-containing additives, known ignition enhancers, a range of proprietary additives provided by Afton Chemicals, and additives produced at the U using a novel micellar synthesis technique particularly suited for the production of multifunctional additives. Limited experimental results were obtained at the U on the effects of additives on soot oxidation kinetics using a two-stage burner, providing data that confirmed that both metallic additives and organic ignition enhancers were effective under oxidizing conditions, but that metal additives produced aerosol residues that would a deterrent to their acceptance. An AMT AT-400 small scale turbine at the U showed limited utility in determining the effects of additives because of the large amounts of unburned fuel, resulting from the use of fuel as a lubricant, that masked the effect of additives on soot formation and suppression.

Modeling capabilities for assessing the effectiveness of additives were also developed. Soot models using the method of moments and sectional methods were combined with detailed kinetics models for surrogates of JP-8. The models were validated with experimental data in the literature for a number of simple fuels. In addition, detailed kinetic mechanisms were developed at New Jersey Institute of Technology for two of the organic ignition enhancers in the study, di-tertiary butyl peroxide (DTBP) and 2-ethyl-hexyl-nitrate. These kinetics were used to augment the mechanism for the JP-8 surrogate providing, for the first time, a theoretical method for evaluating the effect of soot additives. The kinetic model was used in a simple reactor model of a gas turbine combustor. As in the experiments, the reactor model showed that the additives were effective only in a certain range of conditions, those in which the change in time to ignition influenced the soot burnout. Finally the kinetic models were incorporated in the UNICORN CFD code by ISSI to evaluate diffusion flames representative of both the drop tube experiments at the University of Utah and a swirl-stabilized combustor. The computations for one of the laboratory flames showed the reproduction by the model of many of the features of the flame, including a previously unexplained undulation in the flame width. But the model greatly under-predicted the effects of additives on soot emission. The UNICORN model of a swirl-stabilized flame, however, showed that the addition of DTBP to the flame can significantly reduce soot in the flame.

In conclusion, the screening techniques, both experimental and computational, have shown that the effect of additives on soot formation is very sensitive to experimental conditions, explaining the highly variable results that have been observed with additives

in the field. The additives tested in this study were most effective in the oxidation regime. If an additive can be found that is effective under fuel-rich conditions then the micellar synthesis technique developed in this study could be used to synthesize a multi-functional additive that could be valuable over a wider range of operating conditions.

2. Introduction

2.1 Purpose of Work

Reduction of particulate emission from gas turbine engines is motivated by concerns about the impact of soot particles on human health, engine life, and aircraft detection. Prompted by the strong correlations between the concentrations of particles with sizes under 2.5 μm (micrometer) (PM 2.5) and cardiovascular and respiratory illness, the U.S. Environmental Protection Agency has recently promulgated ambient air quality standards for PM 2.5. Further, there is evidence that ultra fine particles, with sizes under 0.1 microns, may be of greater importance than larger particles because of their ability to penetrate deep into the lung and into the interstitial layers (Lighty et al., 2000). Combustion sources are major contributors to the fine particle emissions, particularly ultra fines. Although DoD sources contribute a small part of the total emissions they cannot be overlooked in view of the importance of internal combustion engine vehicles and aircraft. The purchase of 3 billion gallons/year of JP-8 by the DoD accounts for about ten percent of total aviation fuel consumption in the U.S. (Edwards, 2000), which in turn accounts for approximately 14 percent of all petroleum products; therefore their emissions can be a significant fraction of the nation's total.

It has been estimated that the particulate emissions from jet aircraft are approximately 600,000 kg/year (Roquemore, 2001). National efforts to reduce emissions have focused on combustor design rather than on fuel chemistry/combustor interactions. However, turnover of the aircraft fleet is slow; greater short-term impact can be achieved through the use of fuel additives. Additives may suppress particulate emissions via two paths: destruction of soot particles once formed, or prevention of inception reactions. The

latter offers a potential order of magnitude soot particulate reduction; hence it is desirable to develop and tailor jet fuel formulations to mitigate particulate formation.

The goals for such an additive are that it should: (1) be benign to the environment and safe to handle, (2) be low in cost (fractions of a cent per gallon of fuel); (3) be effective at low concentrations (ppm level); (4) not degrade the fuel performance specifications or combustion characteristics; (5) and not reduce engine performance and life. These goals seem attainable when considering that the JP-8 +100 additive that currently $0.005 per gallon and is expected to decrease as production volume increases. The +100 additive, present in the fuel at a concentration of 256 mg/l, has been found in limited tests to decrease both particulate emissions and deposit formation in the lines and engine (Edwards & Harrison 2004). However, more recent experience indicates that +100 effectiveness on particulate emissions is highly variable.

The use of fuel additives is a pervasive and cost-effective approach that has the potential of reducing PM2.5 emissions in all engines in the fleet. Additives have the additional benefits of possibly reducing deposit formation and being applicable to the larger commercial aviation fleet. Howard and Kausch (1980) provide an excellent review of the earlier literature. Additional data since then support their general conclusions and reinforce the observation of apparently contradictory performance of additives under different combustion conditions. The contradictory results for many additives designed to reduce soot noted in the review by Howard & Kausch (1980) demonstrate that the temperature-oxidation history under which the additives act is critical to their effectiveness. Understanding how an additive acts is essential to understanding the

conditions under which it is effective in the field and for designing small scale tests to assess its effectiveness. The problem can be illustrated by a few examples:

- Adding a soot oxidation catalyst such as ferrocene to a sooting premixed flame will not reduce the soot emission but increase it slightly (Feitelberg et al., 1993).
- In diesel engines, and possibly jet engine combustors, soot is formed early and needs to burn out rapidly before the oxidation reactions are quenched either by rapid expansion in a diesel engine or by the injection of the liner cooling air in a gas turbine engine. Decreasing ignition delay will therefore improve soot burnout. By contrast, in diffusion flames decreasing ignition delay will decrease the amount of air premixed with the fuel and therefore will increase soot formation.
- Additives that improve atomization quality of fuels will not show any effect in standard tests such as the smoke lamp since it does not involve atomization.
- Additives that release oxidant in the critical presooting regime will be effective only for temperature histories that lead to the decomposition of the additive in the proper location in a flame.
- The soot formation rates in diffusion and premixed flames that characterize different practical combustors may vary in opposite ways with changes in flame conditions. Increasing flame temperature, for example, will increase soot formation in a diffusion flame and decrease it in a premixed flame.

For the above reasons, correspondence is seldom found between fuel additive effectiveness in suppressing soot in a laboratory test and in an engine, or, additive effectiveness under different engine conditions. To date, additive selection has been a largely empirical process and the reports of the additive effectiveness in field use have been often highly variable.

This project has taken important steps toward a more fundamentally based approach. It aids in understanding why an additive that is effective in one engine may not be effective in another. A fundamental understanding of the action of additives on soot production and oxidation requires a variety of experiments that can separate the effects of various phenomena, along with advanced chemical kinetic, soot production, particle coagulation, and oxidation models.

In this project, Reaction Engineering International (REI) and team members have developed and demonstrated a set of experimental and numerical modeling tools that can screen functional molecular groups for eventual inclusion into a multifunctional additive that will reduce soot emissions through multiple mechanisms.

2.2 Phase II Objectives

The overall goal for this SBIR Phase II program was to develop fundamentally-based screening tools for soot suppression additives for JP-8 fuel in jet aircraft engines. This required improved fundamental understanding of the action of soot-reducing additives under a variety of combustion conditions in order to develop the ability to predict additive effectiveness in engines using screening tools, specifically laboratory tests and

numerical computations. This goal was achieved by completing the following research and development objectives:

- Identify chemical elements or functional groups that could either inhibit the formation of soot or enhance its rate of oxidation.
- Design laboratory scale experiments to determine the role of additives on ignition delay, soot formation potential, and soot oxidation rate.
- Develop codes for modeling JP-8 combustion kinetics, soot formation and soot oxidation.
- Assess the merit of the compounds nominated using laboratory experiments and models.

2.3 Key Technical Accomplishments of Phase II Work

The Phase II objectives were accomplished by integrating key technologies, developed and/or implemented as part of the R&D tasks, to develop and demonstrate a capability for assessing additive performance. Key technical results from the Phase II work included the following:

- The experimental program demonstrated that a laminar drop tube furnace at the University of Utah (the U) could effectively screen a large number of additives relatively rapidly and inexpensively as a function of furnace temperature, injection orifice size, injection pressure, and oxygen concentration. Additives were found to be most effective under highly oxidizing conditions. Soot reductions of over 90 percent were observed for metal-containing additives, known ignition enhancers, a range of proprietary additives provided by Afton Chemicals, and additives produced at the U

using a novel micellar synthesis technique particularly suited for the production of multifunctional additives.

Limited experimental results were obtained at the U on the effects of additives on soot oxidation kinetics using a two-stage burner, providing data that confirmed that both metallic additives and organic ignition enhancers were effective under oxidizing conditions, but that metal additives that produced aerosol residues that would a deterrent to their acceptance.

- An AMT AT-400 small scale turbine at the U showed limited utility in determining the effects if additives because of the large amounts of unburned fuel, resulting from the use of fuel as a lubricant, that masked the effect of additives on soot formation and suppression.
- Modeling capabilities for assessing the effectiveness of additives were also developed. Soot models using the method of moments and sectional methods were combined with detailed kinetics models for surrogates of JP-8. The models were validated with experimental data in the literature for a number of simple fuels.
- Detailed kinetic mechanisms were developed at NJIT for two of the organic ignition enhancers in the study, di-tertiary butyl peroxide (DTBP) and 2-ethyl-hexyl-nitrate. These kinetics were used to augment the mechanism for the JP-8 surrogate providing, for the first time, a theoretical method for evaluating the effect of soot additives.
- The kinetic model was used in a simple reactor model of a gas turbine combustor. As in the experiments, the reactor model showed that the additives were effective only in a certain range of conditions, those in which the change in time to ignition influenced the soot burnout.

- The kinetic models were incorporated in the UNICORN (UNsteady Ignition and Combustion with ReactioNs) CFD code by Innovative Scientific Solutions Inc. (ISSI) to evaluate diffusion flames representative of both the drop tube experiments at the University of Utah and a swirl-stabilized combustor. The computations for one of the laboratory flames showed the reproduction by the model of many of the features of the flame, including a previously unexplained undulation in the flame width. But the model greatly under-predicted the effects of additives on soot emission. The UNICORN model of a swirl-stabilized flame, however, showed that the addition of DTBP to the flame can significantly reduce soot in the flame.

This research demonstrated the design and application of experimental and numerical screening tools for assessing aircraft engine soot suppression additives. The screening techniques, both experimental and computational, showed that the effect of additives on soot formation is very sensitive to experimental conditions, explaining the highly variable results that have been observed with additives in different platforms. The additives tested in this study were most effective in the oxidation regime. If an additive can be found that is effective under fuel-rich conditions then the micellar synthesis technique developed in this study could be used to synthesize a multi-functional additive that could be valuable over a wider range of operating conditions.

The new fundamental understanding and screening capabilities developed in this program provide a method for the U.S. Air Force to more efficiently and cost-effectively identify candidate JP-8 fuel additives for comprehensive testing in jet engine combustion applications.

3. Technical Approach

This section provides an overview of the technical approach and key technical tasks in this research. The program technical objectives were accomplished by completing tasks in the following areas.

3.1 Additive Selection

Additives selection was based on nominations by Drs. Eyring and Dunn, with inputs from consultant Dr. Dan Daly, who has years of experience in the additives industry, and from Dr. Allen Aradi, our contact at Afton Chemical, a commercial additive manufacturer, on classes of ignition inhibitors, oxidation catalysts, and radical-suppressants that were readily available. Also, commercial additives proven to be successful in engine tests were also considered in order to test the ability of the small-scale experiments to explain additive performance in the field. The functional groups considered included metals, peroxy compounds, and nitrates.

3.2 Small-Scale Experiments

Potential additives were screened in the University of Utah laboratory combustors, using fuel droplet arrays to generate soot in an axisymmetric diffusion flame (drop tube furnace) and a two-stage combustor that isolates the effects of soot production and oxidation in two coupled premixed burners. An Aviation Microjet AT-400 Turbine was also tested for feasibility as a screening tool. The key technical tasks for each of the combustors were as follows.

3.2.1 Drop Tube Experiments

The University of Utah Combustion Research Laboratory drop tube facility was used for screening tests. The experimental program began with baseline soot measurements in unaltered JP-8 fuel. Experiments were then carried out with additives designed to delay or accelerate ignition, inhibit soot precursor formation, and augment the rate of soot oxidation.

Using the drop tube furnace as a preliminary screening tool allowed assessment of the following functions of an additive: 1) modified atomization of the droplets, 2) delays in ignition (leading to enhanced premixing), 3) decreased soot formation on the fuel rich side of the diffusion flame front, and 4) increased soot burnout on the fuel lean side. The total soot was collected to determine the net impact of the additive. A similar monosized droplet stream was used to study the effect of fuel composition and inter-droplet spacing on soot formation by Sangiovanni and Liscinski (1985).

3.2.2 Two-stage Burner Experiments

To facilitate isolation of soot oxidation mechanisms from the formation steps, a two-stage, dual-burner soot oxidation reactor was used. The two-stage reactor utilized an initial premixed flame capable of generating soot under a variety of conditions. The soot-laden stream was passed through a dilution/mixing zone where the formation reactions were quenched and the stream was diluted by combinations of oxygen, nitrogen, carbon dioxide and methane to provide the required reactant mixture and temperature for the subsequent oxidation reactions. The stream was then passed into a flat-flame burner where soot oxidation occurred under carefully-controlled conditions.

In addition, specific additives were atomized downstream of the soot formation zone, but upstream of the oxidation zone, to isolate their impact on oxidation mechanisms alone. A comparison of these tests with those performed introducing the additive in the soot formation zone identified whether catalytic additives must be incorporated into the soot matrix to effectively catalyze soot oxidation, or whether the additives function by suppression of gas-phase radicals. An additional mechanism might be surface adsorption onto soot particles with subsequent reaction. A similar comparison between pre- and post-formation zone injection can be made for oxygenated additives. A scanning mobility size analyzer was used to measure the size dependent concentrations with and without additives.

3.2.3 Aviation Microjet Technologies AT-400 Turbine

Discussions with the Phase II Project Officer highlighted a desire by the Air Force to see the most promising additives evaluated at a larger scale and in an actual device as part of the Phase II program. Although this task was not part of the original Phase II Statement of Work, it was proposed that such testing be pursued on a limited basis under existing funding.

An Aviation Microjet AT-400 gas turbine was purchased for feasibility testing as a screening tool. The exhaust is sampled 3 inches from the exhaust exit plane via a ¼ inch stainless steel tube. Steady sample flow is accomplished with an eductor assembly that pulls the exhaust through a critical orifice. The short sample tube length minimizes thermophoretic losses prior to dilution with the motive air in the eductor. The diluted sample is introduced into a manifold, where black carbon is measured with a

photoacoustic analyzer, and particle number and size distribution are measured with a TSI scanning mobility particle sizer.

The base fuel for the tests was Jet A. The additives that were tested were ferrocene, the proprietary Lubrizol additive PA-5, +100, and tert-butyl peroxide, all of which have proven effective in the drop tube under some conditions.

3.3 Modeling

Additives were screened computationally after developing new gas-phase additive kinetics, chemistry, and soot particle dynamics and oxidation models. Computations were performed first with simple reactor models, then in the UNICORN CFD code. UNICORN was then used to model pertinent experiments.

Key development tasks in this area included:

1. Development of a soot formation, agglomeration and oxidation model for jet fuels.
2. Development of detailed chemical kinetic parameters for jet fuel and organic additives.
3. Development of a simple reactor model with soot model and detailed chemical kinetics to test additive effects on ignition delay and soot formation.
4. Implementation of soot model and chemical kinetics into UNICORN. The UNICORN code was used to model the drop tube experiments and provide calculations for a swirl-stabilized combustor.

3.4 Validation

The validity of the models has been established by comparing model predictions with the measurements made at the University of Utah facility and published data.

The technical tasks outlined above required that a number of development and implementation tasks be completed. Figure 1 illustrates conceptually the technical approach and task dependencies for this program.

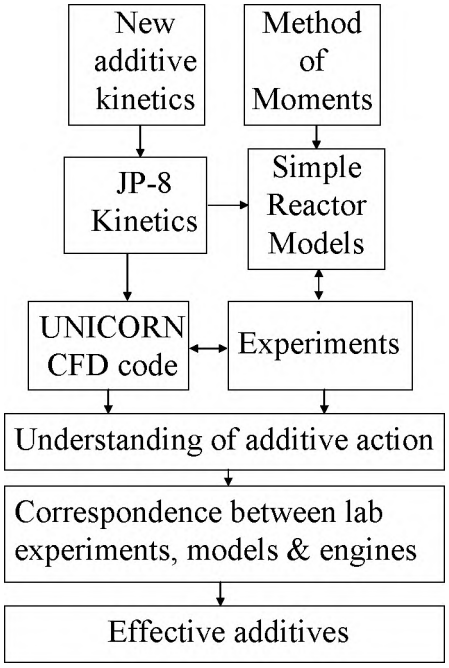

Figure 1. Technical Approach Used in Program

4. Additive Selection

4.1 Introduction

Additives selection was based on nominations by Drs. Daly, Eyring and Dunn, with inputs from a commercial additive manufacturer, Afton Chemical, on classes of ignition inhibitors, oxidation catalysts, and radical-suppressants that were readily available. Also, commercial and proprietary experimental additives proven to be successful in engine tests were also considered in order to test the ability of the small-scale experiments to explain additive performance in engines.

From the literature and our industrial collaborators we first compiled a list of promising additive compounds whose composition is in the public domain. Consultants Professor Edward Eyring, Dr. Brian Dunn, and Dr. Dan Daly have helped us nominate potential jet fuel additives that will decrease soot emissions. One key requirement for the additive is that it be effective at reducing soot at low (<1000 ppm) concentrations in the fuel. This precluded the use of additives that enhance the oxygen content of the fuel mixture because these are only effective at much higher concentrations (5-20 wt%). It has been known for decades that metal-containing fuel additives reduce soot in flames and engines (see Howard & Kausch (1980) and references therein). Therefore, many of the initial nominees were metal-containing compounds. Non-metallic compounds that alter the combustion process by enhancing or inhibiting ignition or act as sources or sinks of radical species were also of interest.

The initial criteria for selecting potential metal-containing fuel additives are listed below:

1) The compound must be soluble in JP-8,

2) The compound must be commercially available in laboratory-scale quantities, and

3) The compound must contain a metal that has been previously shown to reduce PM emissions or

4) The compound must be known to modify the combustion process when added in small amounts.

4.2 Known and Proprietary Compounds

Literature reports were used to identify the most promising metallic elements. However, the bulk of the reported work did not combine the additive directly with the fuel, but rather sprayed an aqueous solution of the additive into the exhaust stream to measure its emission-reducing capabilities. This technique was not applicable to the current project as any potential additives had to be pre-mixed with the jet fuel.

Two well-known additives, ferrocene and methylcyclopentadienylmanganese tricarbonyl (MMT), contain transition metals which serve as oxidation catalysts for soot burnout. Other possible organometallic compounds that may prove useful for reduction of PM emissions are iron pentacarbonyl, dimethyl (1,5-cyclooctadiene) platinum, and ruthenocene. All of these compounds act as oxidation catalysts by incorporating some metal content into the soot particle.

Thirty compounds containing seven different metals (Ba, Ca, Fe, Cs, K, Na, Mn, W) were identified as potential candidates. The initial recommendation was to test a series of compounds that differed only in the identity of the metal. Metal compounds

with cyclohexanebutyrate were suggested, but these compounds proved to be insoluble in jet fuel and could not be tested. Metal compounds with 2-ethylhexanoate were suggested as well as metal naphthenates. Ferrocene (dicyclopentadienyl iron) and ruthenocene (dicyclopentadienyl ruthenium) were also nominated as they are known to be effective at reducing soot emissions.

Ferrocene and ruthenocene possess some unusual properties that other metal-containing compounds do not. They have unusual chemical bonding between the metal center and the cyclopentadienyl groups that leads to increased thermal stability. This property may allow the additive to exist in molecular form even after ignition of the fuel and initiation of soot particle formation. The aromatic nature of the cyclopentadienyl compounds may allow for increased incorporation of the metal into the growing soot particle compared with other, non-aromatic compounds. Soot burnout can be accelerated when the iron or ruthenium are present in the particle, as iron and ruthenium are well-known oxidation catalysts. Another possibility considered was that the cyclopentadienyl groups are influencing free radical formation and availability. Cyclopentadiene can form a relatively stable free radical and may act to quench some of the radical reactions that lead to soot formation. While cyclopentadiene proved to be ineffective by itself, the greatly increased thermal stability of ferrocene and ruthenocene may give rise to the presence of non-combusted cyclopentadiene in the exhaust stream which is most likely not present when cyclopentadiene by itself is added to the jet fuel. Another hypothesis involves the volatility of the additive and its ability to vaporize from the wick used in a smoke lamp or in a droplet spray and to be incorporated into the soot formed.

The following list of potential additives was suggested by consultant Dan Daly,

formerly of Lubrizol and currently at the University of Alabama:

Metal-containing additives:

Bis(cyclopentadienyl)chromium

Bis(cyclopentadienyl)cobalt

Bis(cyclopentadienyl)magnesium

Bis(cyclopentadienyl)nickel

Bis(cyclopentadienyl)ruthenium

Bis(cyclopentadienyl)vanadium

Ferrocene

Lithium cyclopentadienide

MMT

Calcium dodecyl phenate

Non-metallic additives:

2-ethylhexylnitrate

1,2-dimethyl 1,2-dinitrobutane

N,N-diethylhydroxyl amine (anhydrous)

di-tertbutyl peroxide

Dr. Allen Aradi of Afton Chemical (formerly Ethyl Corp.) has sent us several proprietary additives for testing. Test results are reported in Section 5.1.4.

4.3 Novel Metal Micelle Additives

Hydrocarbon-dispersible nanoparticles of platinum, gold, silver, copper, cobalt, and iron have been reported in the open literature, either as a bare nanoparticle or a

monolayer-protected cluster (MPC). A monolayer of a suitable capping agent is used to prevent the metal nanoparticles from agglomerating. The MPCs have very high surface area due to their small size (<10 nm) which should allow for effective catalysis of soot oxidation. The capping agent offers an opportunity for chemical modification. Figure 2 represents a generic MPC. MPCs are typically synthesized in a water-in-oil microemulsion in which an inorganic metal salt is dissolved in the water phase. The metal ion can be chemically reduced with a suitable water-soluble reducing agent like sodium borohydride. The capping agent is added to the solution which allows the MPCs to be collected without forming larger particles.

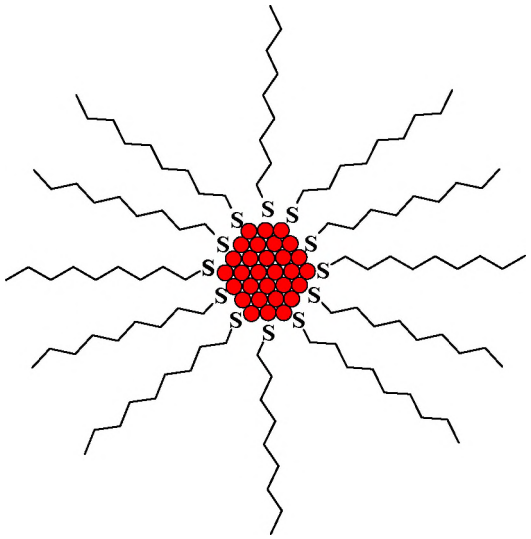

Figure 2. Diagram of a generic monolayer protected cluster.

An approach to creating metal-containing fuel additives similar to MPCs is to use a metal-containing surfactant formed into reverse micelles. Sodium bis(2-ethylhexylsulfosuccinate), NaAOT, can be functionalized with different metal ions. When dissolved in a hydrocarbon solvent, reverse micelles will spontaneously form provided the concentration is above the critical micelle concentration. Mixed-metal

reverse micelles will form if various metal-containing forms of AOT are combined in the same solution. Figure 3 represents a micelle formed using $Fe(AOT)_3$, $Co(AOT)_2$, and NaAOT. Iron and cobalt can serve as oxidation catalysts while sodium (or potassium) can serve to add ions during the combustion process which in turn decreases the soot coagulation rate through electrostatic repulsion. Alkaline earth metals can also be added to produce hydroxyl radicals which react with soot precursors to reduce PM emissions. The proximity of the multiple metals in a reverse micelle may allow for exploitation of any synergistic effects.

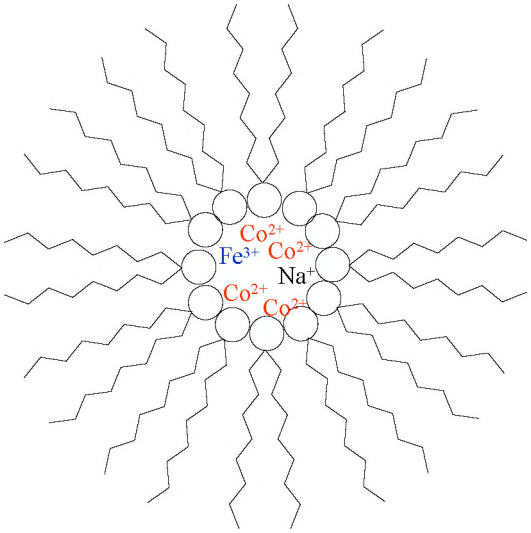

Figure 3. Diagram of a micelle formed using $Fe(AOT)_3$, $Co(AOT)_2$, and NaAOT.

REI consultant Dr. Brian Dunn has synthesized novel additives consisting of sodium, cobalt, and iron, ion-exchanged onto the surfactant AOT (bis-(2-ethylhexyl) sulfosuccinate). Before mixing with JP-8, the additives form waxy solids that are white (sodium) or purplish-red (cobalt) or a yellowish liquid (iron). The additive molecules are expected to form reverse micelles in the fuel-additive solution. Solutions of NaAOT, $Co(AOT)_2$, and $Fe(AOT)_3$ were prepared at concentrations of 250, 500, and 1000 ppm

metal in JP-8. Concentrations are evaluated based on metal content so that different organo-metallic additives can be more easily compared based on the metal atom.

Although these solutions were all prepared at concentrations above the critical concentration for micelle formation (~30 ppm metal), some precipitation was observed for all three iron-containing solutions and also for the 250-ppm cobalt-containing solution. The nature of the precipitate was not determined, but we have speculated that it may be metal oxide, resulting from the mixing of air into the solution during preparation, and the subsequent oxidation of the additive. Soot reduction results for the reverse-micelle additives are given in Section 5.1.5.

5. Small-Scale Experimental Testing

This section describes results for the small-scale experimental testing program. The majority of the results are from the drop tube reactor facility at the University of Utah, which is described below. We also present results from a 2-stage soot burner, the AMT-400 small gas turbine engine and a few results from the smoke lamp (ASTM D 1322–97 standard "Standard Test Method for Smoke Point of Kerosene and Aviation Turbine Fuel"). The facilities are discussed in more detail below except for the smoke lamp, which is a standard instrument.

5.1 Drop Tube Facility

Using the drop tube furnace as a preliminary screening can assess the following functions of an additive: 1) modified atomization of the droplets, 2) delays in ignition (leading to enhanced premixing), 3) decreases in soot formation on the fuel rich side of the diffusion flame front, and 4) increased soot burnout on the fuel lean side. The total soot was collected and weighed to determine the net impact of the additive. A similar monosized droplet stream was used to study the effect of fuel composition and inter-droplet spacing on soot formation by Sangiovanni & Liscinski (1985). A variety of conditions can be simulated in the drop tube by varying the oxygen concentration in the coflowing gas stream. Soot emissions have also been measured in this equipment as a function of oxygen content in the surrounding gas stream (Rah et al. 1987).

5.1.1 Apparatus Description

The drop tube reactor consists of a fuel feed system, furnace and sample collection system. A schematic of the drop tube system is given in Figure 4 and photos of the facility are shown in Figure 5.

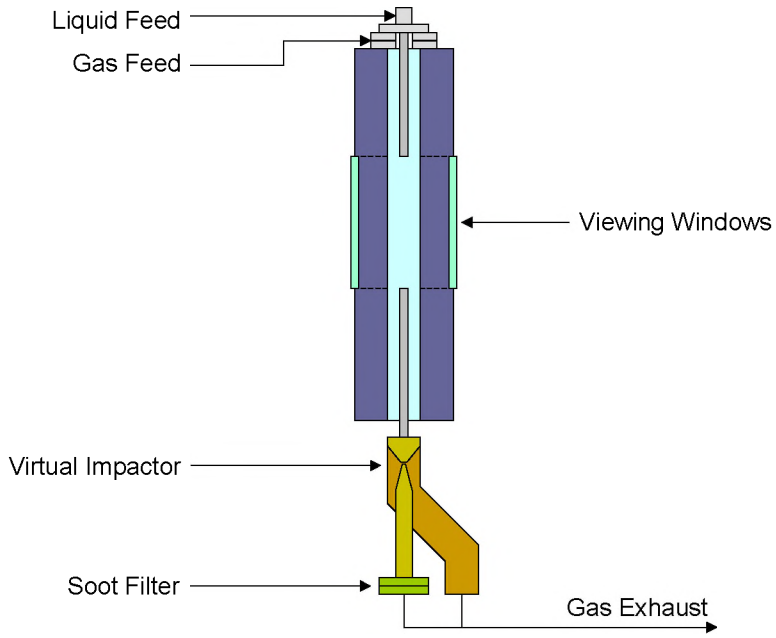

Figure 4. Diagram of the drop tube apparatus.

Parameters that can be varied in the experiments include furnace temperature, gas flowrates, fuel injection pressure, injector orifice size, and composition of the co-flow stream. Droplet size and residence time are functions of both orifice size and injection pressure. The many variable parameters allowed the drop-tube settings to be tuned to find conditions in which additive results most closely resemble those found in actual engines. This provides a screening tool which is considerably easier to run than an engine test and more realistic than the standard smoke-lamp test.

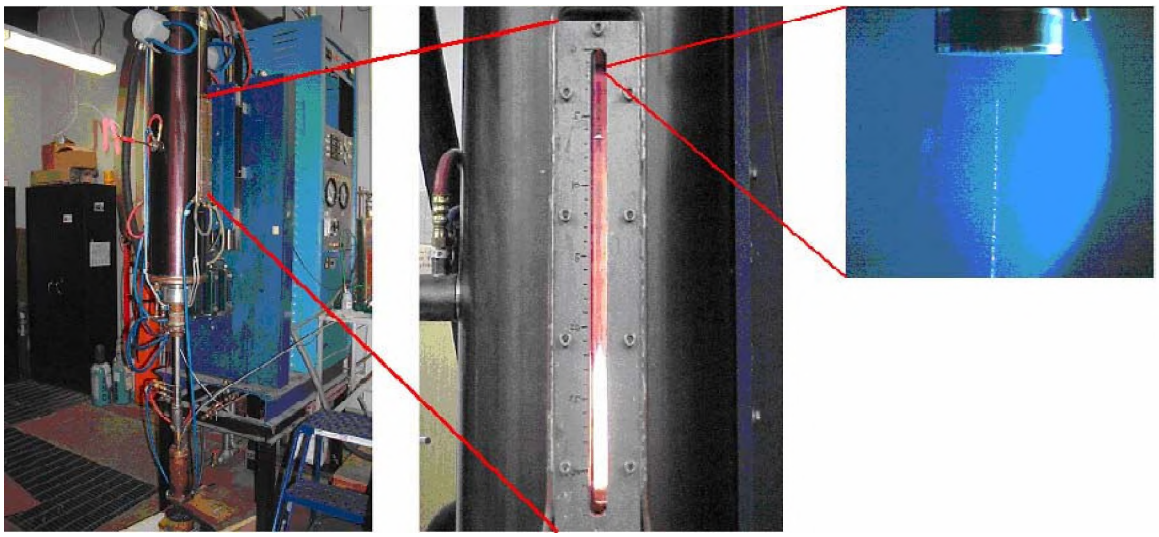

Figure 5. Photos of the drop tube apparatus.

Fuel feed rates, gas flow rates, sampling time, etc. were selected so that the following conditions apply:

- The overall mixture was stoichiometric when the oxidizer was atmospheric air.
- Droplets evaporated and burned before reaching the filter.
- Enough soot was collected for accurate weighing (about 1 g in 10 minutes).
- Sampling was completed before the collected soot exceeded the vacuum pump's capacity to draw enough gas through the filter.

5.1.2 Baseline Results

The drop-tube experiments began with baseline soot measurements in unaltered JP-8 fuel. Experiments were later carried out with additives designed to delay or accelerate ignition, inhibit soot precursor formation, and augment the rate of soot oxidation. Figures 6 and 7 show the baseline soot yield measurements for an expanded

range of operating conditions in the drop-tube furnace. In particular, we have examined a range of oxygen concentrations as well as temperatures. Figures 6 and 7 show soot aerosol yield and percent tar collected on the filter for JP-8 combustion without additives.

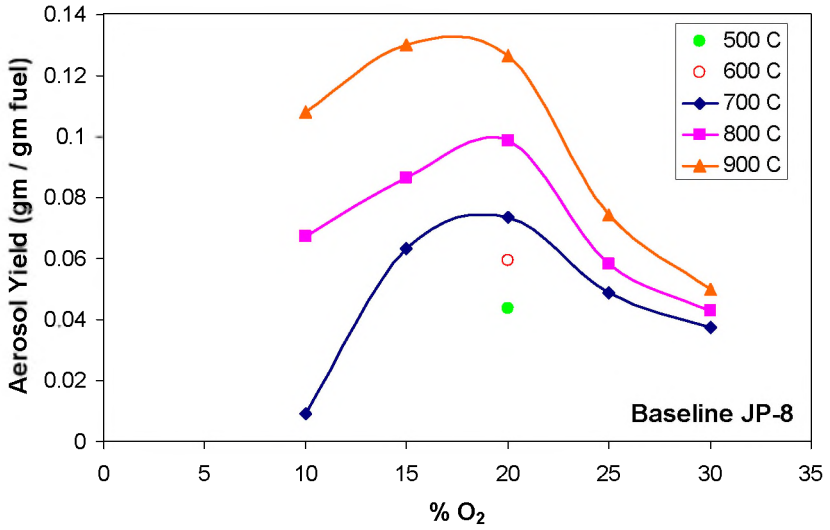

Figure 6. Soot aerosol yield in the drop tube experiment burning JP-8 fuel as a function of temperature and O_2 concentration in the co-flow gas.

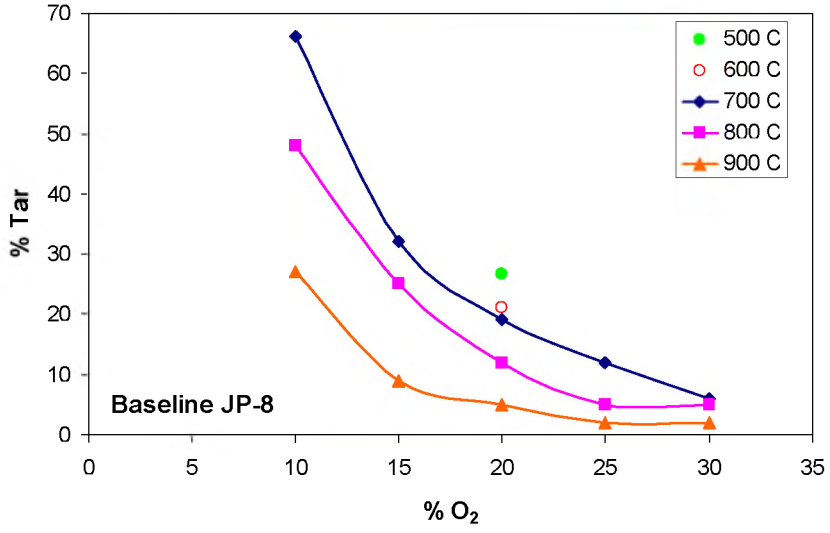

Figure 7. Tar percentage from the collected soot for the drop tube experiment burning JP-8 fuel as a function of temperature and O_2 concentration in the co-flow gas.

The results shown here are for cases in which the O_2 concentration in the oxidizer stream has been varied. The furnace wall temperature in all cases is 1370 K. The droplets are approximately 150 microns in diameter and exit the droplet generator with a downward velocity of about 4 m/s.

Measured parameters are the ignition delay (that is, the distance between droplet injection and ignition) and the mass of material collected on the filter.

5.1.3 Drop Tube Results with Known Compounds in JP-8

Our first series of drop-tube furnace tests examined organo-metallic and organic additives, as well as some proprietary additives whose composition was unknown to us. Figures 8 and 9 show molecular structures of some of the additives tested.

- Betz-Dearborn Spec-Aid 8Q462 (+100) detergent/dispersant (250-10,000 ppm)
- Lubrizol PA-5 detergent (1000 ppm)
- Ferrocene (300 ppm)
- Ruthenocene (300 ppm)
- Methylcyclopentadienyl manganese tricarbonyl (MMT) (300 ppm)
- Iron naphthenate (300 ppm)
- 2-ethyl hexyl nitrate (1000 and 3000 ppm)
- Di-tert butyl peroxide (1000 and 3000 ppm)
- NN diethyl hydroxylamine (1000 and 3000 ppm)
- 2-3 dimethyl 2-3 dinitrobutane (1000 and 3000 ppm)

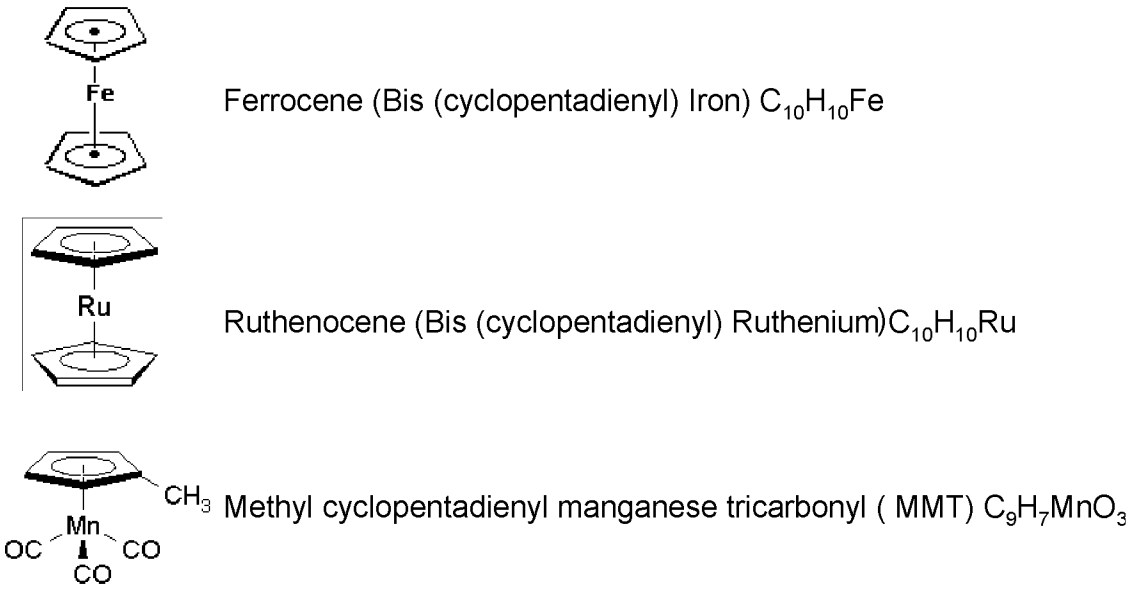

Figure 8. Molecular structure of some of the metallic additives tested in the drop-tube.

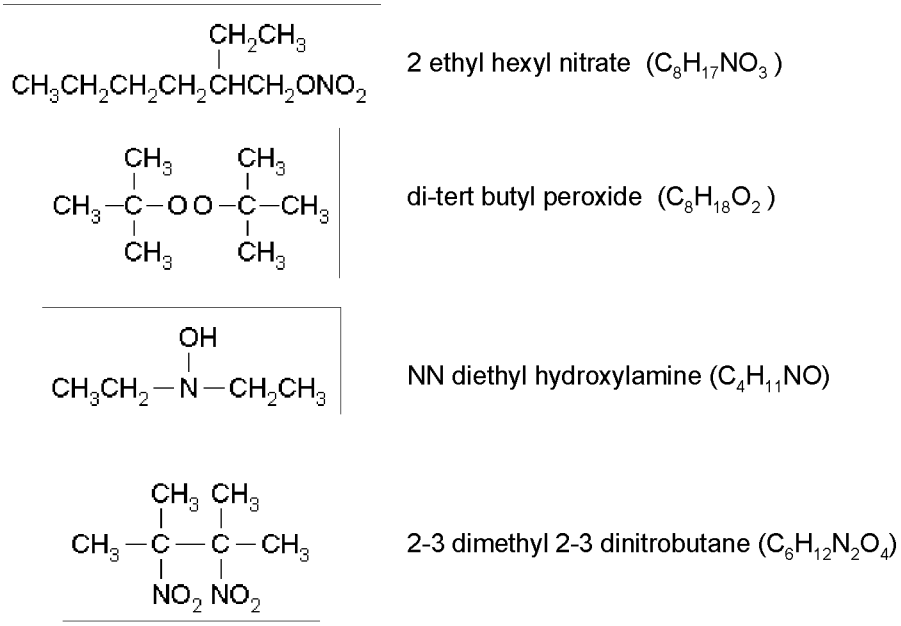

Figure 9. Molecular structure of some of the organic additives tested in the drop-tube.

Test results for the metallic additives are shown in Figure 10, which again shows the soot aerosol yield as a fraction of the soot aerosol produced by JP-8 with no additives at the same conditions. Additive concentrations are given in terms of metal content. Ferrocene is consistently the most effective additive. Iron naphthenate was tested to see

if another soluble iron compound could perform as well as ferrocene. Ruthenocene is identical to ferrocene except for the substitution of ruthenium (the element directly below iron in the periodic table) for iron. It was tested to help determine how important the dual pentadienyl structure is to ferrocene's long-recognized soot reducing effectiveness. MMT contains manganese, another known soot oxidation catalyst. All the metallic additives increase in effectiveness with increasing oxygen concentration, which is consistent with their expected action as soot oxidation catalysts. However, none of the additives was as consistently effective as ferrocene.

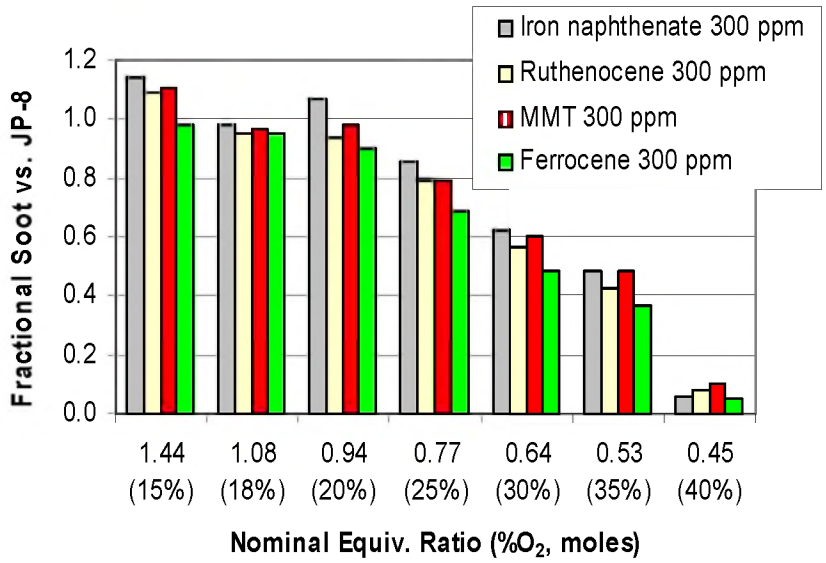

Figure 10. Soot reduction by metallic additives.

In the Phase I smoke lamp tests, ferrocene had showed significant reduction, while iron naphthenate had shown no effect. In order to resolve questions about the performance of iron naphthenate in the smoke lamp vs. the drop tube furnace, samples of soot from a wick lamp were collected. As an alternative to the smoke lamp, a common wick lamp (Shor International "Simplicity Burner") was used to generate larger quantities of soot from a wick-based flame. Solutions of ferrocene and iron naphthenate, each 500

ppm iron in JP-8, were burned individually in the lamp, with the wick raised enough to produce a visible emission of soot. Samples were collected on a Teflon filter of the same variety used for the drop-tube studies for 30 minutes, yielding 0.1–0.5 g soot aerosol material, which likely includes soluble organic material such as PAH. The filters were then delivered to Prof. David Robertson (University of Missouri) for x-ray fluorescence analysis.

In the case of the soot from the ferrocene-doped fuel, we find an iron concentration of 19150 ng/cm^2, corresponding to 1.2% by mass of the total material collected. On the other hand, in the soot from the iron-naphthenate-doped fuel, we observe an iron concentration of 649 ng/cm^2, corresponding to 0.008% by mass of the total material collected. In other words, the soot aerosol produced by the ferrocene-containing fuel had roughly 30 times the iron content (and 1/5 the total mass) of the soot aerosol produced by the iron-naphthenate-containing fuel. We can therefore conclude that the poor performance of iron naphthenate in the smoke lamp is the result of an insufficient amount of iron making its way into the gas phase, probably the result of the relatively higher molecular weight, and corresponding lower volatility, of iron naphthenate compared to both ferrocene and JP-8.

Figure 11 shows photographs of the drop-tube flame for varying oxygen concentrations in the co-flowing stream. In each pair, the left flame is pure JP-8, while the right flame contains 300 ppm ferrocene. The pictures show both the ignition delay and the soot burnout effects of adding ferrocene. The spark-like features visible in the 40 and 45 percent oxygen flames may be iron oxide particles. The flame undulations, most visible in the leftmost picture also occur in the UNICORN simulations to be shown in

Chapter 6. The flame dims when oxygen diffusing from the co-flowing stream is exhausted. The flame re-ignites when more oxygen diffuses in.

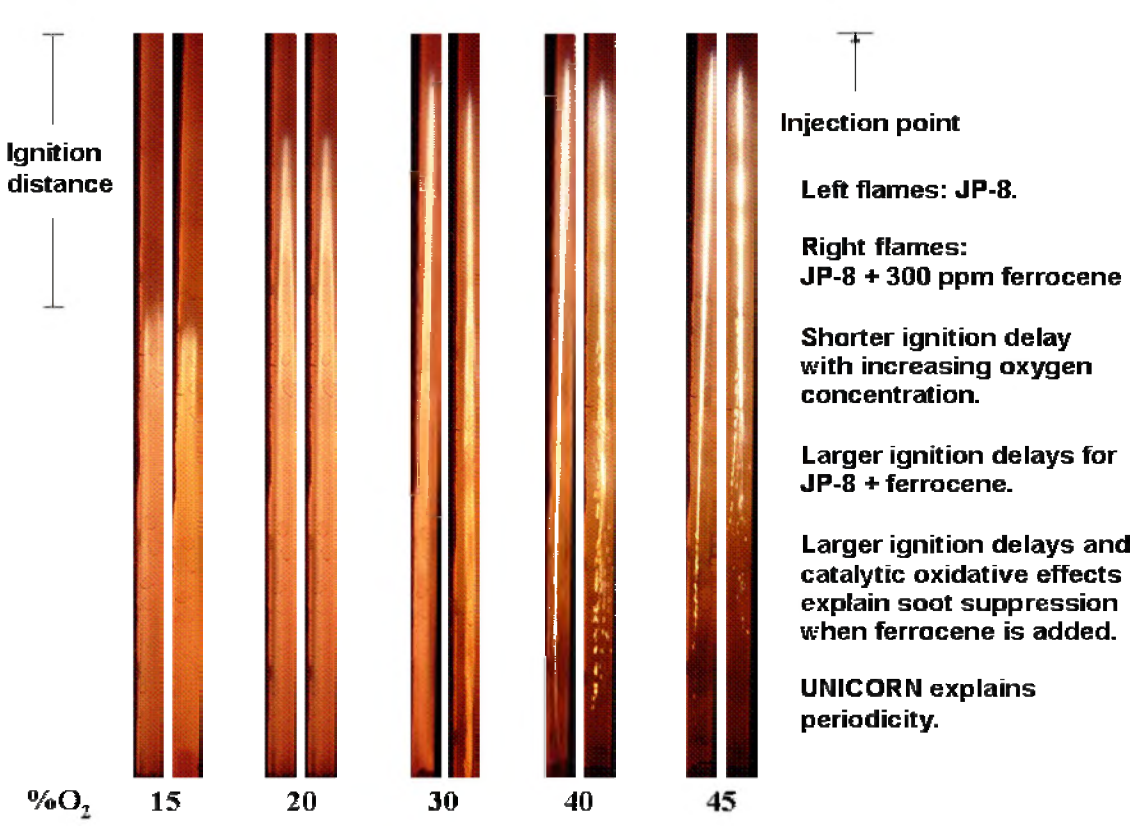

Figure 11. Photographs of the drop-tube flame for varying oxygen concentrations in the co-flowing stream. In each pair, the left flame is standard JP-8, while the right flame contains 300 ppm ferrocene.

Figure 12 shows results for the organic additives. Consistent with previous results, significant soot reductions are observed for the organic additives at 25% and higher oxygen concentration. At these concentrations, all of the additives have a significant soot-reducing effect. In nearly all cases where a significant soot reduction is observed, 3000 ppm results in a larger soot reduction than 1000 ppm.

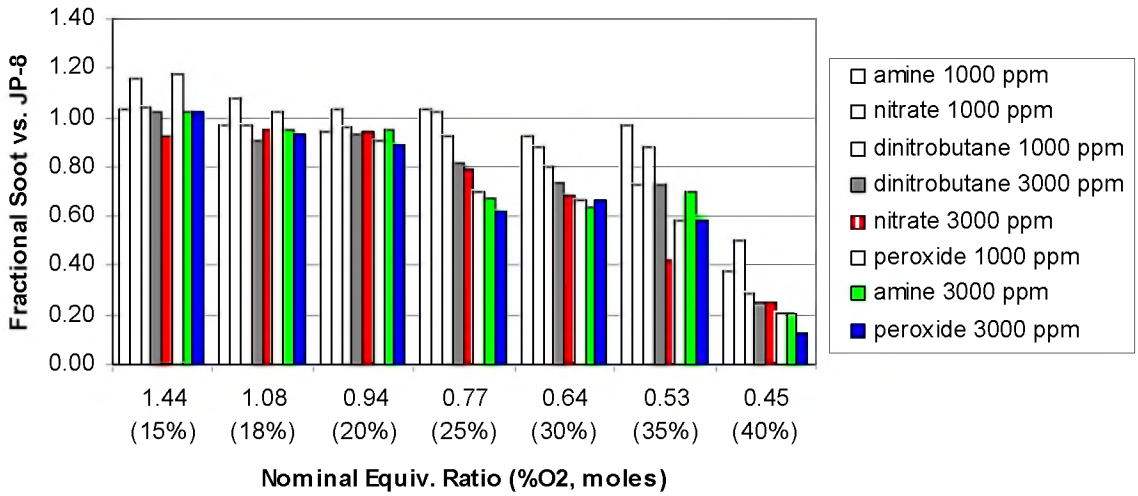

Figure 12. Soot reduction by organic additives. (nitrate = 2-ethyl hexyl nitrate; peroxide = di-tert butyl peroxide; amine = NN diethyl hydroxylamine; dinitrobutane = 2-3 dimethyl 2-3 dinitrobutane).

Figure 13 show the correlation between ignition distance and soot reduction for the additives tested for the 40% O_2 case, where the greatest soot reductions occur for all additives. A clear correlation exists between decreasing ignition delay with decreasing soot yield. In nearly all cases, the additives increase the ignition delay. The results are surprising because the peroxide and nitrate additives are known to be ignition enhancers and the metal-containing additives are not expected to affect the gas-phase chemistry and thus the ignition delay.

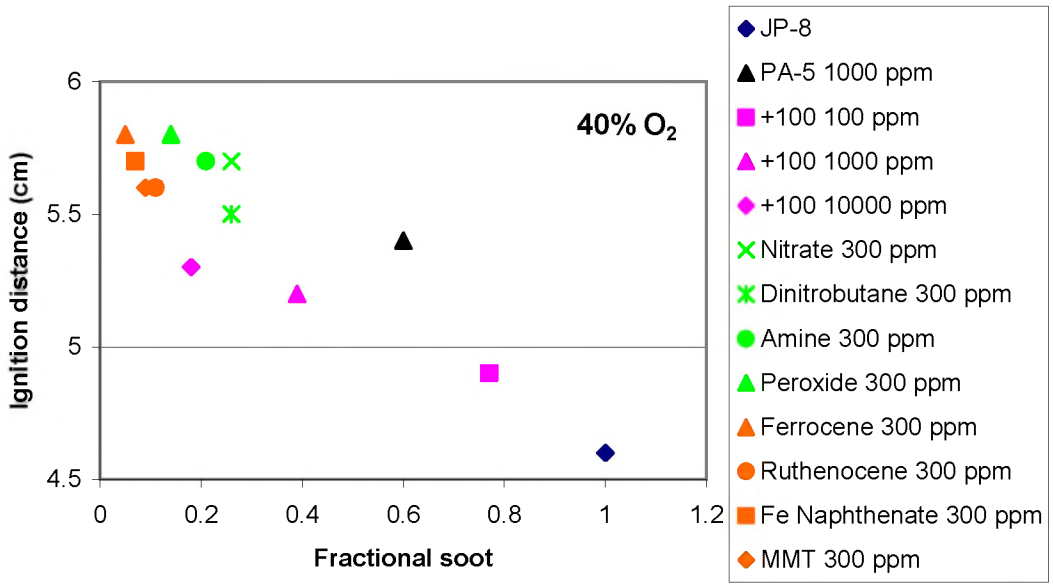

Figure 13. Correlation fraction of soot compared to JP-8 with ignition distance for 40% O_2.

Increased ignition delay for all additives that are effective at reducing soot has been observed even when the additive in question is a cetane improver, which is expected to enhance ignition, i.e. decrease ignition delay. It has been suggested that this trend may have resulted from measuring the ignition delay from the start of the luminous, sooting part of the flame rather than the "true" location of ignition, a much less luminous blue flame (as illustrated in Figure 14). At the high oxygen concentration used for most additive testing, the sooting portion of the flame is so luminous that it makes the blue flame difficult to see or photograph. It was hypothesized that if the additive inhibited soot inception, then the length of the blue portion would be longer. It would therefore be possible to have decreased ignition delay and still see the orange portion of the flame having moved away from the point of ignition.

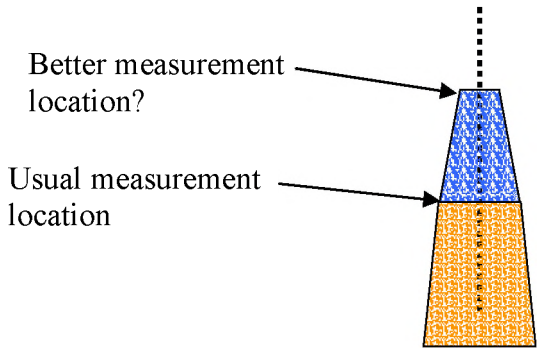

Figure 14. Diagram showing of drop tube flame showing the droplet stream, the dim blue flame, and the bright, soot-laden luminous yellow flame.

In order to better see and photograph the blue part of the flame, several optical filters were tried, with an example photograph shown in Figure 15. In preliminary tests with ferrocene, we do not observe any significant change in the length of the blue flame compared to the flame with no additive. In other words, measuring the ignition delay based on the blue flame gives the same comparison as measuring it based on the luminous orange zone. On the other hand, if the alkane blend Norpar 13 is used instead of jet fuel, the length of the blue flame increases by a factor of four, a result of the significantly lower sooting tendency of the normal alkanes.

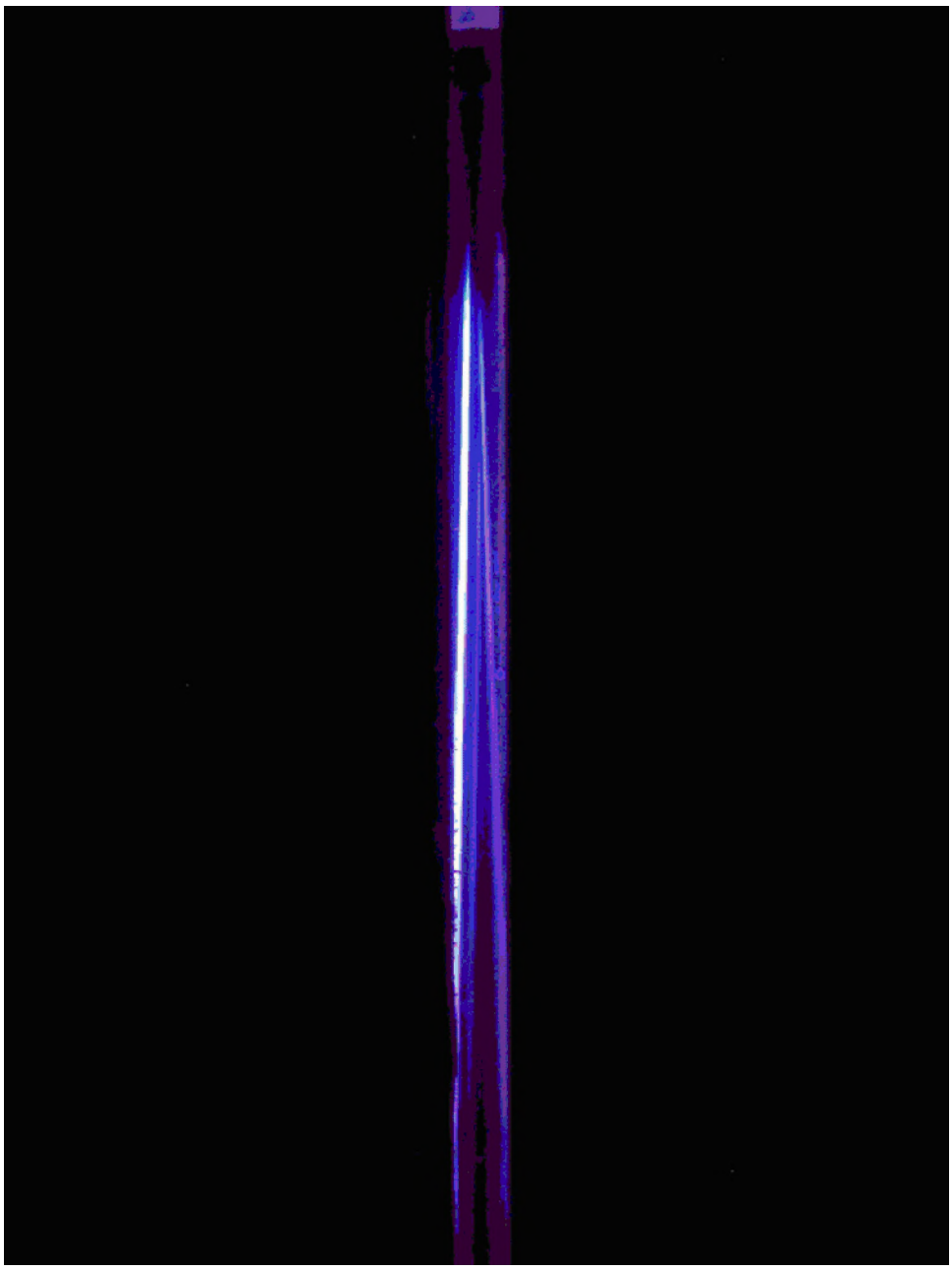

Figure 15. Photograph of the drop tube flame using an optical filter.

5.1.4 Proprietary Additives

Again, the additives have been tested in a variety of oxygen-nitrogen mixtures ranging from 15-40% O_2. In all cases the additives were more effective in the enriched oxygen environment. Figure 16 shows results for the soot mass collected (normalized by the unaltered JP-8 result) for the proprietary PA-5 and +100 additives. PA-5 shows

significant reductions for oxygen-enriched combustion at a concentration of 1000 ppm. The +100 additive shows no effect near its recommended concentration (250 ppm) but shows very significant reductions with increasing concentration, again only for oxygen-enriched conditions.

These results show considerable correspondence with WPAFB gas turbine engine (T63) results (Corporan et al. 2002):

- PA-5 1000 ppm: soot reduction on the order of 40 – 50%.
- +100 Additive at 256 ppm: no soot reduction.

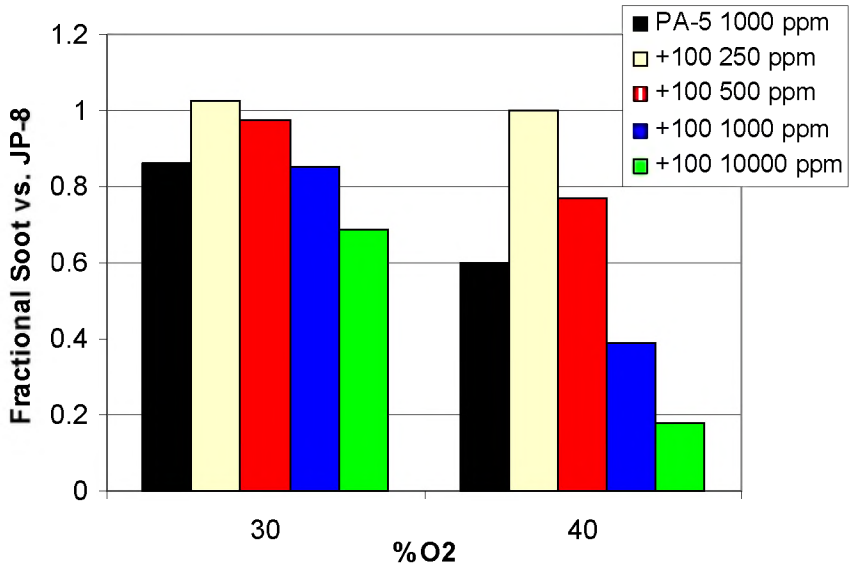

Figure 16. Soot reduction results for proprietary additives PA-5 (Lubrizol) and "+100" (Betz-Dearborn).

We tested 16 additives from Afton Chemical in both the smoke lamp and the drop tube. It is important to note that additives #7 through #16 are mixtures consisting primarily of additives #1 and/or #6 and the additional additive named A-150.

Figure 17 shows results for the 16 Afton additives in the smoke lamp. Three of the Afton additives (#4, #5 and #14) had a clear positive effect on the smoke point (i.e., a

reduction in sooting). These three measurements were repeated. The second measurement was within one millimeter of the first, suggesting that the effect is real. The data plotted in Figure 17 are the average of these measurements. During Phase I we tested several proprietary Lubrizol additives in the smoke lamp and saw little effect. The effects seen for these Afton additives are more substantial than those for the Lubrizol samples.

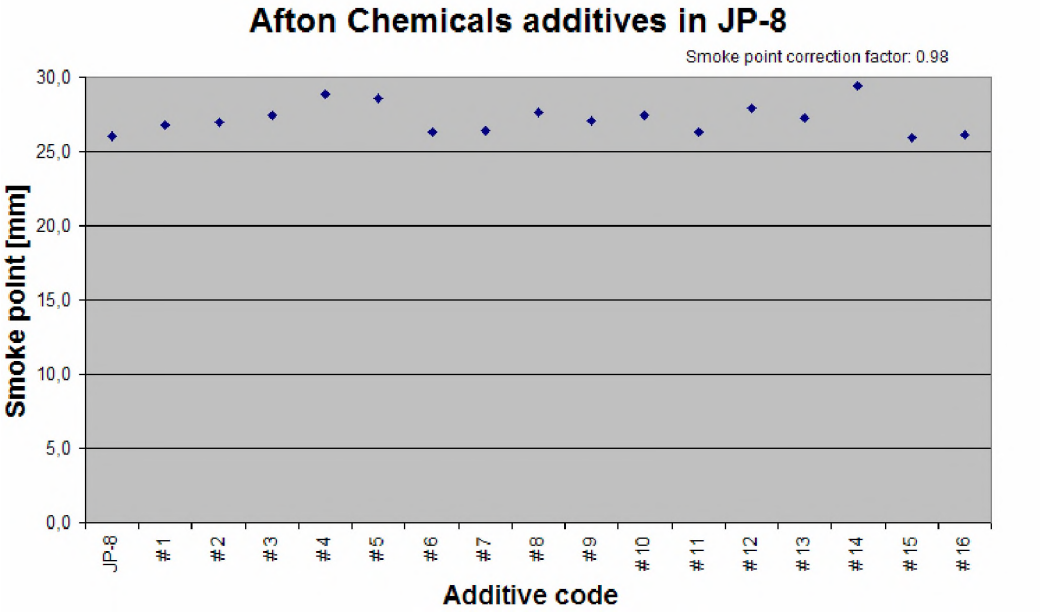

Figure 17. Smoke lamp results for the Afton additives.

The Afton additives were all successfully tested in the drop-tube furnace except additive #3, which increased the viscosity of the fuel to a degree that the droplet generator would not function properly. In addition, additives #1, #10, and #11 produced very bright flames that also have an unusual concentric appearance. Efforts to document the unusual flame structure photographically were unsuccessful. The similar behavior of these three additives is attributed to the incorporation of significant quantities of #1 in the formulations of #10 and #11. Finally, we observe that in solutions of additives #1, #5, #12 and #15, some material precipitates to the bottom of the container several hours after

preparation. It likely that the similar behavior of #5, #12, and #15 is due to the common component #5.

Figures 18 and 19 show the results of the drop-tube tests of the Afton Chemical additives. All experiments were conducted with the furnace set to 1100 C and the coflowing gas mixture containing 40% O_2. Figure 18 shows the soot yield from each test, with additives ordered from least to most effective. In general, nearly all of the additives performed well under these conditions, with the exception of #16, #6, and #12. The remaining additives all had soot yields of 23%–32%, compared to JP-8 alone.

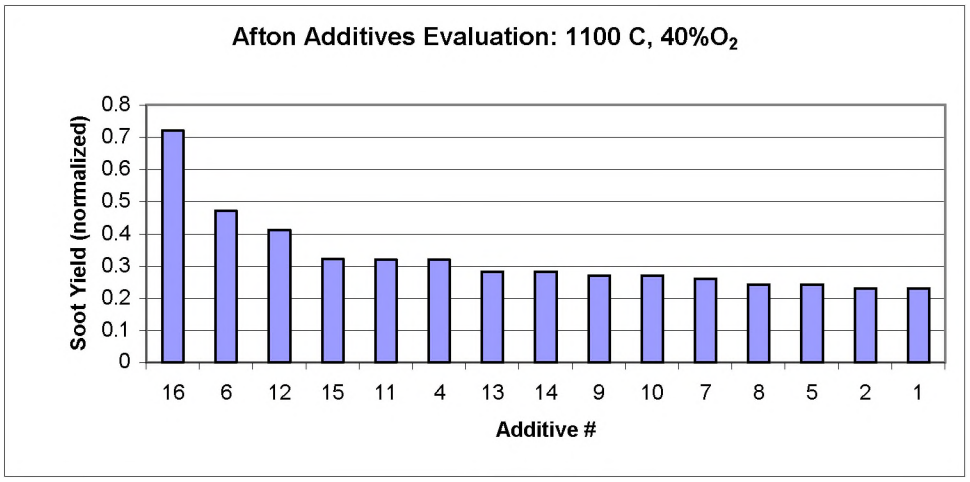

Figure 18. Soot Yield of JP-8 with Afton additives, normalized by the yield from unaltered JP-8.

Figure 19 shows the ignition delay (flame liftoff) resulting from the Afton additives. Additives #16 and #6, the least effective for soot reduction, produced no change in the ignition delay compared to JP-8 alone. The other additives (maintaining, in Figure 20, the order from Figure 19) do not show a clear relation between ignition delay and soot suppression, although they do all slightly increase the ignition delay compared to unaltered JP-8.

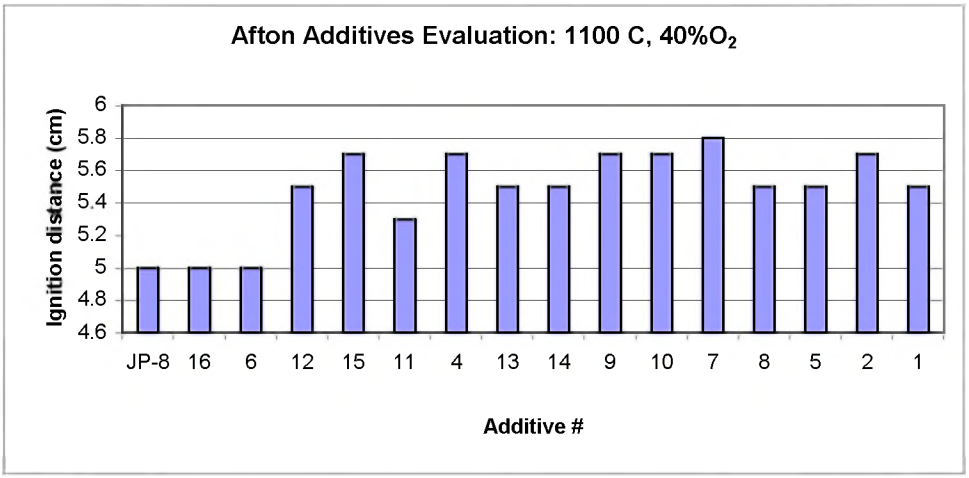

Figure 19. Ignition delay (flame liftoff) of JP-8 with Afton additives

5.1.5 Metal Micelle Additives

The second set of additives, synthesized by REI consultant Brian Dunn (see section 4.3), consist of sodium, cobalt, and iron, ion-exchanged onto the surfactant AOT (bis-(2-ethylhexyl) sulfosuccinate). Before mixing with JP-8, the additives form waxy solids that are white (sodium) or purplish-red (cobalt) or a yellowish liquid (iron). In these additives, the additive molecules are expected to form reverse micelles in the fuel-additive solution. Solutions of NaAOT, $Co(AOT)_2$, and $Fe(AOT)_3$ were prepared at concentrations of 250, 500, and 1000 ppm metal in JP-8. Concentrations are evaluated based on metal content so that different organo-metallics can be more easily compared based on the metal atom.

Although these solutions were all prepared at concentrations above the critical concentration for micelle formation (~30 ppm metal), some precipitation was observed for all three iron-containing solutions and also for the 250-ppm cobalt-containing solution. The nature of the precipitate has not yet been determined, but we have

speculated that it may be metal oxide, resulting from the mixing of air into the solution during preparation, and the subsequent oxidation of the additive.

The JP-8/additive solutions were first tested in the smoke lamp. As can be seen in the smoke lamp measurements shown in Figure 20, none of the micelle compounds showed a significant effect.

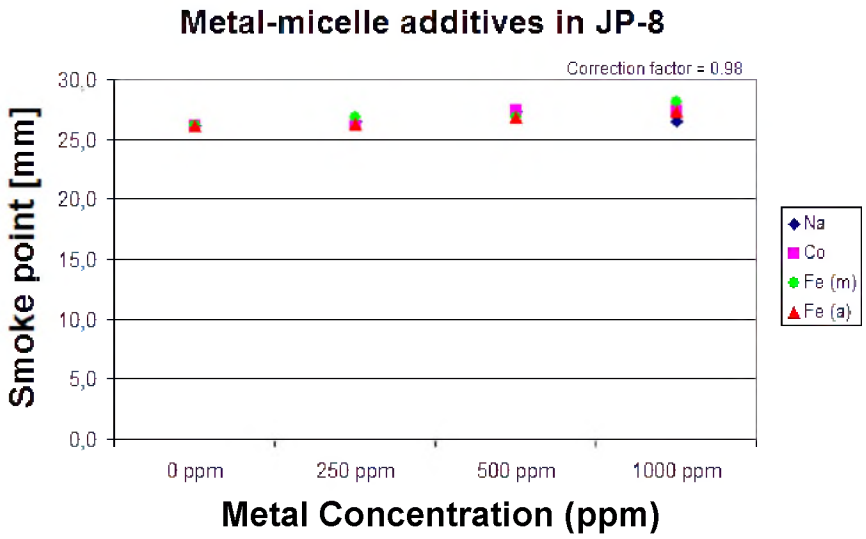

Figure 20. Metal micelle additive results from the smoke lamp.

Figure 21 shows the results from the drop tube experiments with these additives. In general, the iron-containing additive performs much better than the others, although the cobalt additive also has a significant effect at the highest concentration. For reference, ferrocene at 300 ppm metal in JP-8 results in a normalized soot yield of 5% at these conditions. A similar quantity of metal via $Fe(AOT)_3$ in JP-8 results in a normalized soot yield of 13%.

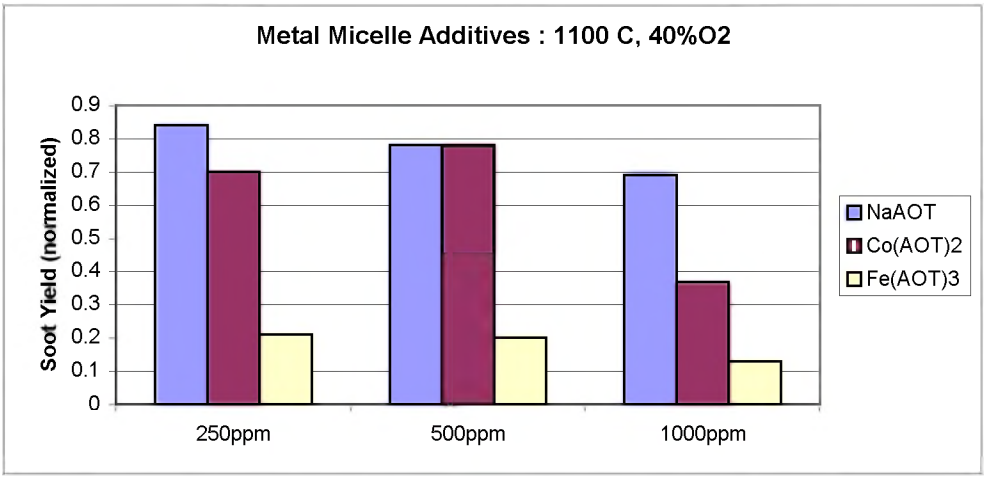

Figure 21. Soot Yield of JP-8 with metal micelle additives, normalized by the yield from JP-8 alone.

Figure 22 shows the correlation of ignition delay (flame liftoff) with soot yield resulting from the use of the metal micelle additives. In this case, there appears to be a clear trend of increasing ignition delay with increasing soot suppression. In particular, it is notable that the cobalt additive spans the range of behavior: at lower concentrations it is not particularly effective and has an ignition delay similar to JP-8 alone, while at the highest concentration it has an increased ignition delay and decreased soot yield in line with the correlation for the iron additive. However, the causal relationship between ignition delay and soot suppression remains unclear, particularly for metallic additives that are expected to act primarily as oxidation catalysts.

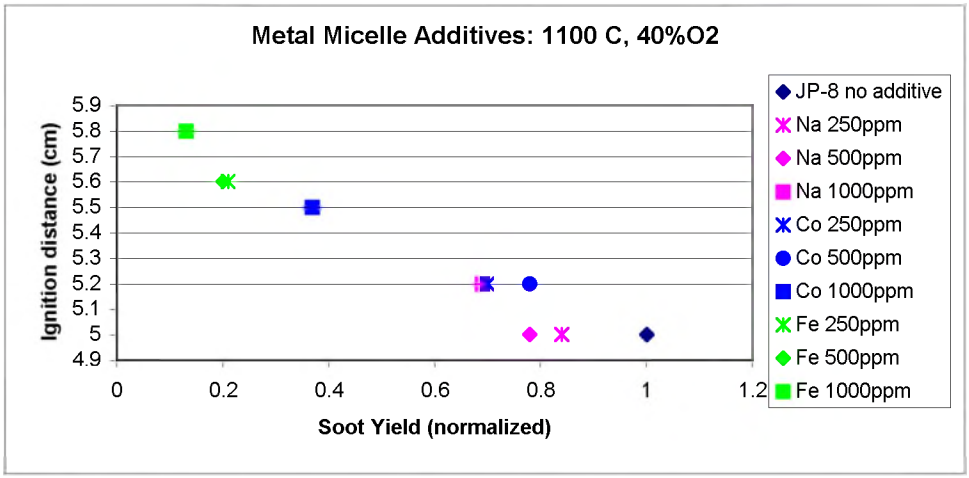

Figure 22. Correlation of ignition delay (flame liftoff) and sot yield for JP-8 with metal micelle additives

5.1.6 Microphotography in the Drop-Tube

Extensive microphotography of droplets in the drop-tube furnace has allowed us to refine our understanding of the droplet behavior. Using this technique, we revised our specification of initial droplet diameter, droplet vaporization rate, and droplet velocity. We have determined that the droplets enter the reactor with much smaller diameters and much larger velocities than previously estimated. We have also observed that shortly after injection the droplets slow and coalesce into larger droplets. These new larger droplets then evaporate at a rate consistent with d^2 theory (which says that individual spherical droplets will evaporate in such that the diameter squared changes linearly with time). Information obtained from the photographs was forwarded to Dr. Vish Katta of ISSI for use in the UNICORN CFD code inputs used for modeling the drop tube.

Figure 23 shows the initial breakup of the liquid column into individual droplets. Similar images were used to make the findings in the above paragraph.

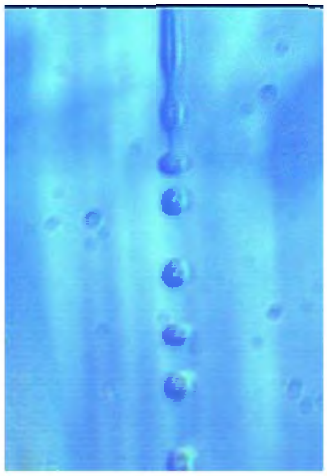

Figure 23. Microphotograph of droplet formation in the drop-tube furnace.

In addition, we have observed sooting behavior on a much larger scale than we had expected. Figure 24 contains photographs taken during drop tube combustion showing large (~100 μm) soot aggregates formed both with and without the addition of ferrocene. These aggregates are much larger than one would ordinarily expect in a sooting flame, but do agree qualitatively with observation of the material collected on the sampling filter. It is unclear how these large aggregates are formed; one possibility is through agglomeration of soot particles.

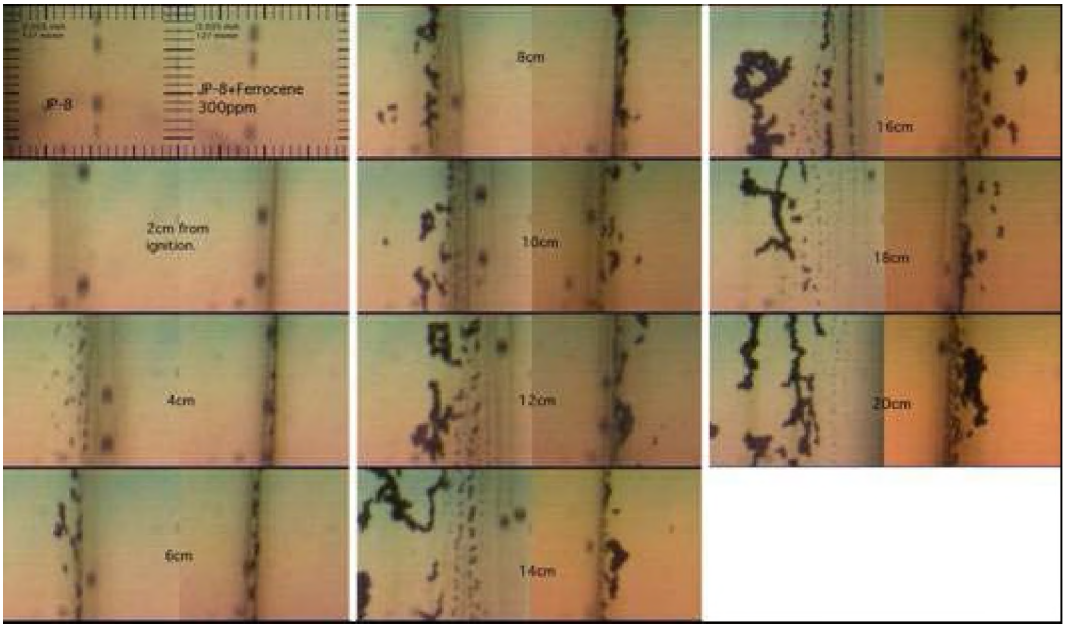

Figure 24. Microphotographs taken during drop tube combustion showing soot aggregates formed both with and without the addition of ferrocene.

5.2 Two-Stage Burner

The two-burner apparatus is a system that allows the generation of soot in a primary premixed flame and subsequent oxidation in a secondary flat flame. The design of the system ensures high flame stability and a one-dimensional flame, both of which aid in the study of soot oxidation kinetics. This system also allows for separation of mixing and chemical kinetic effects due to the long residence time of the soot-laden primary combustion gases in the mixing chamber prior to burnout. Optical techniques, such as light scattering and extinction, can be used in conjunction with this apparatus to measure both soot size and concentration from either flame.

5.2.1 Description of the Apparatus

A detailed description of the dual-burner apparatus is given below and a diagram is shown in Figure 25.

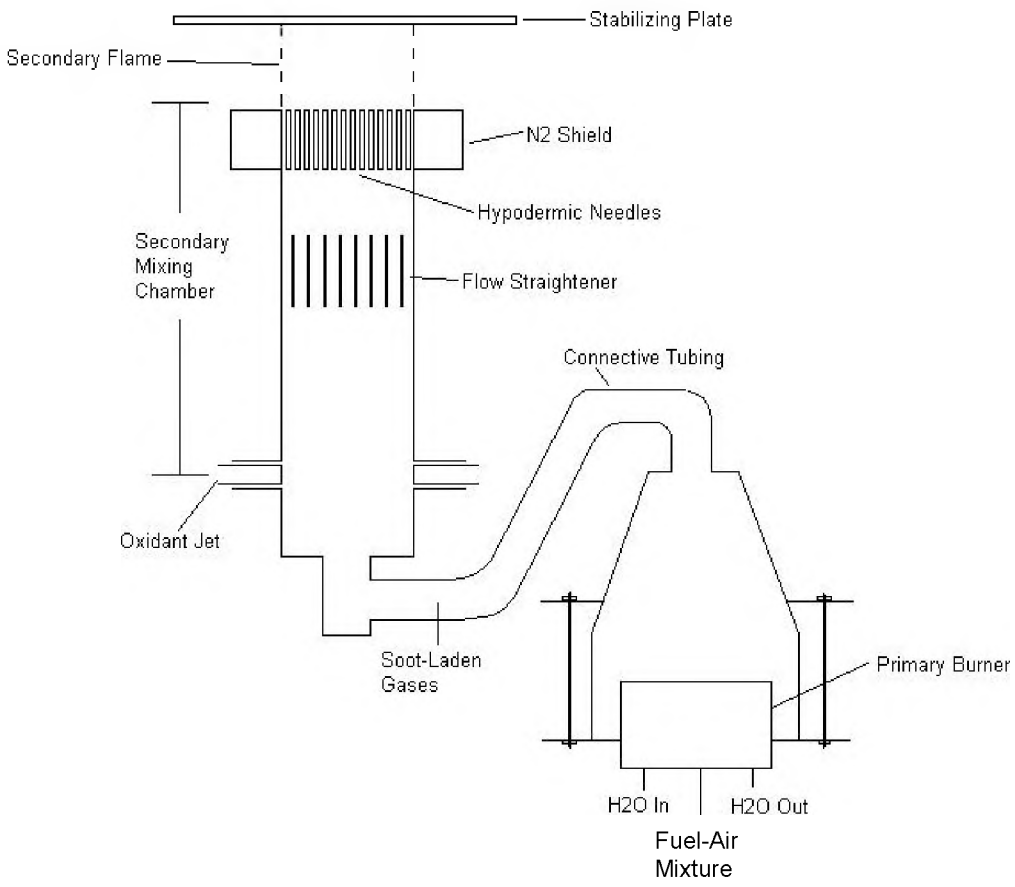

Figure 25. Schematic of the two-stage soot burner experiment.

A fuel-rich gas stream is sent through the primary burner where an igniter rod is used to initiate a soot-forming flame. The combustion products and newly-formed soot then enter a long, vertical secondary mixing chamber where nitrogen and oxygen are injected at high velocity (to ensure good mixing) through four nozzles spaced 90 degrees apart. The capability for carbon dioxide and fuel injection through these nozzles was also available to manipulate the temperature of the secondary flame and the equivalence ratio of the soot-laden mixture to aid in maintaining the secondary flat flame. The gas stream passes through stainless steel flow straighteners that ensure a uniform flow and thus a flat secondary flame. The quenched combustion gases then flow across the "flame plug", a

dense bundle of 17 mm stainless steel hypodermic needles, which acts as a burner from which the secondary flame originates. An annular ring of continuously flowing nitrogen surrounds the flame plug and prevents mixing of the combustion gases with the ambient air. A water-cooled ceramic stabilizing plate is positioned above the flat flame and is used to increase the stability of the flat flame by directing gas flow from the flame through a hole in the center of the plate. The soot then enters a Scanning Mobility Particle Sizer to create a monodisperse stream that then travels to the oxidation burner.

The flow rates of both the combustion fuel and the air entering the burner are controlled by Brooks 5850E mass flow controllers. The fuel (usually ethylene) and air are mixed in a ¼" mixing tube prior to entering the burner. The burner chamber is comprised of a 2" OD Schedule 80 stainless steel pipe that is 5" long. While macromixing occurs in the mixing tube, micromixing of the reactants occurs over a bed of 1/8" quartz beads resting on a stainless steel mesh inside the burner chamber. The burner plate consists of a 2" OD, ½" thick sintered bronze disk with a void fraction of 0.2 from MKI corporation. The use of a sintered metal disk as a burner is quite desirable as the large pressure drop across the disk leads to a uniform flow and the possibility of flashback is completely eliminated. In an adiabatic flat flame burner, there is a very narrow range of conditions in which a stable flame is produced. A non-adiabatic burner allows a stable flame over a wide range of flow conditions. This burner is non-adiabatic and makes use of copper cooling coils. Two 1/8" copper cooling coils are embedded in the sintered disk 1/16" from the bottom. The total flow rate of water through the two cooling tube is 1.4 L/min. This flow rate removes enough heat from the flame to stabilize

it for a variety of flow conditions. It is desirable to embed these coils as close to the bottom of the burner disk as possible to eliminate flow distortion.

To shield the premixed flame from atmospheric interference, a quartz tube was initially used. However, difficulties in sealing the tube after ignition of the reactants in each run and problems with fatigue cracking of quartz at weak points in the wall led to the construction of a steel shield. The steel shield has a port for both ignition and temperature measurements and has eliminated the difficulties inherent in using a quartz tube. The height of this shield, 6", was chosen to give the products residence time for cooling prior to entering the SMPS.

The oxidation chamber has three primary purposes: efficient mixing of the soot-laden combustion gases with new gases injected to alter the properties of the secondary flame, uniform flow of combustion reactants to the secondary flame, and oxidation of the soot from the primary flame.

The secondary burner apparatus is made of stainless steel and has a 2" outer diameter. The soot-laden combustion gases that exit the SMPS enter this chamber through a ¼" swagelock fitting welded to the bottom of the cylindrical chamber. Four gas injection points spaced 90 degrees around the tube allow for the high-velocity injection of fuel, air, CO_2 and other desired reactants. The flow rates of these injected gases are controlled by Brooks 5850E mass flow controllers. The oxidant jets are designed to ensure adequate mixing of combustion gases from the primary burner and newly injected reactants. This setup allows the manipulation of the stoichiometry and temperature of the oxidation flame. Jet momentum calculations indicate that 10" would

be required for proper mixing of the gases. A ceramic honeycomb flow straightener was placed after this mixing zone to insure uniform flow of the gases into the secondary flame. Uniform flow is achieved using a honeycomb with a 1" thickness with a 1/8" cell size.

The use of a sintered disk for the secondary burner is not possible because soot particles need to flow through the burner disk. As done by several other experimenters, the burner consisted of a bundle of stainless steel hypodermic tubes. In this case, a flamelet is created over the top of each tube. The tube size is a compromise between the flame stability given by small tubes and the amount of time that passes before the tubes clog with soot. 1/16" tubes were chosen for these experiments.

To shield the secondary flame from atmospheric interference, a nitrogen sheath flow with a rate of 8 L/min was used. The cooling system in the secondary burner consisted of a small cylindrical cooling tank 1 inch above the burner with a ¼" hole through the center that allowed the soot-laden combustion gases to travel through. The removal of heat stabilizes the flame, increasing the repeatability of the experimental runs.

5.2.2 Two-Stage Burner Results – Soot Oxidation

In the initial tests a premixed ethylene-air flame generated the soot stream. The equivalence ratio of this rich flame varied from 2.4 to 3.2. The soot stream was injected with the appropriate amount of air to reach the desired equivalence ratio. Also, methane was injected to stabilize the secondary flat flame. The soot-laden gas stream then passed through a flow straightener and then to the secondary flame. This flame was stabilized

by removing heat via a cooling chamber directly above the burner tip. The equivalence ratios for the secondary flame ranged from 1.6 to 2.25. The oxidized soot was then sent through ¼" copper tubing to the SMPS for size analysis. Typical results are shown in Figures 26 and 27. The pre-oxidation data in the figures are soot size distributions for the same system with no secondary flame and no methane injection. The distributions have not yet been adjusted for the dilution effects from the additional methane flow present in the post-oxidation runs, because this is expected to be a very minor correction.

As seen in these two figures, oxidation decreases the particle concentrations for the entire range of soot size diameters; these data were consistent for the entire range of stoichiometries that were used in these experiments. Previous studies have shown that under these fuel-rich conditions, hydroxyl radical are the primary species responsible for this oxidation (Neoh et al 1981). In the case of the equivalence ratio of the primary flame being 2.4, both runs showed up to a 60% burnout of the entering soot (Figure 26). The truly remarkable aspect of these runs is the comparison between the particle count decrease in large particles to that of small particles. It appears from the figure that the decrease in large particles is much larger than that of small particles (observe the 15-50 nm range vs. the 150-250 nm range). What is most likely occurring here is that the large particles are fragmenting into smaller particles. There is a small size range, near the limits of the instrument, where the particle numbers *increased* during the oxidation process.

Runs with primary equivalence ratios of 2.8 (Figure 27) again show the obvious decrease in particles from oxidation. However, the fragmentation mechanism is not as distinct as shown in Figure 26.

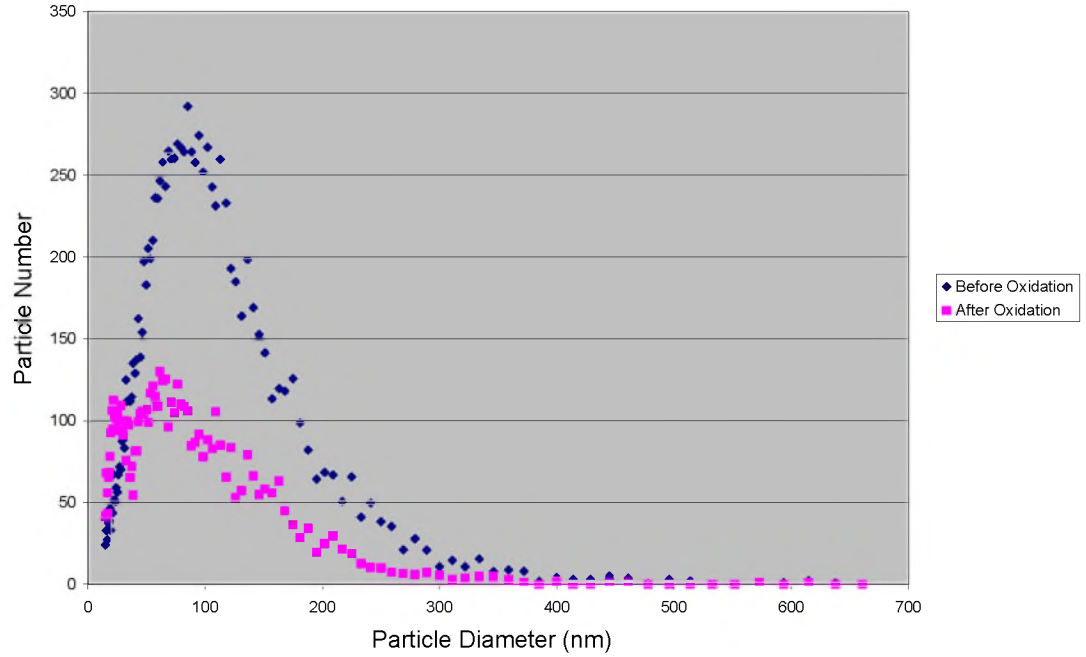

Figure 26. Results before and after oxidation. The equivalence ratio is 2.4 in the primary burner and 1.6 in the secondary burner.

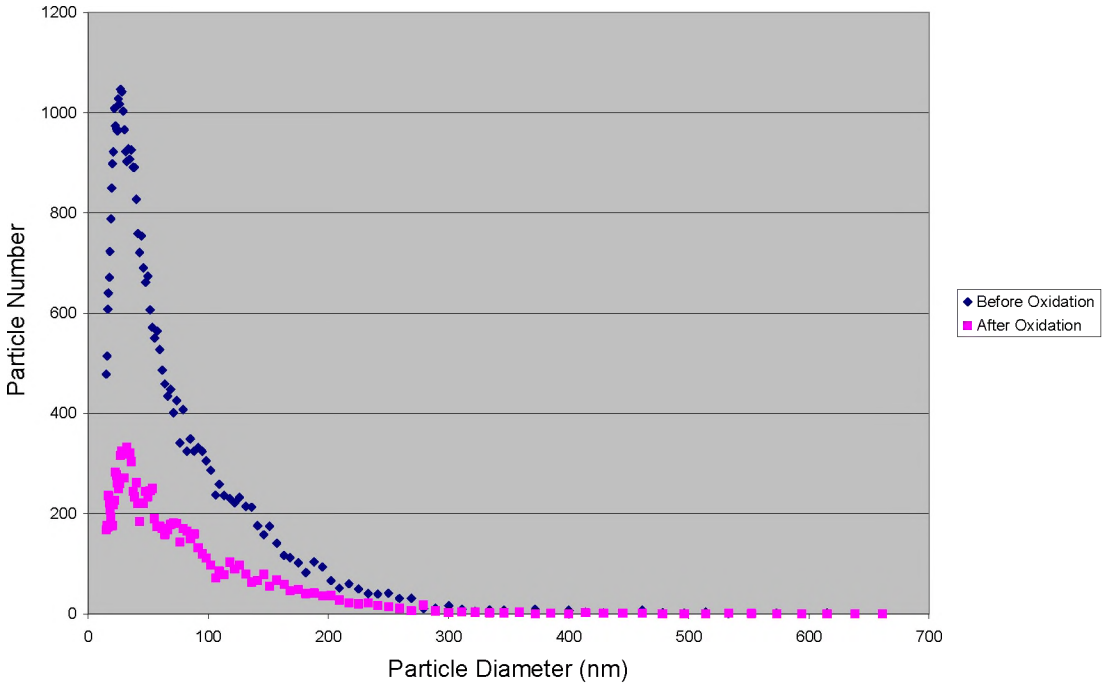

Figure 27. Results before and after oxidation. The equivalence ratio is 2.8 in the primary burner and 1.75 in the secondary burner.

Fuel rich experiments were run at an equivalence ratio of approximately 1.4 for these tests. The temperature of the premixed oxidation flame, measured by a type R thermocouple and corrected for radiation, was 1000 ± 20^{o} C. Figure 28 shows the effect of fuel-rich oxidation on the primary particle size distribution. The average particle diameter remained essentially constant at 59.4 ± 1.1 nm before oxidation and 58.3 ± 3.7 nm following oxidation; in addition, the peak diameter decreased slightly from 59.4 nm to 53.3 nm. A 10-fold decrease in peak particle number occurred on oxidation and the average extent of burnout was 77%. Calculations suggest that the primary oxidant under these conditions was OH, with O_2 playing a minor role. As observed by previous investigators (Neoh et al 1981), there is no evidence of any fragmentation in these runs.

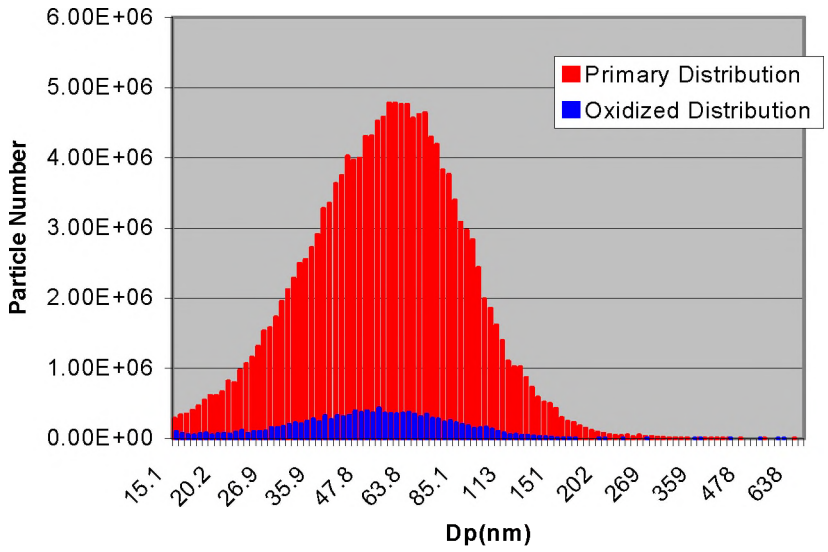

Figure 28. Fuel rich soot oxidation ($\phi = 1.4$) results.

The high level of repeatability in these experiments is visible in Figure 29.

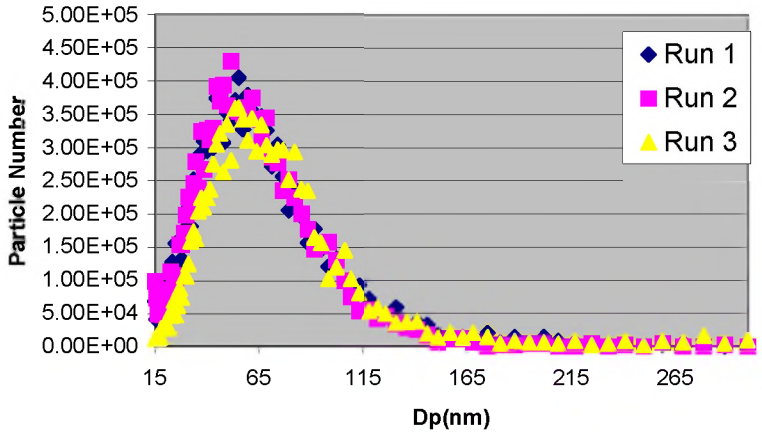

Figure 29. Repeatability of Oxidation Experiments

The oxidizing environment used in this study for fuel-lean oxidation had an equivalence ratio, , ϕ of 0.80). Again, a temperature of $1000 \pm 20^{\circ}$ C was measured (after radiation corrections). Temperature was measured at the sampling location, approximately 5 mm above the burner surface. Figure 30 shows the fuel-lean oxidation particle size distributions.

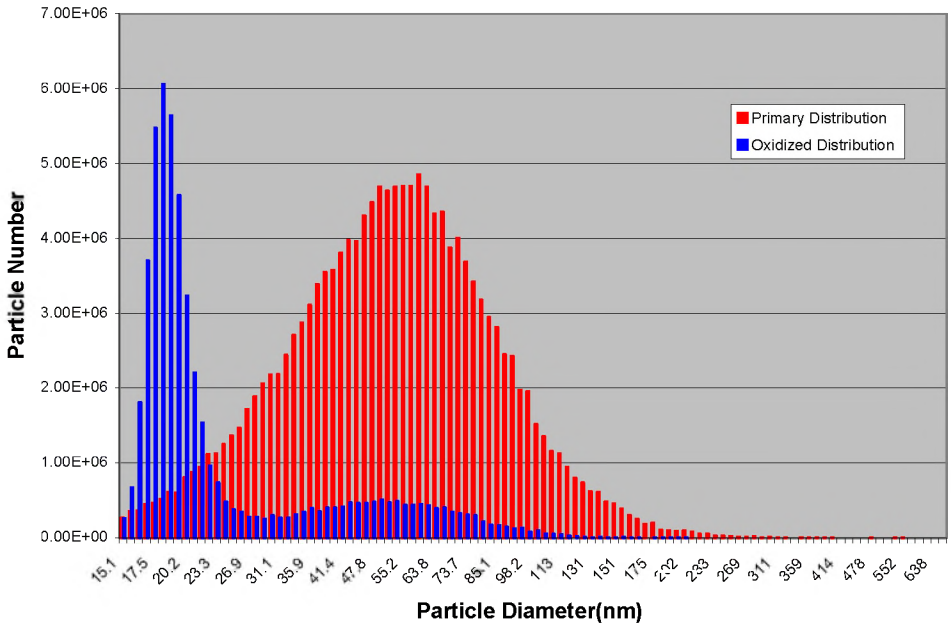

Figure 30. Fuel-lean oxidation results.

Figure 30 shows that a significant fragmentation peak was generated, most likely the result of large aggregates burning and fragmenting. The mean particle diameter for the smaller particles is on the order of 19 nm, typical of the size of primary particles in soot aggregates, and the number of particles is significantly higher than the larger particle peak which occurs around 55 nm. In this case, oxygen was the primary oxidant. It is hypothesized that oxygen diffuses into the soot aggregate, as opposed to OH, which is believed to only be involved in surface oxidation leading to the disintegration of the bridges between particles. The extent of burnout for the fuel-lean runs was 84%.

Later experiments explored the effect of temperature on oxidation by diluting the secondary flame with nitrogen to lower the temperature. Temperature measurements were carried out with type R fine gage thermocouples. Three thermocouples with diameters of 0.003 in., 0.008 in., and 0.015 in. were used. Flame temperatures were measured with each thermocouple then extrapolated to a zero diameter bead, which gives the radiation-corrected temperature of the flame. Soot oxidation experiments were carried out at temperatures of 1250 K, 1296 K and 1336 K. Three runs were carried out for each temperature. The particle size distribution measurements from these experiments are shown in Figure 31.

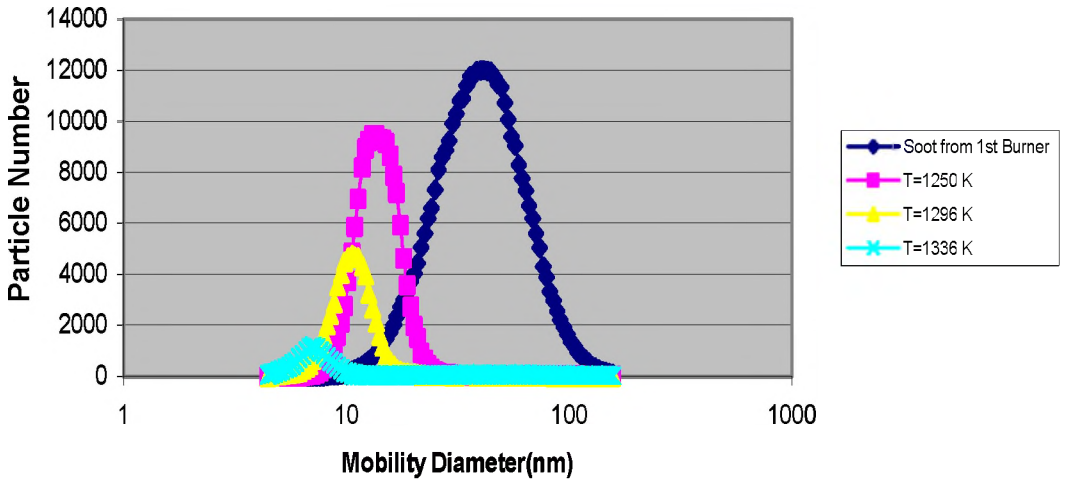

Figure 31. Effect of temperature on fuel-rich soot oxidation as a function of temperature for H_2/CO oxidation, $\phi = 1.2$.

Without exception, the particle number and average diameter decreased with oxidation as the temperature increased. Under fuel-rich conditions, the oxidant of interest is OH radical which decreases the diameter of soot particles by surface oxidation. The soot particle distribution from the first burner had an average diameter of 43.6 nm. The average diameter of the oxidized soot size distributions was 13.1, 11.4 and 7.1 nm for 1250 K, 1296 K and 1336 K, respectively. The soot mass burnout ranged from 98 % at 1250 K to 99.5% at 1336 K. Using the oxidized mass, the calculated surface area of the soot and the residence time in the oxidation zone, soot oxidation rates were calculated for all three temperatures and were compared to those predicted by the Neoh hydroxyl oxidation equation (Neoh, 1981), as shown in Figure 32.

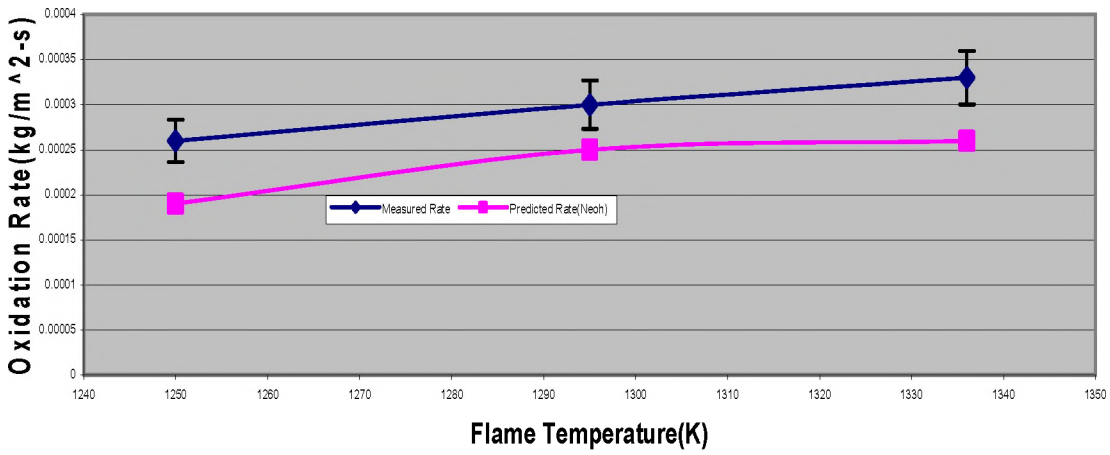

Figure 32. Comparison of measured and predicted soot oxidation rates.

For calculation of rates predicted by the Neoh equation, a collision efficiency of 0.28 was used and OH concentrations were calculated using the PREMIX code. The values for the oxidation rates are very close to those of Neoh and follow the trend of Neoh's equation, but are higher for every temperature. A critical aspect of this research is to be able to calculate collision efficiencies for OH radical. The value of the collision efficiency is the fraction of successful reactions that occur with OH collides with a soot particle and this value should be independent of temperature. Collision efficiencies were calculated for all 3 temperatures and were found to be 0.41 for 1336 K, 0.38 for 1295 K, and 0.37 for 1250 K. These values are slightly higher than those calculated in Neoh's oxidation flame. However, she was using a different fuel, higher temperatures and had a higher degree of scatter in the data than was found in the experimental data of this work.

The University of Utah team acquired a fuel vaporizer from Mesoscopic, Inc. The vaporizer is capable of producing fuel flowrates of 0.05 – 0.5 ml/min. In order to verify that the vaporization process does not chemically alter the fuel (either through catalyzed/thermal chemical reactions or preferential vaporization of some compounds),

vaporized fuel was captured in a solvent impinger and analyzed by gas chromatography. The vaporized fuel was found to be identical to the original fuel.

The Mesoscopic Inc. vaporizer was incorporated into the 2-stage premixed flat-flame experiment. First, the vaporizer and a gas preheat system were mounted to the existing "tube-bundle" stage for testing. The use of the "tube bundle" (as opposed to a sintered metal disk) is intended to reduce the possibility of fuel vapor condensation and reaction on the burner surface. The air preheating system, maintained at 300 °C, is an additional measure to prevent fuel condensation inside the burner. This assembly was tested at a variety of flowrates and equivalence ratios, and successfully established a uniform premixed flame of air and JP-8.

In addition, a new burner plenum and chimney were manufactured, to replace the existing sintered disk burner that has been used as the first stage of the 2-stage system. Figure 33 shows photographs of the apparatus.

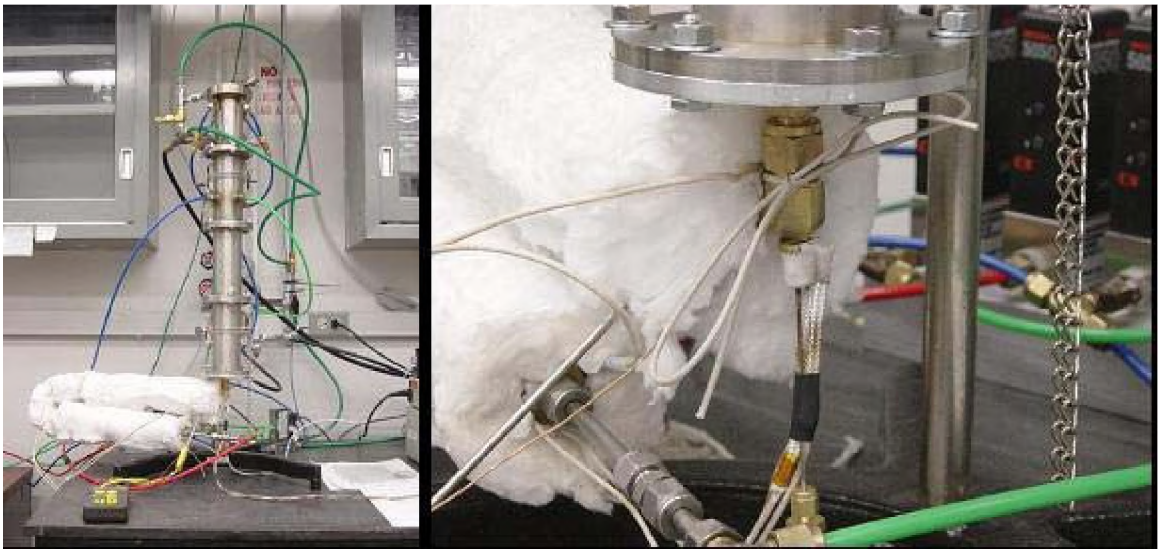

a) b)

Figure 33. a) The vaporizer, burner plenum, and chimney assembly. The insulated portion is the air pre-heater. b) Close-up of the fuel vaporizer

After several hours of use, the Mesoscopic Inc. vaporizer ceased to function, behaving as if it were clogged internally. The unit was returned to the manufacturer for cleaning, but was determined to be irreparable. The manufacturer indicates that they expect a lifetime of more than 500 hours. Disassembly of the unit by the manufacturer has led to more questions than answers. The biggest surprise is that the vaporizer came back with virtually no copper foam in the unit. There was clogging at the end of the inlet tube, where it enters the body of the vaporizer. This appeared to be from oxidation of the brass body and/or from the copper foam but it did not completely block the passage.

5.2.3 Additives in the Two-Stage Burner

Due to these problems with the vaporizer, no liquid fuels were run in the two-stage burner. The results below examine the effects of additives on ethylene flames. Soot formed from an ethylene flame is not expected to be appreciably different from soot formed in a JP-8 flame. Therefore we expect the additive results found for ethylene flames in the two-stage burner to be applicable to JP-8 combustion also.

In all cases, we compare the PSDs, with and without additives, from the second flame. (Other experiments with this setup have compared PSDs from the first flame to the second flame.) The additives evaluated are the organo-metallic additive ferrocene and the oxygenated additive 2-ethyl-hexyl nitrate. To introduce the additives into the flame, the air stream is sent into a heated glass flask containing the liquid additive. As the air passes through the flask, the air is saturated with the additive vapor. This saturated air is then mixed with the fuel (ethylene) prior to entering the burner. All of the plumbing involved in delivering the fuel and air to the burner is maintained at 100 °C by electrical heating. This temperature is well above that of the flask where the additive vapor is

produced, so the additive does not condense out of the gas before reaching the first flame. Concentrations were calibrated by sending the saturated air through a solvent bubbler, then quantifying the ferrocene in the solvent (dichloromethane) by gas chromatograph. Table 1 summarizes the experimental air and fuel flow rates. Table 2 gives the iron content for the experimental runs.

Table 1. Experimental conditions for additive experiments in the two-stage burner.

		First burner	Second burner
ϕ (Equivalence ratio)	Ethylene (lpm)	Air (lpm)	Air (lpm)
1.5	0.78	4.8	4.3
1.2	0.78	4.8	6.3
0.9	0.78	4.8	8.3

Table 2. Iron (Fe) content for the experimental runs.

Glass flask Temperature (C)	Ferrocene feed rate (mg/min)	Fe content (ppm) in ethylene
30	0.644	220
33	0.985	300
40	1.98	680
50	3.43	1180

5.2.3.1 Ferrocene The PSDs for overall equivalence ratios of 1.2 and 0.9 are shown in Figures 34 and 35 respectively. The results are presented as $dM/d\log D_p$ (units of micrograms/m^3) as a function of particle diameter D_p (nm).

In Figure 34, the peak particle diameter with no additive is 82 nm. The peak particle diameter for Fe concentrations 220, 300, 680 and 1180 ppm are 50, 37, 40 and 49 nm respectively. In other words, there is a smaller average diameter when ferrocene is present at any concentration. The smallest reduction in particle diameter corresponds to 220 ppm, suggesting that this concentration is lower than optimal; higher concentrations of iron result in larger reductions in peak diameter. However, at 680 and 1180 ppm the

peak particle diameter is somewhat larger than at 300 ppm. We suspect that in addition to soot particles, iron oxide particles are also present, which could contribute to the larger diameters. This is supported by the fact that the mass of particles (determined by assuming a particle density of 1.2 g/cc) produced is much larger at Fe concentrations above 300 ppm. We also observe the presence of iron oxide (orange deposits) on the burner and sampling probe (see Figure 36).

Figure 34 presents the results at an equivalence ratio of 0.9. In this case, the peak particle diameter with no additive is 98 nm. The peak particle diameter for iron concentrations of 220, 300, 680 and 1180 ppm are 22, 26, 33 and 43 nm respectively. Thus we observe the same trends discussed above for the rich second flame: although there is a significant reduction in particle diameter when ferrocene is used, the diameter and the mass of particles both increase with higher Fe concentrations, which can be explained by the presence of iron particles in the exhaust stream.

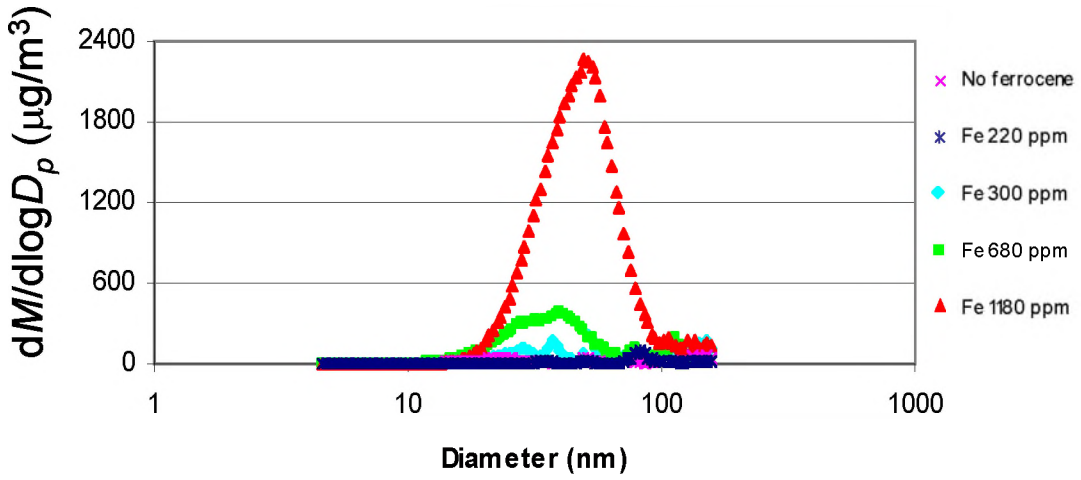

Figure 34. PSDs observed in the rich second flame.

Figure 35. Second-stage burner (left) and sampling probe (right), showing iron oxide deposition.

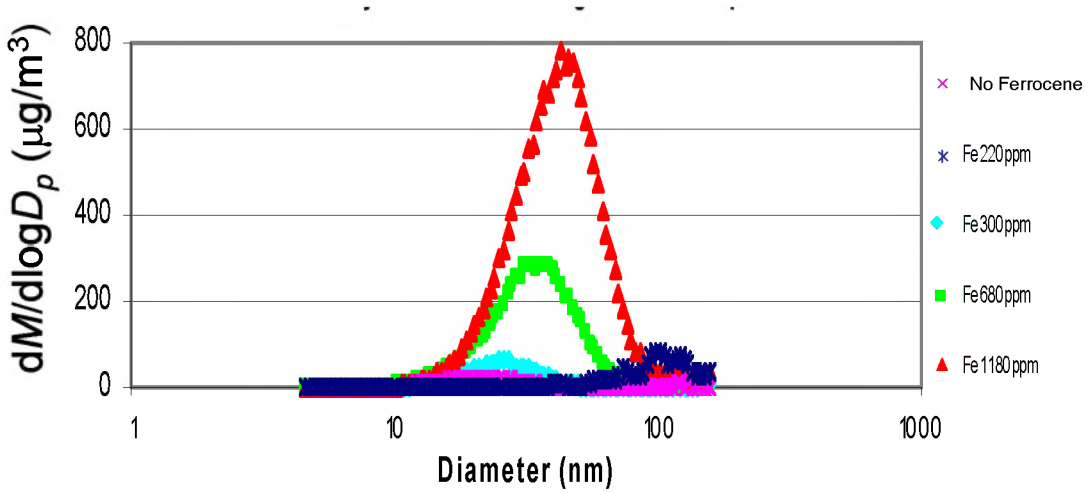

Figure 36. PSDs observed in the lean second flame.

Figure 37 compares the experiments without additive and 300 ppm Fe content. At fuel rich conditions (ϕ = 1.5) a slight reduction in peak particle diameter is observed when the additive is used (152 nm vs. 122 nm). It is not clear whether this change is the result of a small degree of oxidation or simply an artifact of iron particles that are slightly smaller on average than the soot particles. On the other hand, at fuel lean conditions, there is a significant decrease in both peak diameter and particle mass when ferrocene is added at 300 ppm.

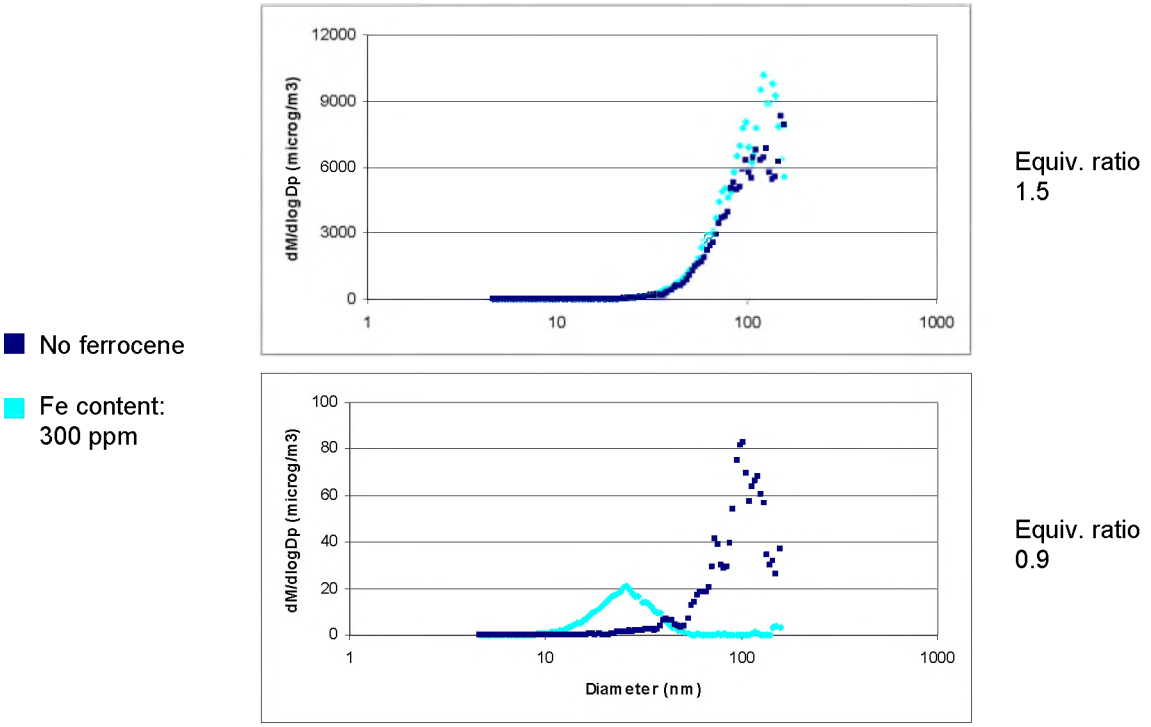

Figure 37. PSDs observed under rich and lean conditions with 300 ppm iron.

5.2.3.2 2-ethyl-hexyl nitrate Figure 38 shows the PSDs found when 2-ethyl-hexyl nitrate is added at 6000 ppm, the vapor concentration achieved at room temperature for our setup. Under fuel rich conditions (1.5 equivalence ratio) a change in particle diameter is not detected (95 nm in both situations, with and without additive) and the mass of particles produced is slightly larger with the additive. At 1.2 equivalence ratio, there is a considerable reduction in particle size distribution when the additive is used. The peak diameter decreases to 37 nm (vs. 98 nm without the additive) and the mass of particles produced is also much lower. Under fuel lean conditions, the addition of 2-ethyl-hexyl nitrate results in particle counts below the detection limit of the instrument, so no particle size distributions could be measured.

The results obtained for the nitrate additive are consistent with those obtained in the drop tube experiments for the oxygenated additives. In some situations at fuel rich

conditions the oxygenated additives increased the soot production, but as the system went to more fuel lean conditions the soot reduction was more significant.

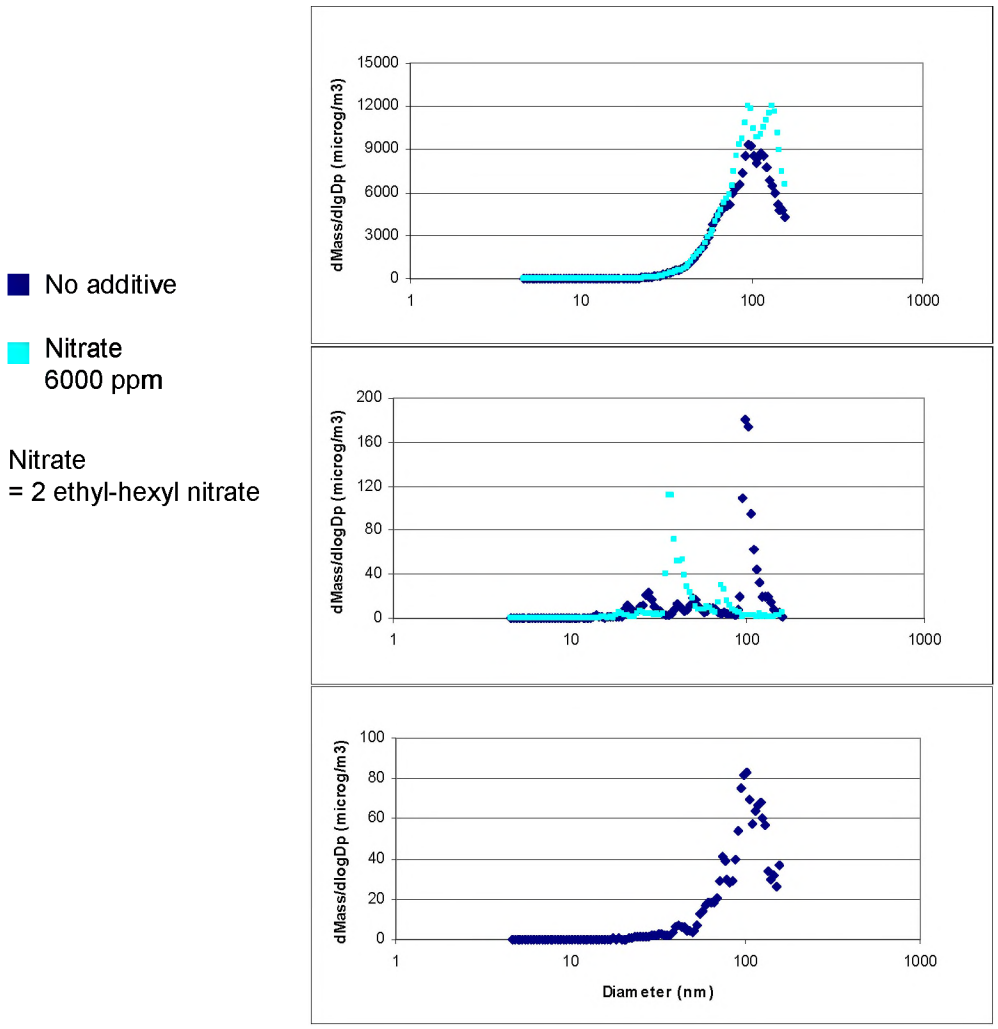

Figure 38. PSDs observed under rich and lean conditions with 6000 ppm nitrate.

5.3 Small Gas Turbine Engine

During the project REI purchased a US Aviation Microjet Technology AT-400 gas turbine engine and associated hardware and software. Support hardware, including a computer, was contributed by the University of Utah.

5.3.1 Apparatus Description

The AMT-400 turbine is housed in an up-right rectangular enclosure measuring 6 ft × 4 ft × 3 ft. The enclosure is constructed from 1.5 in angle iron and divided into an upper section, containing the turbine, and a bottom section containing electronic controls and start-up equipment. For safety, the top section is enclosed with 0.5 inch thick polycarbonate plate. Mounting brackets have been attached to the air intake side of the frame to allow filters to be attached. Two fuel tanks are mounted to the base of the top section to allow for separate starting and shutdown fuel (containing lubricant) and testing fuel (containing additive). The enclosure is illustrated in Figure 39.

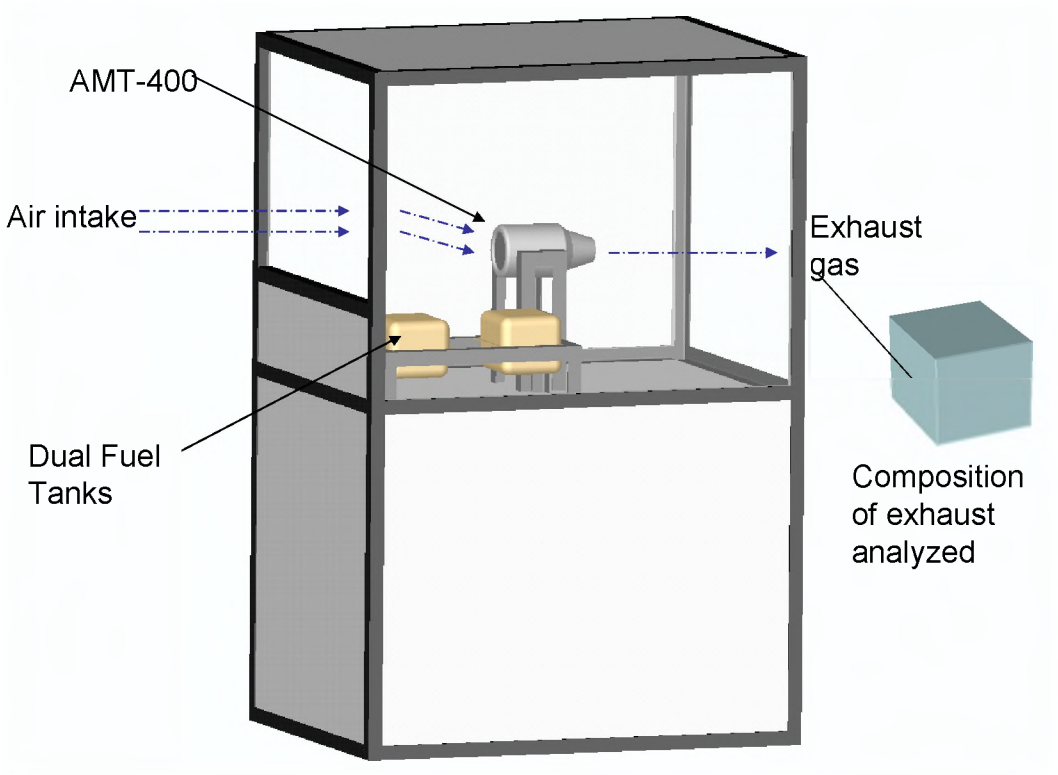

Figure 39. Illustration of the AMT-400 gas turbine engine enclosure.

The exhaust is sampled 3 inches from the exhaust exit plane via a ¼ inch stainless steel tube. Steady sample flow is accomplished with an eductor assembly that pulls the exhaust through a critical orifice. The short sample tube length minimizes thermophoretic

losses prior to dilution with the motive air in the eductor. The diluted sample is introduced into a manifold, where black carbon and particle size number and distribution are measured. Black carbon is measured with a photoacoustic analyzer, particle number and size distribution are measured with a TSI scanning mobility particle sizer. The PM 10 is measured on a mass basis with a laser photometer (TSI model 8520 DustTrak).

Testing of various jet fuel additives was performed at the University of Utah in the fall of 2005. Standard operating procedure for the engine is to run fuel with a 5% mixture of Aeroshell 500™ turbine lubricant. The lubricant component provides residual lubricant upon shutdown to the front and rear bearings. The fuel evaporates in the hot bearing casings upon shutdown, but the lubricant remains. A small fraction of the fuel pumped to the engine is split off to the bearing casings. This small split flows though the bearings and lubricates during steady state operation. The engine bearings are not sealed. In an effort to eliminate interactions between the fuel additive under study and the Aeroshell 500 lubricant, the engine is started up on the fuel/lubricant mixture and then switched (with a three way valve) to the test fuel. After testing, the fuel is switched back to the Aeroshell 500 mixture and the engine is shut down.

A problem arose during testing that made data collection problematic. The manufacturer's claim that the fuel split to the bearings is routed to the combustor section and burned appears to be wrong. Black carbon, as measured with a photoacoustic analyzer, was consistently very low, when compared to overall particle counts from a PM 10 monitor and a TSI scanning mobility particle sizer (SMPS). In the course of several conversations with the engine designer, the fate of the fuel split used for bearing lubrication was discussed. This fuel split is not burned, as was claimed initially by the

manufacturer. The lubrication fuel exits the bearing casings after the combustor and is entrained into the exhaust. The unburned fuel in the exhaust is atomized.

The atomized fuel in the sample accounts for the high particle counts. The inordinately low black carbon levels could be a result of interactions with the atomized fuel. Further investigations should be conducted to eliminate this effect. The inability to gather valid data on the AMT 400 leads to the larger issue of the effects of unburned fuel on data from larger scale engines that have sealed bearings. While the masking effect of atomized fuel in the exhaust of the AMT 400 is exaggerated, the same effect could result in inaccurate data on sealed bearing engines burning under inefficient conditions. Options for eliminating the effect of atomized fuel include using thermal denuder technologies to selectively eliminate the liquid phase fuel in the exhaust prior to analysis.

Diluting the sample in conjunction with a thermal denuder could keep the remaining hydrocarbons in vapor phase, reducing the interference effects.

5.3.2 AMT 400 Jet Engine Results

Tests were performed in the AMT 400 engine on four additives: ferrocene, tert-butyl peroxide and two commercial products: Plus 100 and PA 5. Baseline tests were also run for the fuel with the 5% Aeroshell 500 lubricant and fuel with no additive or lubricant. In all cases, the base fuel is Jet A fuel drawn from the same 50 gallon barrel. The tests were typically conducted by starting the engine on Jet A with Aeroshell 500, throttling to the test rpm and running for approximately two minutes before switching over to the test fuel. Once the instruments indicated the emissions were at steady state, data was logged for 20 minutes. The fuel was then switched over to the Jet A/Aeroshell

500 mixture for five minutes before shutting the engine down. Each fuel was tested at 30,000 and 50,000 rpm. The fuels tested and values for back carbon and PM 10 are summarized in Table 3.

Table 3. Black Carbon and PM 10 for Tested Fuels.

Additive	Concentration	Engine rpm	Black carbon ($\mu g/m^3$)	PM 10 ($\mu g/m^3$)
Aeroshell 500	5% by volume	30,000	4562	84.74
Aeroshell 500	5% by volume	50,000	10,359	100.13
none	n/a	30,000	31,488	131.48
none	n/a	50,000	43,972	324.9
ferrocene	300 ppm*	30,000	22,383	115.71
ferrocene	300 ppm*	50,000	35,444	212.8
tert-butyl peroxide	1000 ppm	30,000	29,123	174.42
tert-butyl peroxide	1000 ppm	50,000	39,628	298.3
tert-butyl peroxide	3000 ppm	30,000	23,526	133.19
tert-butyl peroxide	3000 ppm	50,000	40,061	296.4
Plus 100	256 ppm	30,000	31,985	186.77
Plus 100	256 ppm	50,000	47,631	427.5
Plus 100	1000 ppm	30,000	31,728	141.36
Plus 100	1000 ppm	50,000	45,704	315.4
PA 5	1000 ppm	30,000	30,822	122.36
PA 5	1000 ppm	50,000	44,751	273.6
PA 5	3000 ppm	30,000	25,522	124.64
PA 5	3000 ppm	50,000	47,857	292.6

*Concentration of iron.

Gas phase data logged included O_2, CO_2, CO, and NO_x. Particulate emissions data were recorded for real time black carbon, PM 10 and particle size distribution from 14 nm-673 nm. PM 2.5 was not measured, but based on previous experience the mass loadings fall heavily in the small (<1 nm) size range so the PM 10 measurements reported here are likely very similar to PM 2.5 measurements. The CO and CO_2 were measured with a California Analytical non-dispersive infrared analyzer. The O_2 analyzer was a

Yokagawa™ zirconia oxide analyzer and the NO_x is a Thermoelectron chemiluminescent analyzer. Real time black carbon was measured with a prototype photoacoustic analyzer. PM 10 is monitored with a TSI model 8520 DustTrak and particle size distributions are generated with a TSI scanning mobility particle sizer. The photoacoustic analyzer, used for real time measurements of black carbon, is a laser based instrument that directs a laser through a volume of airborne sample. The black carbon in the sample is heated by the laser, expanding the gas around the carbon particle. This thermal expansion is translated into an acoustic signal that is detected with sensitive microphones. In this manner, the black carbon is measured real time on a mass basis. Black carbon results are shown in Figure 40. PM 10 measurements are given in Figure 41.

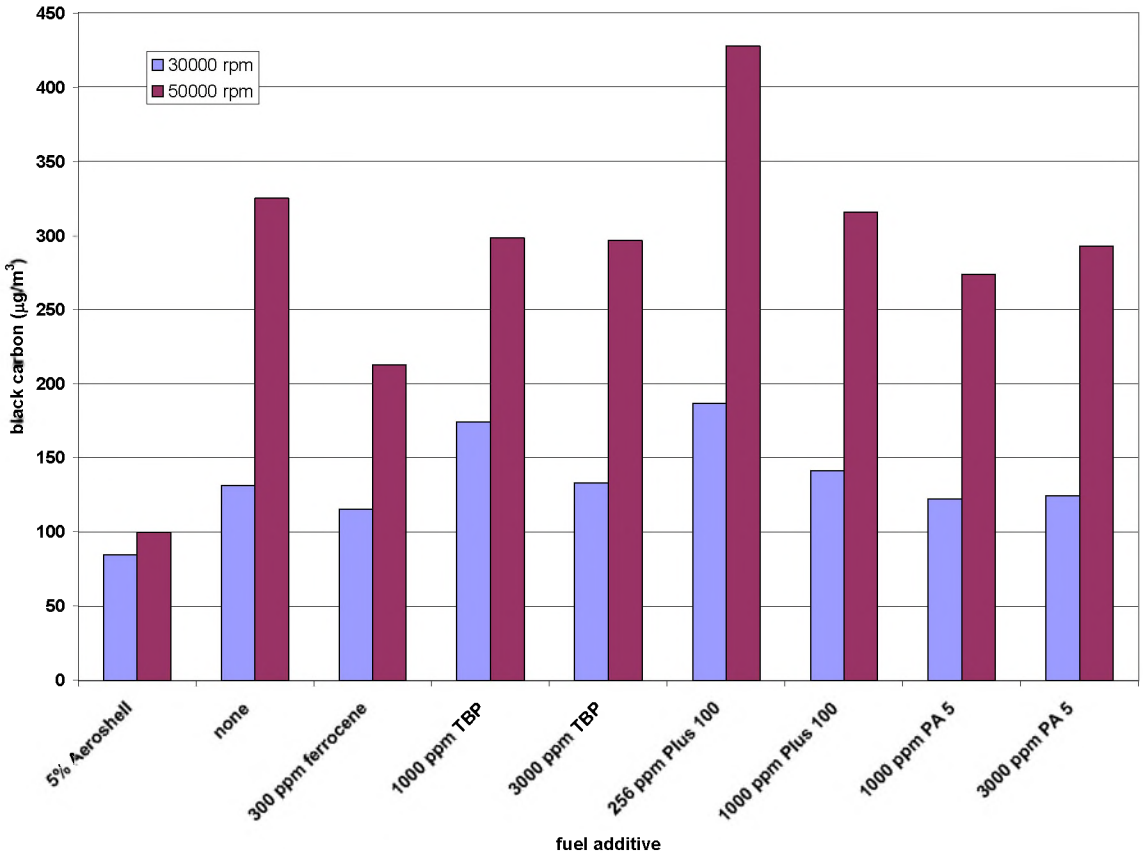

Figure 40. Measured black carbon for various fuels.

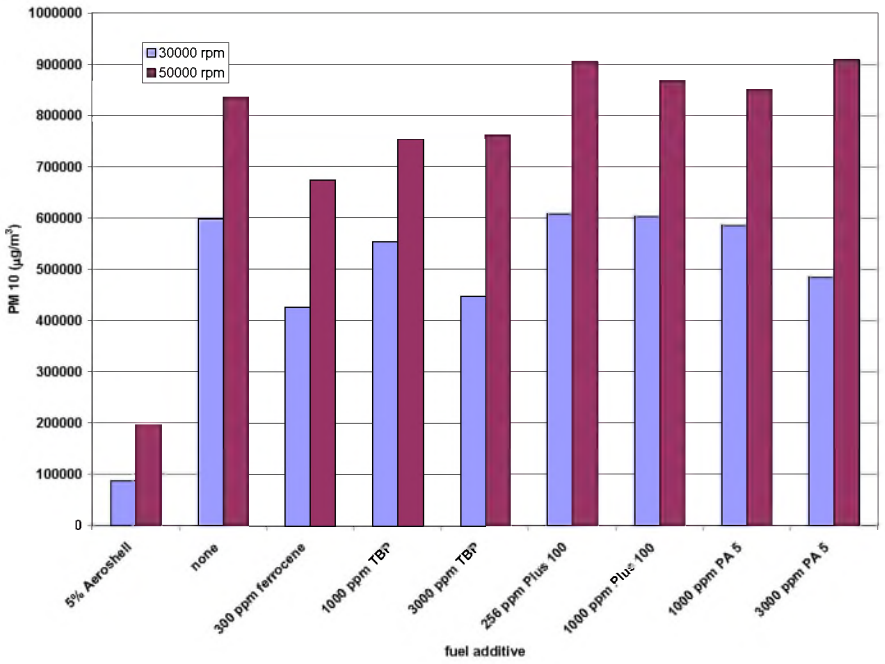

Figure 41. Measured PM 10 for various fuels.

The atomized fuel in the sample accounts for the high particle counts. The inordinately low black carbon levels could be a result of interactions with the atomized fuel.

This problem leads to the larger issue of the effects of unburned fuel on data from larger scale engines that have sealed bearings. While the masking effect of atomized fuel in the exhaust of the AMT 400 is exaggerated, the same effect could result in inaccurate data on sealed bearing engines burning under inefficient conditions. Options for eliminating the effect of atomized fuel include using a thermal denuder to selectively eliminate the liquid phase fuel in the exhaust prior to analysis. Diluting the sample in conjunction with a thermal denuder could keep the remaining hydrocarbons in vapor phase, reducing the interference effects. Eliminating both the photoacoustic analyzer and PM 10 monitor in favor of gravimetric measurements of black carbon and PM 10 could also mitigate the problem of the fuel aerosol in the exhaust. Sampling through a heated

sample line and filter assembly, to keep the atomized fuel in the vapor phase would provide a gravimetric means of determining the mass of black carbon generated per unit of run time. Alternatively, the current battery of real time instruments could be used by using denuders, specific to the jet fuel, to eliminate hydrocarbons prior to the instruments. Such a method, if applicable, would be checked with a hydrocarbon analyzer to validate efficiency.

6. Numerical Modeling

This section describes efforts to better understand the effects of additives on soot emissions through numerical modeling. Efforts were focused in three areas:

- Soot particle dynamics modeling,
- Chemical kinetics of additives
- CFD Simulation

The following subsections describe our efforts in these three areas.

6.1 Soot Particle Dynamics Modeling

Two different approaches to modeling soot particle dynamics modeling were evaluated during this project- a sectional soot model and the method of moments..

The first method was a sectional soot model which integrates the aerosol dynamics equations using a discrete size spectrum with particle inception, surface growth, oxidation, and coalescence terms. The soot particle size range of interest is divided into discrete intervals or classes with a logarithmic transformation of the size range, as shown in Figure 42. The model was coupled with REI's proprietary gas kinetics solver, REKS, to model soot formation in Plug Flow Reactor (PFR) cases for rich ethylene-air combustion.

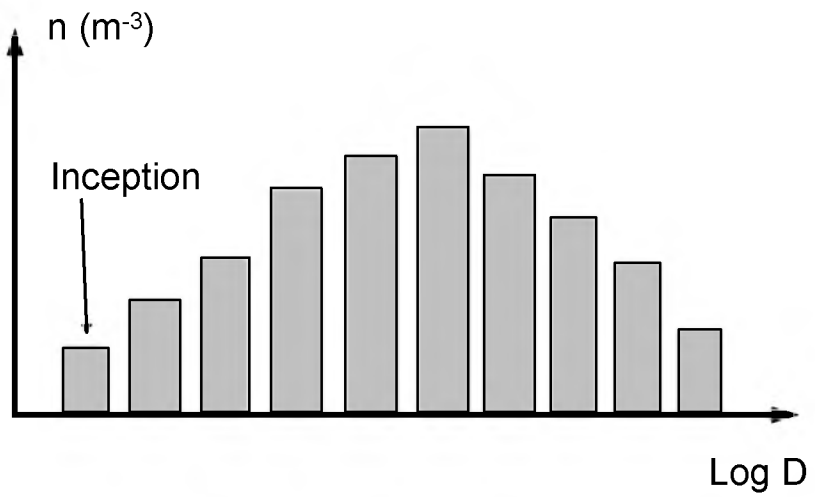

Figure 42. Discretization of the soot size spectrum.

The change of particle number concentrations *n*, due to coagulation, is given by:

$$\left.\frac{\mathrm{d}n_i}{\mathrm{d}t}\right|_{vj} = \left.\frac{\mathrm{d}n_j}{\mathrm{d}t}\right|_{vi} = -\left.\frac{\mathrm{d}n_k}{\mathrm{d}t}\right|_{vi,vj} = -C_{ij}n_i n_j \qquad \text{(Eqn. 1)}$$

where *i, j,* and *k* are bin indices and *v* is the bin volume. C_{ij} is the collision frequency between particles in bins *i* and *j*, which is calculated using the method of Fuchs (1964).

The growth algorithm was devised by Dr. Montgomery. It preserves numbers when there is growth but no inception or coagulation and always conserves mass. The change in particle number in a given size bin is given by Equation 2 and illustrated in Figure 43. The growth term, *G*, comes from the gas phase chemistry and is calculated by the Hydrogen Abstraction C_2H_2 Addition (HACA) mechanism (Frenklach & Wang, 1990; Appel et al., 2000).

$$\frac{dn_i}{dt} = \frac{G}{\rho_p}\left(\underbrace{\frac{a_{i-1}n_{i-1}}{v_i - v_{i-1}}}_{\text{Gain from smaller size}} - \underbrace{\frac{a_i n_i}{v_{i+1} - v_i}}_{\text{Loss to larger size}}\right) + C \qquad G > 0,\ 1 < i < M \qquad \text{(Eqn. 2)}$$

where

n_i is the number density for size bin i (particles/m^3),

a_i is the particle area for size bin i (m^2),

v_i is the particle volume for size bin i (m^3),

G is the surface growth rate from HACA (kg/m^2·s),

ρ_p is the soot particle density (kg/m^3),

C is the coagulation rate (particles/m^3·s), and

M is the number of size bins.

Equation 2 is for net positive particle growth. If particles are shrinking, as in an oxidizing environment then some minor rearrangements are needed to Equation 2. The smallest bin has a source term from the gas-phase chemistry for inception replacing the term representing gain from a smaller bin size. The largest bin does not have a sink term for loss to a larger size so the bin range needs to be large enough that significant mass does not build up in the largest bin.

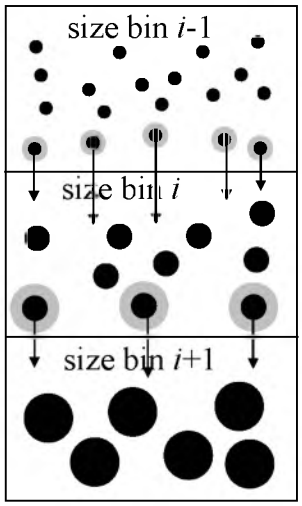

Figure 43. Illustration of surface growth dynamics in the sectional method.

The entire sectional soot algorithm was integrated into REI's REKS kinetics solver. The gas-phase chemistry and sectional equations are fully coupled and integrated

simultaneously using the stiff numerical integrator CVODE. The sectional soot model was implemented only for a constant-temperature plug flow reactor. Figures 44 and 45 show particle size distributions calculated using the sectional method, with Figure 44 showing only the smallest part of the distribution. The particle size distributions are from a run using 80 sections to resolve the PSD better. The total soot volume only changes a few percent when changing from 20 to 80 sections.

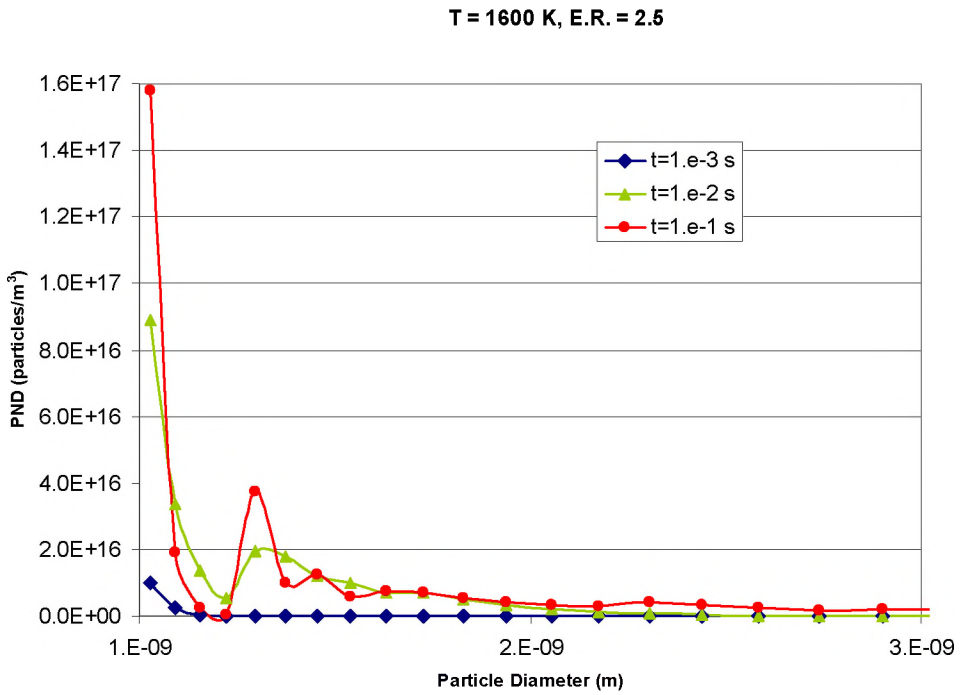

Figure 44. Particle Size Distributions from Sectional soot model for ethylene-air combustion for T = 1600 K, equivalence ratio of 2.5 and P = 1 atm after an integration time of 0.01 s.

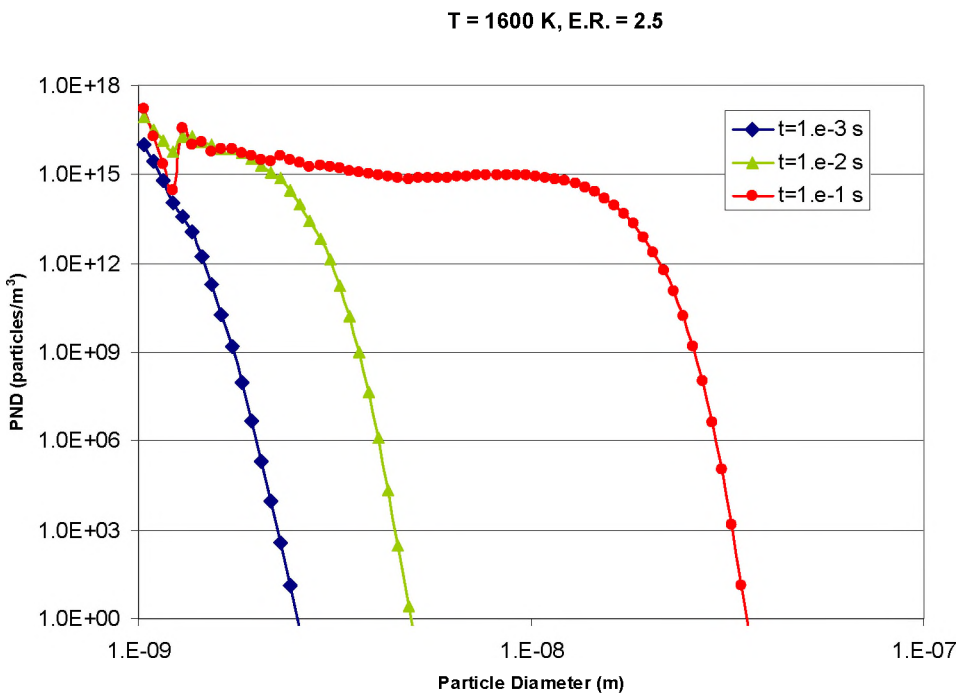

Figure 45. Same as Figure 44 but in log-log form.

The sectional soot model that was implemented as part of this project has been compared to the second method of interest in the project, the Method of Moments (MoM) soot model (Frenklach & Wang, 1990; Appel et al., 2000) as implemented by Frenklach in a commonly used kinetics code. The MoM model calculates six statistical moments of the soot particle size distribution, from which other quantities of interest can be derived. The model couples to the gas-phase chemistry through particle inception, surface growth and oxidation models.

All of these comparisons use the same gas-phase kinetics (Appel et al., 2000). The sectional code uses the coagulation algorithm of Jiang (2003) (translated by REI from Matlab to C++). Soot inception is the rate of A4 (pyrene) dimerization (as in the MoM code). Growth is by the HACA scheme, rates again the same as Frenklach's MoM code. The oxidation rates are also the same as in Frenklach's code.

Results for ethylene-air combustion at 1 atm are shown in Figures 46-48. Overall, the agreement was quite good – well within the uncertainties in the model parameters. The comparisons with MoM use 20 sections with a diameter ratio of about 1.25.

The MoM code runs about 20 times faster. The slowdown in the sectional method seems to come not so much from integrating the additional equations, but because the sectional model makes the gas-phase chemistry stiffer (i.e. the system contains very small time scales requiring very small timesteps and a great deal of cpu time to perform the integration).

The sectional code is identical in gas-phase and surface chemistry to the MoM code except that the MoM code includes PAH condensation. This may be why the sectional code predicts less soot under high soot conditions. The reasons that the sectional method predicts more soot at the high and low temperature ends of the soot dome are not presently understood.

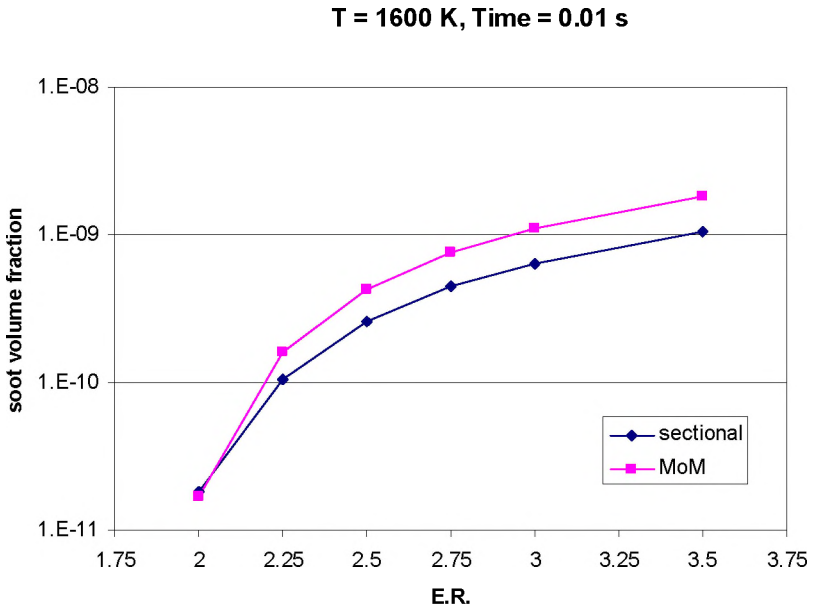

Figure 46. Comparison of Sectional and Method of Moments (MoM) soot models for ethylene-air combustion at T = 1600 K and P = 1 atm. as a function of Equivalence Ratio (E.R.). The integration time is 0.01 s.

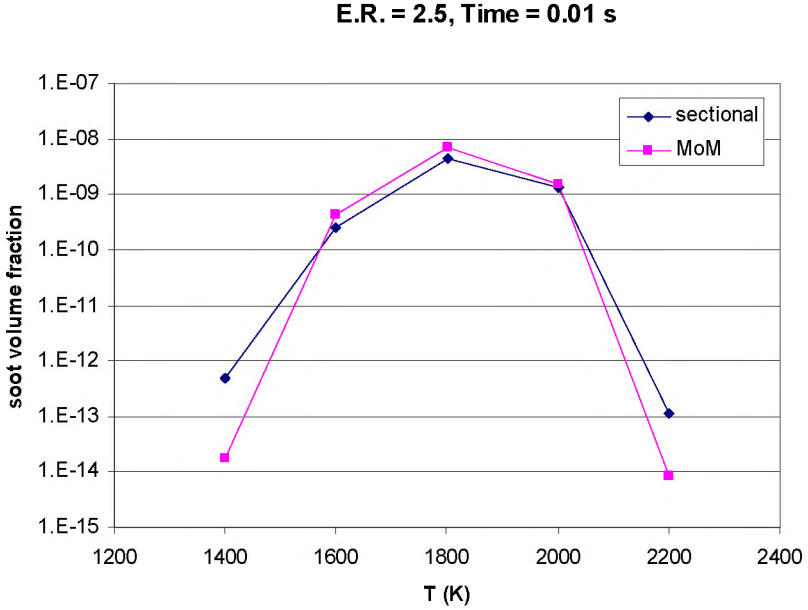

Figure 47. Comparison of Sectional and Method of Moments (MoM) soot models for ethylene-air combustion at an equivalence ratio of 2.5 and P = 1 atm. as a function of temperature. The integration time is 0.01 s.

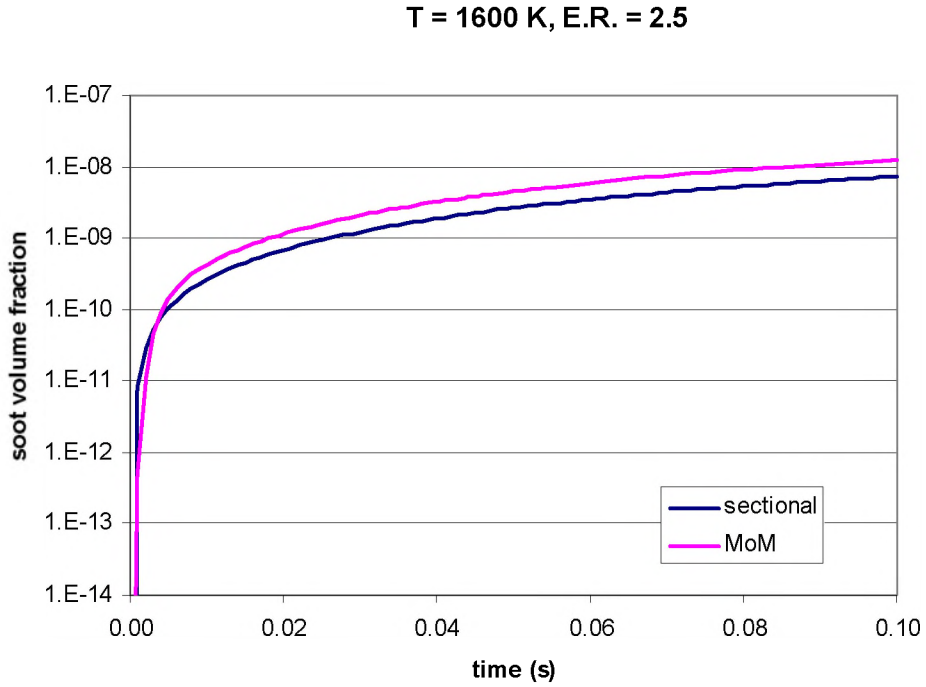

Figure 48. Comparison of Sectional and Method of Moments (MoM) soot models for ethylene-air combustion for T = 1600 K, equivalence ratio of 2.5 and P = 1 atm. as a function of time.

Because of its considerable speed advantage, the Method of Moments (MoM) soot model (Frenklach et al. 1990, Appel et al. 2000) was chosen for use in this project and was implemented into REI's in-house kinetics solver REKS. The integrated JP-8 combustion and soot model can be run for plug flow reactor (PFR) and perfectly stirred reactor (PSR) cases. The augmented REKS code can now run plug flow reactor (PFR) cases either for fixed temperature and pressure or for fixed enthalpy and pressure. We can also run perfectly stirred reactor (PSR) cases for fixed temperature and pressure or for fixed pressure and specified heat loss. A new solution procedure was implemented for the PSR code in which it first solves for gas-phase equilibrium, then finds a gas-only solution, followed by a fully coupled gas-soot solution to the PSR equations. Both the PSR and PFR codes are very fast and robust.

The REKS-MoM code was modified to work with the state-of-the-art JP-8 mechanism of Zhang (2005). Since the Zhang mechanism does not track pyrene, acenaphthylene ($C_{10}H_7CCH$), a major PAH species, was used as the dimerization species for soot particle inception using the same rate as for pyrene dimerization with Frenklach's ethylene model.

We have compared the soot producing tendency of several hydrocarbons in a stirred reactor as calculated with the Zhang (2005) mechanism and the MoM soot model with the experimental results of Wright (1968). Wright reported the critical O/C ratio for soot formation in a well-stirred reactor for a number of compounds. Because the model predicts smoothly varying soot production with changing equivalence ratio it is difficult to define a critical O/C ratio from the model. However, we used Wright's results to qualitatively rank the soot producing tendency of hydrocarbon fuels. Figure 49 plots

Wright's critical sooting O/C ratio vs. the soot volume fraction calculated for a PSR with a residence time of 0.1 sec, and equivalence ratio of 2.0, a temperature of 1600 K at 1.0 atm. Overall, the correlation was quite good, giving us some confidence that the model can predict sooting tendencies based on the chemical characteristics of fuels. Results for the JP-8 + MoM soot model are shown in Section 6.3.

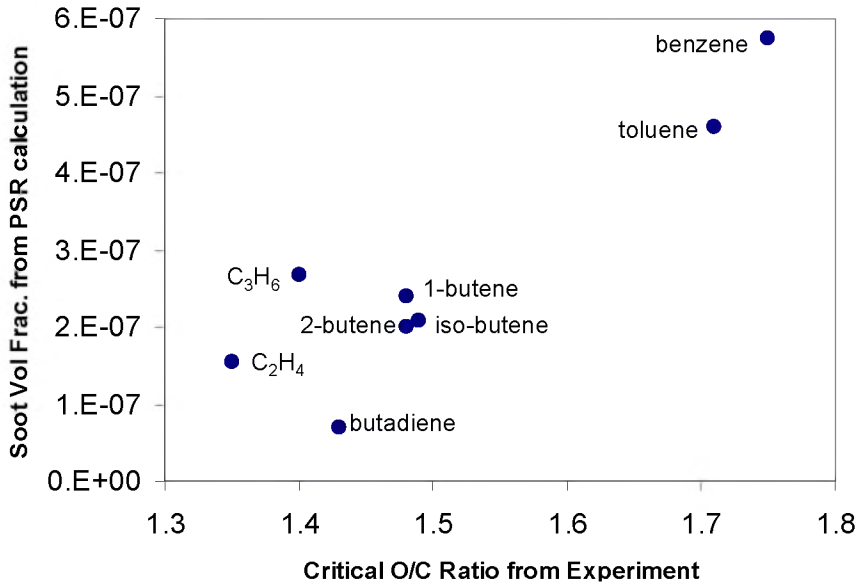

Figure 49. Comparison of the measured critical sooting O/C ratio (Wright, 1968) vs. the soot volume fraction calculated for a PSR with a residence time of 0.1 s, and equivalence ratio of 2.0, a temperature of 1600 K at P = 1.0 atm.

6.2 Additive Kinetics

A study on the thermochemistry and kinetics relating to the initial chemistry of di-tertbutyl peroxide and nitro-hydrocarbons is presented below. These two compounds have been shown experimentally to alter both gas-phase combustion and soot production. They act through very different chemical pathways so insight can be gained into differing ways of affecting soot production with additives.

A modeling effort was undertaken to understand the effects of additives on soot production. The action of oxidation catalysts such as the metal-containing additives can presently only be modeled empirically. Additives that act in the gas phase, however, can be modeled with very high accuracy by chemical kinetic mechanisms that can be developed through *ab initio* and density functional calculations and other estimation techniques. Drop tube results indicated that nitro-hydrocarbons and di-tertbutyl peroxide (C_3COOCC_3, DTPB) reduce the amount of soot produced. However, mixed results have been seen in other laboratory tests and in engines. To help understand the action of DTBP, a detailed chemical kinetic mechanism for the gas-phase reactions of DTBP has been completed and integrated into the Zhang JP-8 mechanism.

With help from Professor Joseph Bozzelli, program consultant, new detailed kinetics for two additives, di-tert butyl peroxide and 2-ethyl-hexyl nitrate were developed. A thermochemical data set of enthalpy, entropy and heat capacity properties were developed for parent, transition state and intermediate reaction species in an elementary reaction mechanism for combustion and thermal oxidation of di-tert-butyl peroxide and 2 ethyl-hexyl-nitrate.

These mechanisms were integrated into the JP-8 mechanism of Zhang (2005) and tested in simple reactor simulations over a wide range of conditions coupled with Method of Moments model and in CFD simulations coupled with the simpler Lindstedt (1994) model.

Knowledge of the thermochemical data, reaction pathways and the kinetics allows a fundamental understanding of the ignition acceleration and the soot inhibition. This

initial analysis also provides a basis on further detailed, elementary reaction modeling of these systems for verification and further evaluation of the temperature, pressure and time regimes that are most important to achieve soot reduction.

6.2.1 Di-tert butyl peroxide

6.2.1.1 DTBP Kinetics Summary The O-O bond in DTBP is weak, with a bond energy of about 43.5 kcal/mol. At high temperatures, DTPB will dissociate quickly via simple bond scission to form two tertiary butoxy radicals. These butoxy radicals will undergo beta scission to form acetone and the CH_3 radical. Acetone will decompose at high temperatures to form two methyl radicals and CO or will react with the radical pool or O_2 to form an acetonyl radical. Further reactions of the acetonyl radical produce additional methyl radicals, O, and OH. DTBP may also react with the radical pool or O_2 to form hydrocarbon peroxide radicals. Further reactions of these radicals release energy and produce methyl, O, and OH radicals through chain-branching processes. All of these processes are represented by elementary reaction steps within the chemical kinetic mechanism.

Thus, DTBP can speed ignition by exothermically enhancing the radical pool. The enhanced radical pool can decrease soot production by speeding oxidation of soot precursor species and of the soot particles themselves. Decreasing the ignition time may increase or decrease soot production depending on the system. One possibility is that quicker ignition leaves less time for mixing of fuel and air, leading to more fuel-rich combustion conditions and thus more soot. Another possibility is that faster ignition increases the flame residence time available for combustion, leading to more complete soot burnout before the combustor exit.

6.2.1.2 Di-tert butyl peroxide kinetic mechanism details The RO-OR bond in hydrocarbon peroxide molecules is weak with a bond energy of only about 45 kcal/mol. This bond in the di-tertbutyl peroxides is a bit weaker than for normal hydrocarbons due to gauche interactions. At high temperatures di-tertbutyl peroxide will dissociate via simple bond scission to two tertiary butoxy radicals:

$$C_3CO\text{-}OCC_3 \rightarrow 2\ C_3CO\bullet \text{ radicals} \qquad \Delta Hrxn = +43.5.\ \text{kcal-mol}^{-1}$$

The tertbutyl alkoxy radicals $C_3CO\bullet$ will undergo unimolecular reaction via beta scission to acetone $CH_3(C{=}O)CH_3$ plus a methyl radical, $CH_3\bullet$.

$$C_3CO\bullet \rightarrow CH_3(C{=}O)CH_3 + CH_3\bullet$$

Reactions of the methyl radical are well described in standard combustion mechanisms. Acetone will decompose at high temperatures to two methyl radicals + carbon monoxide. Under normal combustion initiation the acetone molecule will react with the radical pool or molecular oxygen to form an acetonyl radical, $CH_2\bullet\ (C{=}O)CH_3$.

$$CH_3(C{=}O)CH_3 + X\bullet \rightarrow CH_2\bullet\text{-}C(=O)CH_3 + XH$$

where X• represents a radical (OH, O, HO_2, CH_3, etc.) or O_2.

The acetonyl radical will react via beta scission to form ketene, $CH_2{=}C{=}O$, and a methyl radical or react with molecular oxygen to form an acetone peroxy radical, CH2(OO•)C(=O)CH_3.

$$CH_2\bullet\text{-}C(=O)CH_3 \rightarrow CH2{=}C{=}O + CH3$$

or

$$CH_2\bullet\text{-}C(=O)CH_3 + O_2 \rightarrow CH_2(OO\bullet)C(=O)CH_3$$

Decomposition of the acetone peroxy radical leads to active species plus energy:

$$CH_2(OO\bullet)C(=O)CH_3 \rightarrow CH_2{=}C{=}O + CH_2{=}O + OH \qquad \Delta Hrxn = -25\ \text{kcal/mol.}$$

The reaction above occurs via intramolecular H shift:

$$CH_2(OO\bullet)C(=O)CH_3 \rightarrow CH_2(OOH)C(=O)CH_2\bullet \rightarrow CH_2=C=O + CH_2\bullet OOH$$

$CH_2\bullet OOH$ dissociates quickly with no barrier to lower energy products $CH_2=O + OH$:

$$CH_2\bullet OOH \rightarrow CH_2=O + OH \quad \Delta Hrxn = -40 \text{ kcal mol}^{-1}$$

Reactions of the di-tertbutyl peroxide with the radical pool At low and moderate temperatures the above bond scission reaction will compete with reactions between reaction of the parent C_3COOCC_3 with the radical pool (X•, where as above X• equals OH, H, CH_3, or HO_2) and with molecular oxygen (O_2). Reaction with the radical pool or with molecular oxygen generates a radical on a primary methyl ($-CH_3$) group of the di-tertbutyl peroxide. This reaction forms a hydrocarbon peroxide radical $C_3\bullet COOCC_3$. The radical site is on one of the three methyl groups of one tertbutyl moiety; but it can not be on the quaternary ($C/C_3/O$) central carbon of the tertbutyl group. These are conventional reactions of the radical pool with hydrocarbons and are common in combustion reaction mechanisms:

$$C_3COOCC_3 + X\bullet \rightarrow XH + C_3.COOCC_3$$

$$C_3COOCC_3 + O_2 \rightarrow HO_2 + C_3.COOCC_3$$

Reactions of di-tertbutyl peroxide alkyl radicals formed by reaction with X• or O_2 The primary alkyl radical ($CH_2\bullet C(C_2)OOCC_3$) in $C_3.COOCC_3$ will under go one of two reactions: 1) unimolecular elimination, or 2) association with O_2 to form a peroxy radical.

1) Unimolecular beta scission reaction to cleave a methyl group and form a very unstable vinylic hydroperoxide, isopropenyl-tertbutyl peroxide (C=C(C)OOC3C + CH3); or it will react with molecular oxygen to form a new peroxy radical ($C_3(OO\bullet)COOCC_3$), tertbutyl peroxide – tertbutylperoxy radical. The reaction with molecular oxygen is a

chemical activation reaction and has two channels to chain branching; this will be discussed further below.

$C_3•COOCC_3$ → unimolecular, beta scission) → $C=C(C)OOC_3C + CH_3$

2) Reaction with O_2:

$C_3COOCC_3 + O_2 \leftrightarrow [C_3(OO•)COOCC_3]^* \rightarrow$ New Products

$[C_3(OO•)COOCC_3]^*$ is an activated intermediate, which has excess energy resulting from the new bond that is formed from the association. It can be stabilized by collisions with the bath gas or react to new products before it is stabilized. The reactions of this activated species are therefore pressure dependent. At higher pressures there will be more collisions and stabilization can dominate reaction to new products. At lower pressure the dissociation reactions of the $[C_3(OO•)COOCC_3]^*$ intermediate can dominate. The activated and the stabilized $C_3(OO•)COOCC_3$ react to chain branching pathways.

Reaction of the unstable vinylic peroxide: isopropenyl-tertbutyl peroxide The vinylic peroxide bond is very weak, only 17 to 22 kcal-mol^{-1}, where the normal peroxide bond is near 45 kcal-mol^{-1}. This $C=C(C)OOCC_3$ molecule will rapidly dissociate, cleaving the peroxide bond forming two radicals (chain branching). It will form tertbutyl alkoxy radical $C_3CO•$ plus an acetone-radical ($CH_2•-C(=O)CH_3$). This $CH_2•-C(=O)CH_3$ radical is formed by electron rearrangement of the alkoxy radical $CH_2=C(O•)CH_3$, where the formation of the C=O bond is 20 kcal-mol^{-1} stronger than the olefin ($CH_2=CH•--R$) bond:

$CH_2=C(O•)CH_3$ → $CH_2•-C(=O)CH_3$

The 80 kcal-mol^{-1} gained in the new carbonyl bond relative to the loss of 60 kcal/mol lost from the olefin pi bond via electron rearrangement results in a 20 kcal/mol

added energy to the reaction. This energy is seen by the transition state of the peroxide bond cleavage resulting in a reduction of 20 to 25 kcal/mol needed to cleave the 45 kcal/mol peroxide bond. The reason for the very low stability of the vinyl peroxide bonds is the formation of a very strong carbonyl bond, some 20 kcal-mol^{-1} more stable than the carbon-carbon double bond:

$C=C(C)OOC_3C$ – fast → CH_2•-C(=O)CH_3 + C_3CO• $\Delta Hrxn$ = + 20 kcal mol^{-1}

The acetonyl radical will react to ketene, $CH_2=C=O$, plus a methyl group or react with molecular oxygen to form a acetone peroxy radical, $CH_2(OO•)C(=O)CH_3$, as described more completely above.

$$CH_2•\text{-}C(=O)CH_3 \rightarrow CH_2=C=O + CH_3$$

or

$$CH_2•\text{-}C(=O)CH_3 + O_2 \rightarrow CH_2(OO•)C(=O)CH_3$$

Decomposition of the acetone peroxy radical leads to active species plus energy:

$CH_2(OO•)C(=O)CH3$ → → $CH_2=C=O + CH_2=O + OH$ $\Delta Hrxn$ = -25 kcal/mol

Reaction of the tertbutyl peroxide–tertbutylperoxy radical Both the chemically activated and the stabilized $C_3(OO•)COOCC_3$ will undergo the following reactions; but the chemically activated moiety will need less energy relative to the stabilized adduct, because of the excess energy it contains from the newly formed bond.

$$C_3.COOCC_3 + O_2 \leftrightarrow [C_3(OO•)COOCC_3]^* \rightarrow \text{Products}$$

$$[C_3(OO•)COOCC_3]^* \rightarrow [C_3(OO•)COOCC_3] \text{ (stabilized)} \rightarrow \text{Products}$$

The discussion below applies to both the activated and stabilized intermediate.

Intermolecular H-atom shift and subsequent reactions The forward reaction of the tertbutylperoxide–tertbutyl peroxy radical will undergo intramolecular hydrogen shift reaction to form a hydroperoxide peroxide alkyl radical (C_2•(CH_2OOH)$COOCC_3$):

$$(C_3(OO•)COOCC_3) \leftrightarrow \text{H-shift} \leftrightarrow C_2•(CH_2OOH)COOCC_3$$

and the hydroperoxide - peroxide radical will undergo unimolecular elimination (beta scission) to chain branching products which include formaldehyde, CH_2=O, OH radical, and the very reactive-vinylic, isopropene – tertbutyl peroxide described above, C=C(C)OOC_3C:

$$C_2•(CH_2OOH)COOCC_3 \rightarrow C•H_2OOH + CH_2=C(CH_3)COOCC_3$$

$$CH_2=C(CH_3)COOCC_3 \rightarrow CH_2•C(=O)CH_3 + C_3CO•$$

Here both the C•H_2OOH and the isopropene-tbutyl peroxide rapidly (microsecond time scale under applied conditions) dissociate, as described above to CH_2=O + OH and to CH_2•C(=O)CH_3 plus tertbutyl peroxy radicals respectively.

C•H_2OOH is not a stable species that exists for any length of time; it immediately dissociates and should not be considered as a species in any reaction system.

$$C•H_2OOH \rightarrow CH_2=O + OH$$

The CH_2•C(=O)CH_3 will undergo beta scission (elimination) to ketene plus methyl radical, as above):

$$CH_2•C(=O)CH_3 \rightarrow CH_3 + CH_2=C=O$$

A summary of the overall reaction process for the reaction of the di-tertbutyl peroxide–alkyl radical (C_3•$COOCC_3$) .with O_2 system reacting via intramolecular H-atom shift to chain branching paths is:

$$C_3•COOCC_3 + O_2 \rightarrow C_3(OO•)COOCC_3$$

$(C_3(OO\bullet)COOCC_3) \leftrightarrow$ H-shift $\leftrightarrow C_2\bullet(CH_2OOH)COOCC_3$

$C_2\bullet(CH_2OOH)COOCC_3 \rightarrow C\bullet H_2OOH + CH_2=C(CH_3)COOCC_3$

$C\bullet H_2OOH \rightarrow CH_2=O + OH$

$CH_2=C(CH_3)COOCC_3 \rightarrow CH_2\bullet C(=O)CH_3 + C_3CO\bullet$

$C_3\bullet COOCC_3 + O_2 \rightarrow CH2\bullet C(=O)CH_3 + C_3CO\bullet + CH_2=O + OH$

The overall result of these reactions is chain branching; two radicals are produced from one relatively non-active peroxy radical.

Chain Branching path from the $C_3\bullet COOCC_3 + O_2 \rightarrow C_3(OO\bullet)COOCC_3$ reaction

The second reaction of this intermediate is a simple dissociation of the weak peroxide bond:

$C_3\bullet COOCC_3 + O_2 \rightarrow C_3(OO\bullet)COOCC_3 \rightarrow C_3(OO\bullet)CO\bullet + C_3CO\bullet$

Here a diradical $C_3(OO\bullet)CO\bullet$ and a tertbutoxy radical $C_3CO\bullet$ are formed. Reaction paths of the terbutoxy radical are discussed above. This $C_3(OO\bullet)CO\bullet$ radical can react to acetone plus HC(=O) + OH:

$C_3(OO\bullet)CO\bullet \rightarrow CH_3C(=O)CH_3 + HC\bullet(=O) + OH$

This reactions occurs via the path, $CH_3C(=O)CH_3$ (acetone) plus $C\bullet H_2OO\bullet$ which dissociates to HC=O + OH.

$C_3(OO\bullet)CO\bullet \rightarrow CH_3C(=O)CH_3 + C\bullet H_2OO\bullet \rightarrow CH_3C(=O)CH_3 + HC\bullet(=O) + OH$

The overall reaction for this second oxygen addition to the $C_3\bullet COOCC_3$ radical is

$C_3\bullet COOCC_3 + O_2 \rightarrow C_3CO\bullet + CH_3C(=O)CH_3 + HC\bullet(=O) + OH$

This is again a chain branching process where reaction of one radical with molecular oxygen results in formation of three active radicals.

We have integrated the kinetics for di-tert-butyl peroxide (DTBP), a known ignition enhancer into the JP-8 chemical kinetic mechanism of Zhang (2005). The DTBP kinetics add an additional 125 species and 408 reactions steps to the mechanism.

6.2.2 Combustion Kinetics of 2-Ethyl-Hexyl Nitrate

2-ethyl-hexyl nitrate (2EHN) was chosen as the second additive for which detailed oxidation and combustion chemistry reaction mechanism would be developed. The postulated paths for ignition acceleration and for soot inhibition are delineated below.

The simpler molecule ethyl nitrate ($CH_3CH_2ONO_2$), shown in Figure 50, is used as a model compound for calculating the decomposition rates of 2EHN. Its smaller size allowed the use of reasonable level *ab initio* and density functional calculations for a more accurate study of the thermochemical and kinetic parameters. The approximation of using a simpler molecule for these calculations is not expected to affect the accuracy of the calculated parameters.

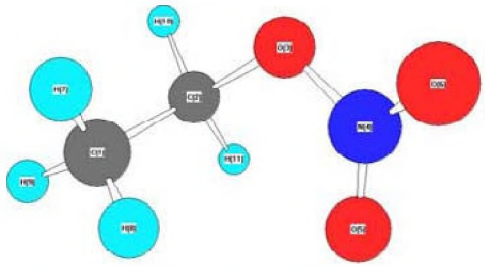

Figure 50. Ethyl Nitrate

Initiation reactions of 2 ethyl-hexyl-nitrate There are three important initiation reactions of 2 ethyl-hexyl-nitrate, that is three channels with quite low reaction barriers that lead to low temperature or rapid decomposition of hydrocarbon nitrate molecules.

The initiation (decomposition) paths for ethyl nitrate are:

1. Simple dissociation of the weak (46 kcal/mol) RO—NO_2 bond to form the corresponding alkoxy radical (CH_3CH_2O▪) plus NO_2. As this is a simple dissociation class reaction, the activation energy is the energy of reaction, ΔHrxn – RT for the gain of a second species.

$$CH_3CH_2ONO_2 \rightarrow (CH_3CH_2O\text{▪}) + NO_2 \quad \Delta Hrxn = +46.4 \text{ kcal mol}^{-1}$$

2. The second reaction is intramolecular abstraction of a hydrogen atom from the nitrate carbon by an oxygen on the NO_2 group and simultaneous (concerted reaction) cleavage of the CH_3CH_2O-NO_2 bond with formation of a double carbonyl bond in CC=O

$$(CH_3CH_2ONO_2) \rightarrow CH_3CH{=}O + HONO \quad Ea = 42.4; \Delta Hrxn = +21.5 \text{kcal/mol}$$

3. The third reaction is the molecular elimination of $HONO_2$ with concerted formation of a carbon=carbon double bond. In the case of ethylnitrate the products are ethylene + $HONO_2$:

$$(CH_3CH_2ONO_2) \rightarrow CH_2{=}CH_2 + HONO_2 \quad Ea = 43. \quad \Delta Hrxn \text{ is } -16.3 \text{ kcal/mol}$$

<u>The mechanism of hydrocarbon oxidation acceleration by organo-nitrates</u> A short summary of the thermochemistry and kinetics relating to the initial chemistry of nitro-hydrocarbons is presented here. The discussion below applies to nitro-hydrocarbons, which have a nitro group bonded to a carbon in the hydrocarbon such as nitromethane (CH_3-NO_2) and nitroethane CH_3CH_2-NO_2).

There are two important initiation steps for nitro-hydrocarbons. These are dissociation to a radical plus NO_2 or to HONO or HNO_2 plus an olefin. Reaction examples for 2-nitro-propane are illustrated below:

$CH_3CH(NO_2)CH_3 \rightarrow CH_3CH\bullet CH_3 + NO_2$ + 62 kcal mol^{-1}

$CH_3CH(NO_2)CH_3 \rightarrow CH3CH{=}CH_2$ + cis-HONO + 21 kcal mol^{-1}

$CH_3CH(NO_2)CH_3 \rightarrow CH_3CH{=}CH_2$ + trans-HONO + 24.5 kcal mol^{-1}

$CH_3CH(NO_2)CH_3 \rightarrow CH_3CH{=}CH_2 + HNO_2$ + 25. kcal mol^{-1}

Note that the ΔHrxn is not the energy needed for reactions. The barrier to the reaction for the HONO eliminations reactions is significantly higher, 40 to 45 kcal/mol. The pre-exponential factors for these reactions are near 1.0×10^{12} sec^{-1}. The barrier for the NO_2 bond cleavage is similar to the bond energy, 61 kcal/mol, but the pre-exponential factor is high, near 1.0×10^{16} sec^{-1}.

Data above illustrates the delta ΔHrxn for these nitro-hydrocarbons is positive, (endothermic) for the reactions forming the olefins and HONO or HNO_3; but very low relative to typical bond cleavage of about 90 kcal mol^{-1}. All of these reactions occur much more rapidly than any hydrocarbon oxidation reaction.

The HNO_2 molecule will isomerize to the slightly more stable HONO with a barrier of 40 kcal mol^{-1}.

The thermochemistry of these initiation reactions for these nitrate molecules is even faster than for the nitro-hydrocarbons. The example below is for ethylnitrate (CH_3CH_2-ONO_2); but the thermochemistry is similar to that of larger hydrocarbons.

$CH_3CH_2\text{-}ONO_2 \rightarrow CH_3CH_2\bullet + \bullet ONO_2$ ΔHrxn = 80 kcal mol^{-1}

$$CH_3CH_2\text{-}ONO_2 \rightarrow CH_3CH_2O\bullet + \bullet NO_2 \quad \Delta Hrxn = 39 \text{ kcal mol}^{-1}$$

The CC-ONO_2 bond in the nitrate is about 10 kcal mol-1 weaker than a normal carbon-oxygen bond in a hydrocarbon, but still relatively strong compared to the very weak CCO-NO_2 bond of less than 40 kcal/mol. These two reactions will both occur with no added barrier to that of the bond energy, thus the nitrate will form an alkoxy radical plus NO_2.

In combustion reactions the alkoxy radical will primarily form an aldehyde and hydrogen atom:

$$CH_3CH_2O\bullet \rightarrow CH_3CH{=}O + H\bullet \quad \Delta Hrxn = +18, \quad Ea = 28 \text{ kcal mol}^{-1}$$

Reactions of the H atom with oxygen are well known to give HO_2 as well as chain branching products OH + O.

The NO_2 and the HONO moieties appear to be the more important here as they undergo a series of reactions that lead to catalytic enhancement of the reaction system. These reaction processes are described below.

HONO will undergo unimolecular dissociation via collisions with the bath gas, (this reaction is pressure dependent and the kinetics need to include fall-off appropriate for the target pressure(s)).

$$HONO \rightarrow HO + NO \quad \Delta Hrxn = 48.5 \text{ kcal mol}^{-1}$$

This is a weak bond and this reaction is likely the main path for the HONO molecule.

OH is an active radical and will react in conventional abstraction and association reactions, well known to the combustion and oxidation literature. It is NO that continues the catalysis of the NOx system; it will further react with a number of species

regenerating NO_2 and ultimately, via abstraction reactions closing the catalytic cycle reforming HONO.

NO in this early reaction process will react with peroxides and hydroperoxides

$NO + CCOO\bullet \rightarrow NO_2 + CCO\bullet$ ΔHrxn is now exothermic –15 kcal mol^{-1}

$NO + HOO\bullet \rightarrow NO_2 + OH$ $\Delta Hrxn = -9.5$ kcal mol^{-1}

The NO_2 will abstract a hydrogen atom from a hydrocarbon and form HONO. The favored process forms a hydrocarbon radical and HONO.

$NO_2 + CH_3CH_2CH_3 \rightarrow HONO + CH_3C\bullet HCH_3$ $\Delta Hrxn = +21.5$ kcal mol^{-1}

The hydrocarbon radical reacts with molecular oxygen to form a peroxy radical:

$CH_3C\bullet HCH_3 + O_2 \rightarrow CH_3CH(OO\bullet)CH_3$

The peroxy radical will react with the NO and form an alkoxy radical. This catalytic process continues as illustrated below:

Reaction	**ΔHrxn (kcal/mol)**
$HONO\ (+M) \rightarrow OH + NO\ (+M)$	+ 48.5
$NO + CCOO\bullet \rightarrow NO_2 + CCO\bullet$	- 8
$NO_2 + CC\text{-}H \rightarrow HONO + CC\bullet$	+ 20
$CC\bullet + O_2 \rightarrow CCOO\bullet$	- 35
---------- **Sum**	**+ 25**

or $H + O_2 \rightarrow HOO$ - 49.

$CC\text{-}H + O_2 \rightarrow CCO\bullet + OH$ (homogeneous catalysis)

Summing these four reactions we have a catalytic cycle for formation of hydrocarbons with an oxygen atom on one of the carbons. This is important because each carbon with an oxygen bond will react to carbon monoxide and then carbon dioxide; it will *not* result in a soot carbon.

Remember the CCO• radical reactions as well and the reactions of the hydrogen atoms produced from the alkoxy dissociation:

$CCO\bullet \rightarrow CCH{=}O + H\bullet$

$CCO\bullet + O_2 \rightarrow CCH{=}O + HO_2\bullet$

$H + O_2 \rightarrow HOO$ or $(H + O_2 \rightarrow OH + H)$

The HO_2 can react with the NO as part of the catalytic cycle or the H can lead to chain branching.

Adding the ethoxy (CCO•) radical dissociation reaction to the reaction sequence

	ΔHrxn (kcal/mol)
$CC\text{-}H + O_2 \rightarrow CCO\bullet + OH$ (from homogeneous catalysis	+ 25)
$CCO\bullet \rightarrow CCH{=}O + H\bullet$	(+ 18)
$CC\text{-}H + O_2 \rightarrow CCH{=}O + H\bullet + OH$ (Catalyzed Chain Branching -6 kcal mol^{-1})	

or

	ΔHrxn (kcal-mol^{-1})
$CC\text{-}H + O_2 \rightarrow CCO\bullet + OH$ (from homogeneous catalysis	+ 25)
$CCO\bullet + O_2 \rightarrow CCH{=}O + HO_2\bullet$	(- 31)
$CC\text{-}H + O_2 \rightarrow CCH{=}O + HO_2\bullet + OH$ (Catalyzed Chain Branching -6 kcal mol-1)	

This chain branching is less active one than that immediately above because H is a much more active radical than HO_2 is.

To summarize, the peroxy compounds enhance oxidation and possibly reduce soot by enhancing the radical pool. The nitro-hydrocarbons create the same effect by

catalyzing the bonding of oxygen and carbon. Carbons bonded to oxygen will not participate in soot formation. The nitro compounds also enhance the radical pool.

6.3 JP-8 Plus Additive Calculation Results in Simple Reactors

The Method of Moments soot model described previously was integrated with JP-8 and additive kinetics. In this section we show results of this combined model over a wide range of conditions.

6.3.1 Di-Tert-Butyl Peroxide

6.3.1.1 Ignition Delay Figure 51 shows the calculated effect of DTBP on JP-8 ignition delay, plotting the ignition time normalized by the result for unaltered JP-8. Ignition delays were calculated for adiabatic, constant pressure reaction. Ignition was defined as the time when the temperature had increased 400 K. A much greater effect can be seen for fuel-rich conditions ($\phi > 1$) than for lean mixtures. In all cases the stoichiometric ratio, ϕ, was calculated including the oxygen in the additive to eliminate purely stoichiometric effects. Almost no soot was produced in these calculations because the system passed rapidly through the 1600-1800 K temperature range where the most soot production occurred.

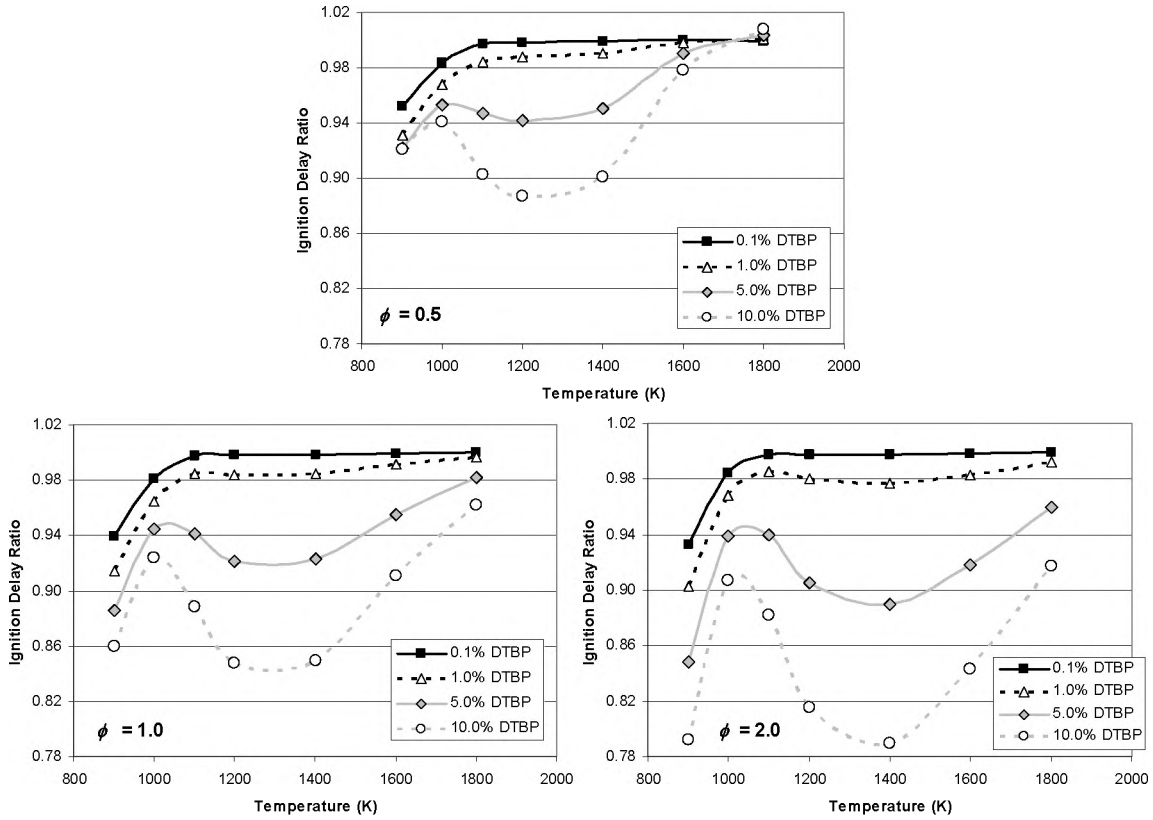

Figure 51. Calculated constant pressure (1.0 atm) and enthalpy ignition delays for DTBP in JP-8 for a range of temperatures, stoichiometries and additive concentrations. The results are plotted as the ignition delay with additive normalized by the ignition delay without additive at the same conditions.

6.3.1.2 Soot Calculations in a PSR Figure 52 shows the calculated soot volume fractions from fixed-temperature PSR calculations for JP-8 and for JP-8 with 5% DTBP added. Figure 52a shows results as a function of temperature for $\phi = 2.0$, $P = 1.0$ atm, and a residence time of 0.1 s. The relatively high concentration (5% by moles) of DTBP resulted in only a few percent reduction in soot volume fraction. Figure 52b shows that the soot reduction due to the additive increased for richer mixtures, where more soot was produced. As in the ignition delay calculations, the equivalence ratio was calculated including oxygen in the additive to screen out purely stoichiometric effects.

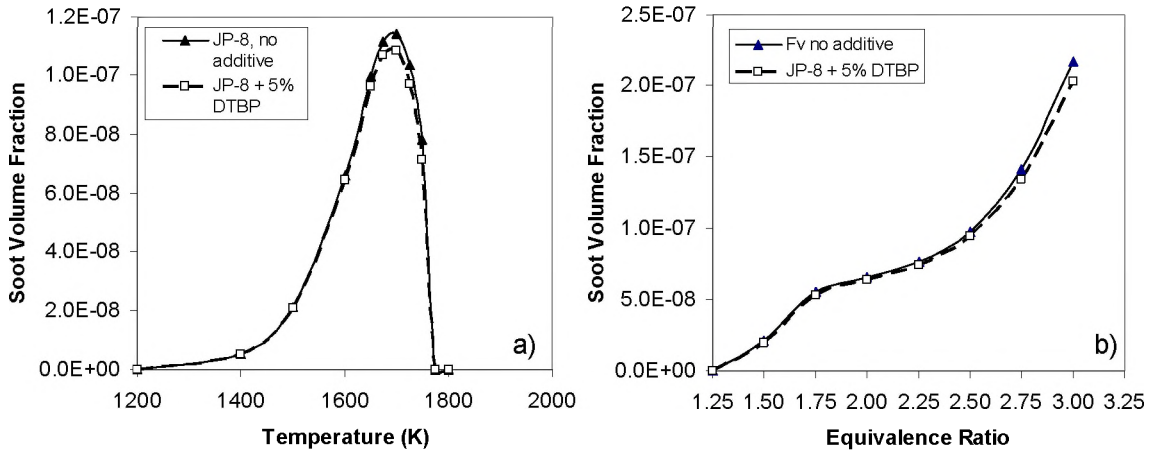

Figure 52. Comparison of fixed-temperature PSR calculation results for JP-8 and JP-8 with 5% di-tert-butyl peroxide added. P = 1 atm., residence time = 0.1 s. Soot volume fraction is plotted a) as a function of temperature for equivalence ratio = 2.0, and b) as a function of equivalence ratio for T = 1600 K.

Figure 53 shows results for adiabatic PSR calculations with P = 1 atm., residence time = 0.1 s, and an inlet temperature of 300 K. Again a comparison was made between JP-8 and JP-8 with 5% DTBP added. In these calculations, the soot increased until about ϕ = 2.1, beyond which soot decreased due to decreasing temperatures. For the richest conditions (ϕ > 2.3) the addition of DTBP increases soot production by raising the calculated reactor temperature. No conditions were found where the PFR or PSR models predicted the large soot reductions with small amounts of DTBP found in the drop tube. Calculations done with an oxidizer consisting of 40% O_2 and 60% N_2 gave similar results to those for air at the same stoichiometry.

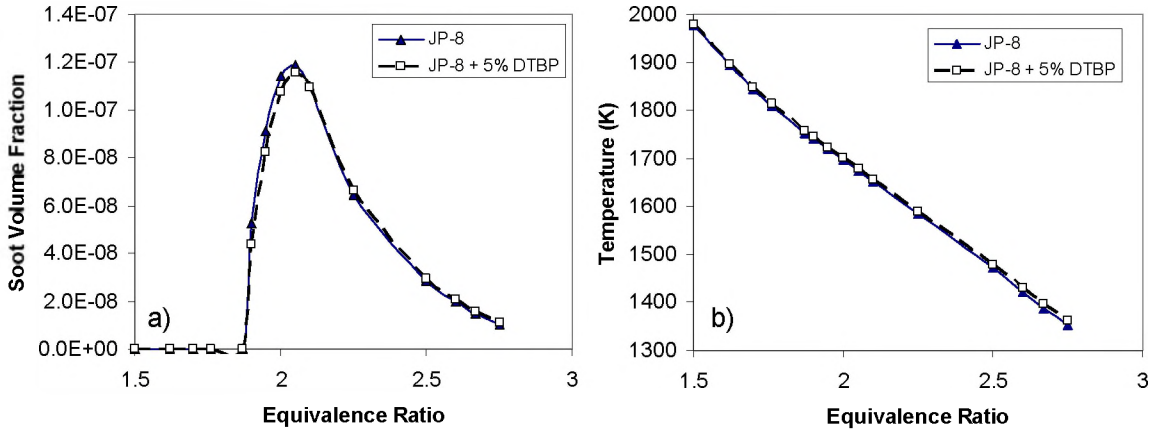

Figure 53. Comparison of adiabatic PSR calculations results for JP-8 and JP-8 with 5% di-tert-butyl peroxide added. P = 1 atm., residence time = 0.1 s, inlet temperature = 300 K. For a) soot volume fraction and b) temperature as functions of equivalence ratio.

6.3.1.3 Simple Gas-Turbine Combustor Model with Detailed Chemistry and Soot Modeling The effects of mixing were modeled by modifying the often-used plug flow reactor (PFR) simulation to account for in-mixing of a diluent such as air. To derive the appropriate mixing term we first define two fluid masses, an original, fixed fluid with species mass fractions Y_0 and mass m_0 and an in-mixing fluid with species mass fractions Y_χ and mass $m_\chi(t)$.

For the nonreacting case the mass fraction of species i, $Y_i(t)$, is given by

$$Y_i(t) = \frac{m_0 Y_{i0} + m_\chi(t) Y_{i\chi}}{m_0 + m_\chi(t)}. \qquad \text{(Eqn. 3)}$$

Differentiating with respect to time and defining the ratio $\chi \equiv m_\chi/m_0$ gives the mixing equation for nonreacting flow:

$$\frac{dY_i}{dt} = \frac{d\chi}{dt}\left(\frac{Y_{i\chi} - Y_i}{\chi + 1}\right). \qquad \text{(Eqn. 4)}$$

The right hand side of Equation 4 was added to the chemical source term to create a model in which chemical reaction occurs along with mixing at a specified rate.

$\chi(t)$ was chosen to model the average equivalence ratio vs. time history that might be found in a typical gas turbine combustor. A fuel-rich primary zone was considered with a residence time of 2 ms and a secondary zone with a residence time of 6 ms as illustrated in Figure 54. At $t = 0$ the composition consists of pure JP-8 surrogate. In the primary zone, air is added at a constant mass rate until the equivalence ratio, $\phi = 1.5$ at $t =$ 2.0 ms. In the secondary zone air is again added at constant (but different) mass rate until $\phi = 0.5$ at $t = 8.0$ ms. Figures 55b and 55c show $\chi(t)$ vs. time and ϕ vs. time. We also specify the temperature history (shown in Figure 55a), which increases linearly from 900 to 2400 K in the primary zone ($t = 0$-2 ms) and decreases linearly in the secondary zone from 2400 to 2000 K. The pressure is constant at 35 atm. This, of course does not take into account turbulent fluctuations that would cause higher and lower temperature and rich and lean gas pockets that would influence the soot production in an actual device.

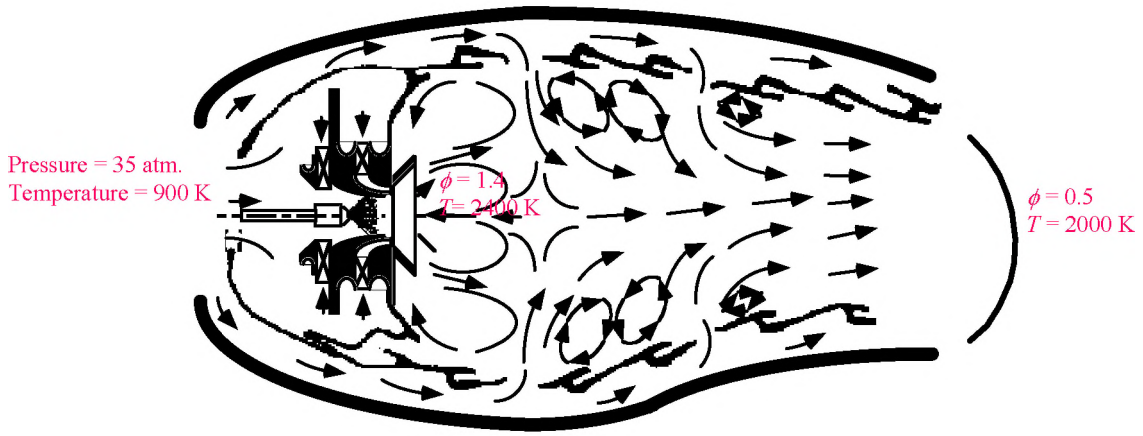

Figure 54. Diagram of a gas-turbine combustor showing average conditions in the inlet, primary zone and exit (Courtesy of Dr. Mel Roquemore).

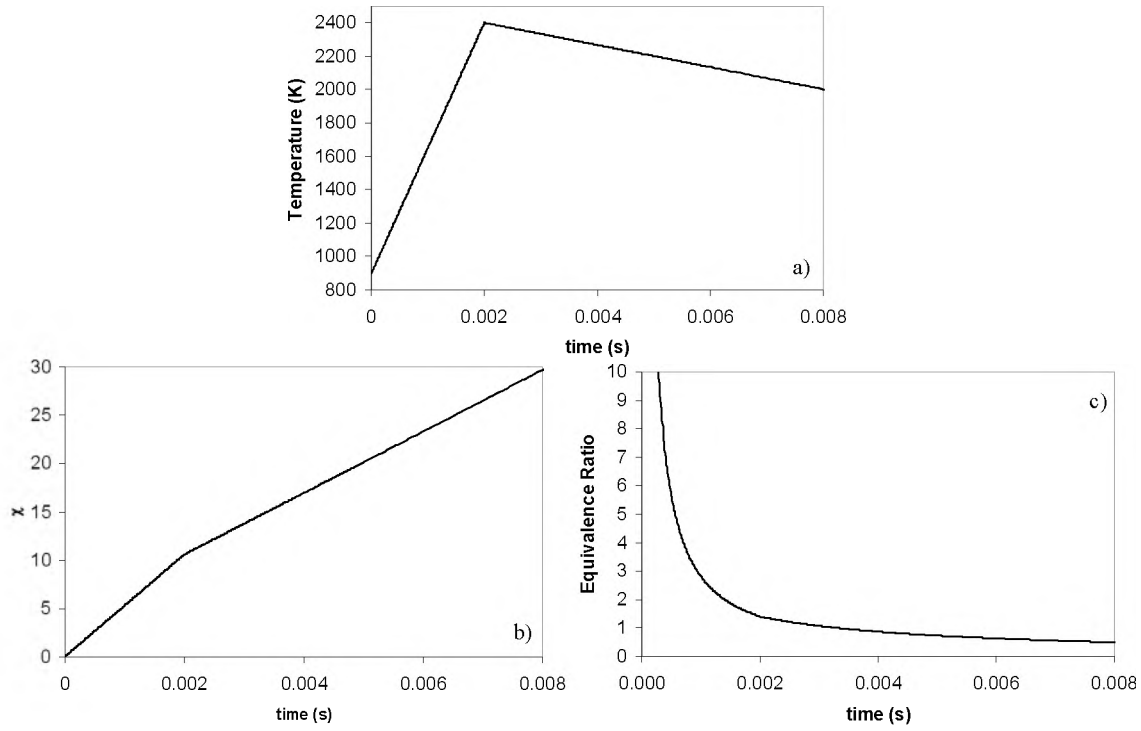

Figure 55. Temperature and mixing histories for the simplified gas-turbine combustor model.

Figure 56 shows the calculated soot volume fractions for JP-8 and JP-8 with 5% DTBP added. In both cases soot production occurs in the rich primary zone when the temperature is high enough. As additional air is added this soot is oxidized until early in the secondary zone effectively all the soot is oxidized. In an actual combustor turbulent mixing irregularities could allow some soot to exit the combustor. The effect of the additive is to speed ignition which also causes soot to be produced sooner. However, the peak soot volume fraction is about 12% lower with 5% additive present. Soot oxidation also occurs sooner in the case with the additive present. It can be seen that soot suppression depends on the soot burnout time relative to the combustor residence time. If the combustor exit were at the time indicated by the vertical red line in Figure 56 then the soot reduction by 5% DTBP would be about 65%.

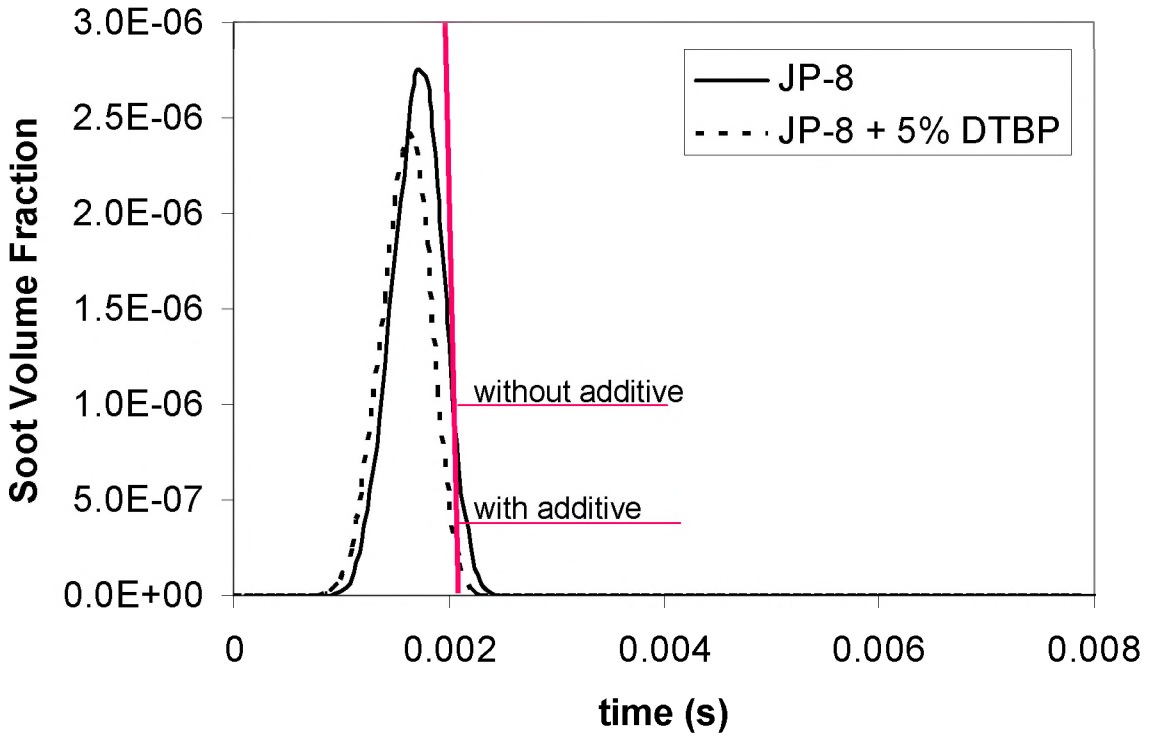

Figure 56. Soot model results for the simplified gas turbine combustor model for JP-8 and JP-8 with 5% DTBP added.

Figure 57 shows the effects of adding DTPB to the radical species. As expected from the kinetics the CH_3 concentration is boosted temporarily. The O and OH (not shown) concentrations are also increased but with a longer lasting effect.

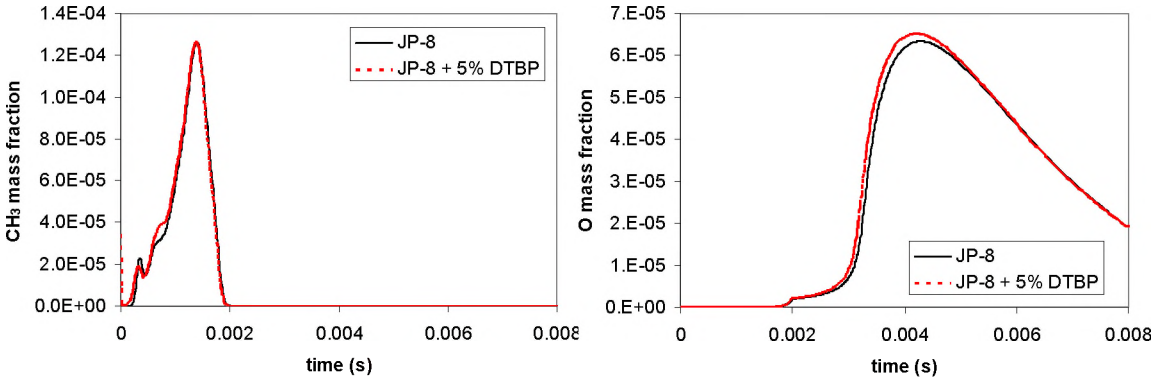

Figure 57. Predicted effects on radical species CH_3 and O for the simplified gas turbine combustor model for JP-8 and JP-8 with 5% DTBP added.

6.3.2 2-Ethyl-Hexyl Nitrate In JP-8 Modeling Results

6.3.2.1 Ignition Delay Figure 58 shows the computed effect of 2EHN on JP-8 ignition delay at 1 atm. Much more significant effects are seen than were found using the di-tert-butyl peroxide (DTBP) kinetics. Even at concentrations as low as 0.1% (by moles) 2EHN can reduce the ignition delay by 20% for mixtures initially at temperatures near 1000 K. At temperatures above 1400-1600 K no effect is found on ignition delay. As with DTPB, a greater effect is seen under rich conditions.

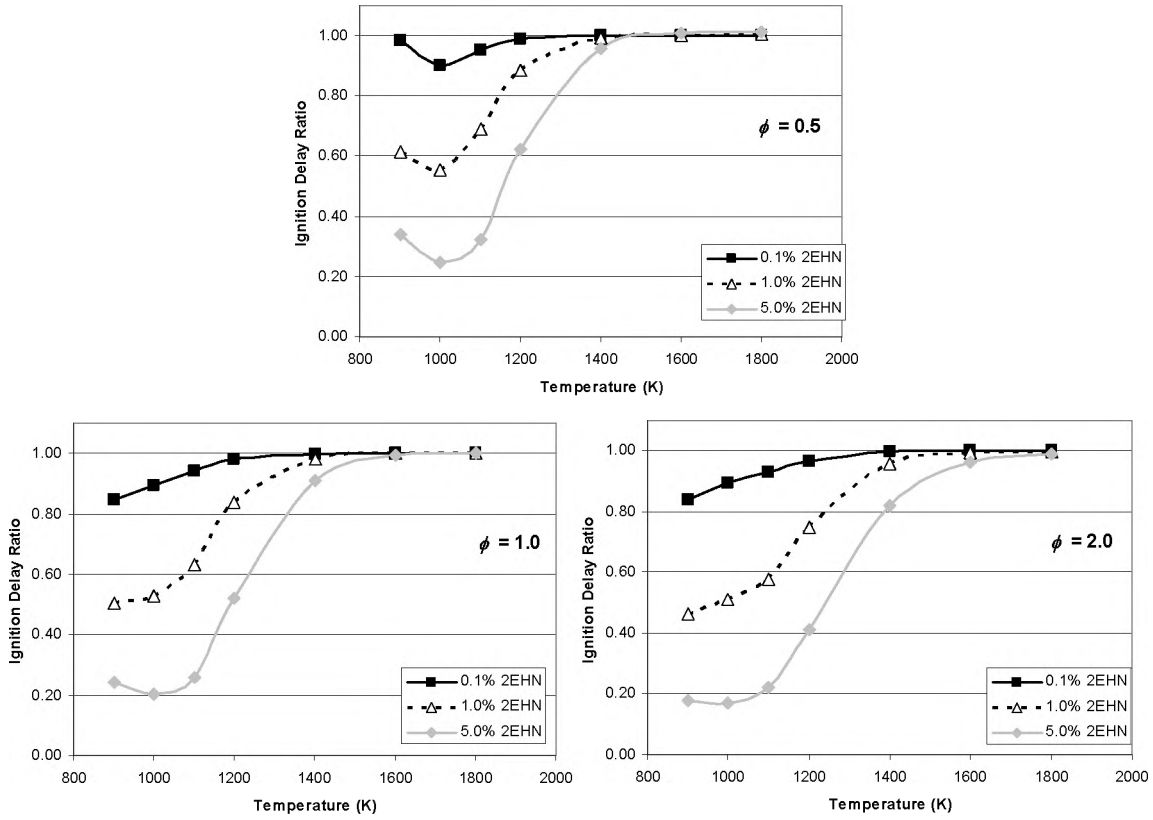

Figure 58. The effect of 2-ethyl-hexyl nitrate (2EHN) on JP-8 ignition for various concentrations, temperatures, and equivalence ratios (ϕ). "Ignition Delay Ratio" is the ratio of computed value for the treated verses untreated fuel.

6.3.2.2 Calculated Effects of 2EHN in a Sooting PSR Figure 59 shows the calculated effect of adding of 5% 2EHN to JP-8 on soot production in a fixed-

temperature perfectly stirred reactor (PSR) as a function of temperature. For these calculations the equivalence ratio = 2.0, residence time = 0.1 s, pressure = 1 atm. The effect of 2EHN on soot reduction in a PSR behaves much differently than the effect on ignition delay. The percentage of soot reduction increases with increasing temperature. However, at temperatures above about 1800 K little soot is produced, so the absolute amount of soot removed peaks at about 1750 K, where only 7.3% soot reduction is achieved. The higher percentage reductions occur where there is little soot in the unaltered JP-8 case. All soot results in this section were calculated using the Method of Moments soot model (Frenklach & Wang 1990, Appel et al. 2000).

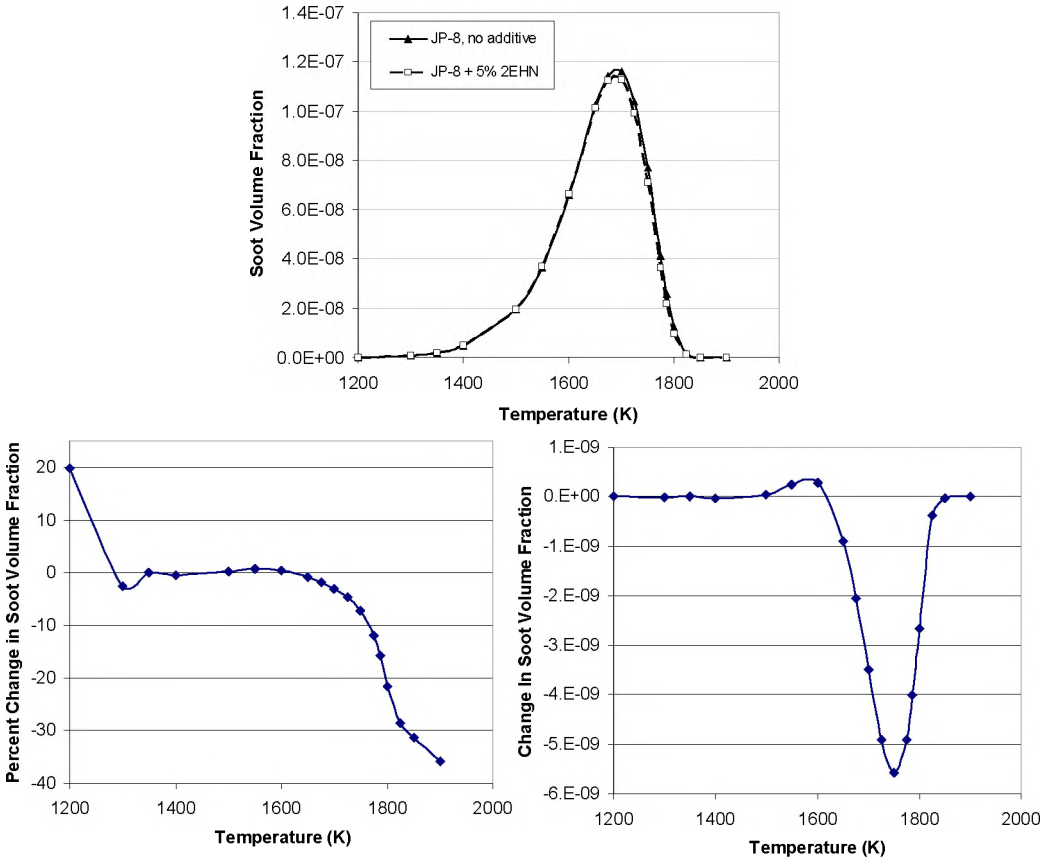

Figure 59. The effect of addition of 5% 2-ethyl-hexyl nitrate (2EHN) to JP-8 on soot production in a fixed-temperature PSR as a function of temperature. Equivalence ratio = 2.0, residence time = 0.1 s, pressure = 1 atm.

Figure 60 shows the calculated effect of adding of 5% 2EHN to JP-8 on soot production in a fixed-temperature perfectly stirred reactor (PSR) as a function of equivalence ratio. For these calculations the temperature is fixed at 1750 K, residence time = 0.1 s, pressure = 1 atm. As expected, soot production increases with increasing equivalence ratio. The soot volume fraction change due to the additive addition also increases with increasing equivalence ratio. The maximum percentage soot volume fraction reduction occurs for an equivalence ratio of about 1.6 (40% removal) however, the actual soot volume fraction is only about 1.e-11 so not much soot is actually removed under these conditions.

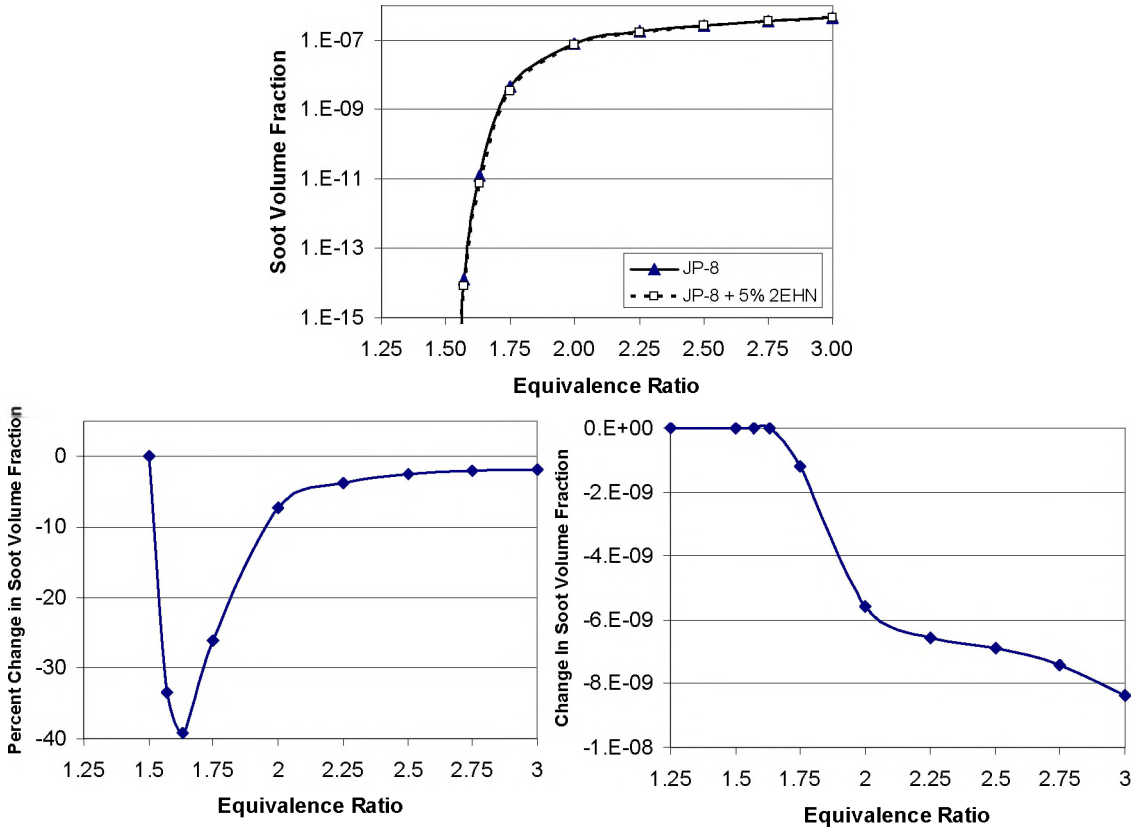

Figure 60. The effect of addition of 5% 2-ethyl-hexyl nitrate (2EHN) to JP-8 on soot production in a fixed-temperature PSR as a function of equivalence ratio. Temperature = 1750 K, residence time = 0.1 s, pressure = 1 atm.

Figure 61 shows the calculated effect on temperature of adding 5% 2EHN to JP-8 in an adiabatic PSR with an inlet temperature of 300 K as a function of equivalence ratio. With increasing equivalence ratio the PSR temperature decreases nearly linearly. The effect at all equivalence ratios is to raise the temperature. Greater temperature increases are found at richer conditions.

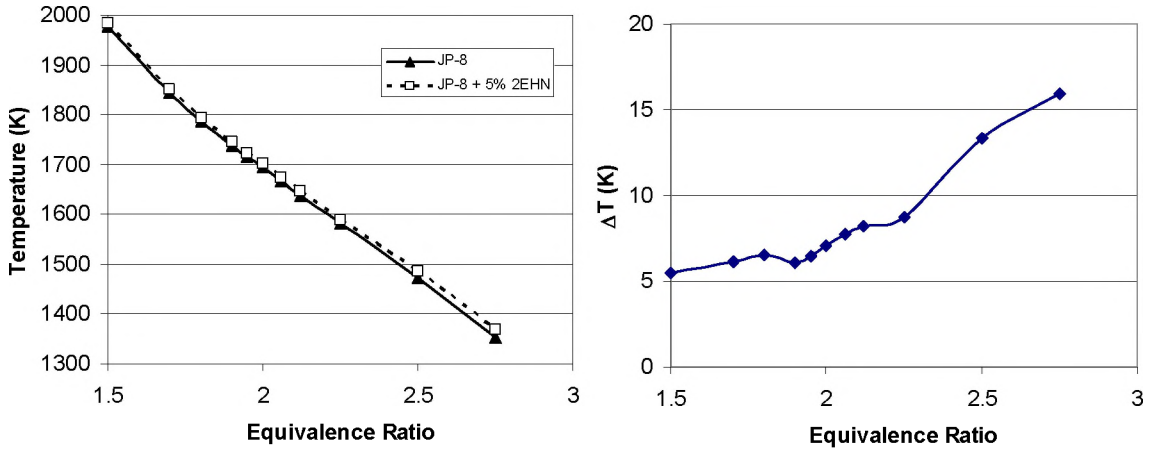

Figure 61. The effect of addition of 5% 2-ethyl-hexyl nitrate (2EHN) to JP-8 on temperature in an adiabatic PSR as a function of equivalence ratio. Inlet temperature = 300 K, residence time = 0.1 s, pressure = 1 atm.

Figure 62 shows the calculated effect on soot production of adding 5% 2EHN to JP-8 in an adiabatic PSR with an inlet temperature of 300 K as a function of equivalence ratio. The interaction of different effects is likely to be complicated in this case. Soot reduction can be expected as seen in the constant-temperature PSR cases. The additive increases soot at higher equivalence ratios, probably due to the temperature increase caused by exothermic reactions of 2EHN. Note that that adding 2EHN begins to increase soot production at the equivalence ratio that gives the temperature at the peak of the "soot bell" as seen in Figure 58, which occurs for an equivalence ratio of about 2 and a temperature of about 1700 K. For equivalence ratios richer than this, the increased temperature causes more soot formation, which is a stronger effect than the soot

reduction due to the additive. At leaner conditions, 2EHN decreases soot by enhancing the radical pool, which in can do more effectively when more oxygen is present. This effect is apparently stronger than the soot increase which is to be expected from the increased temperature.

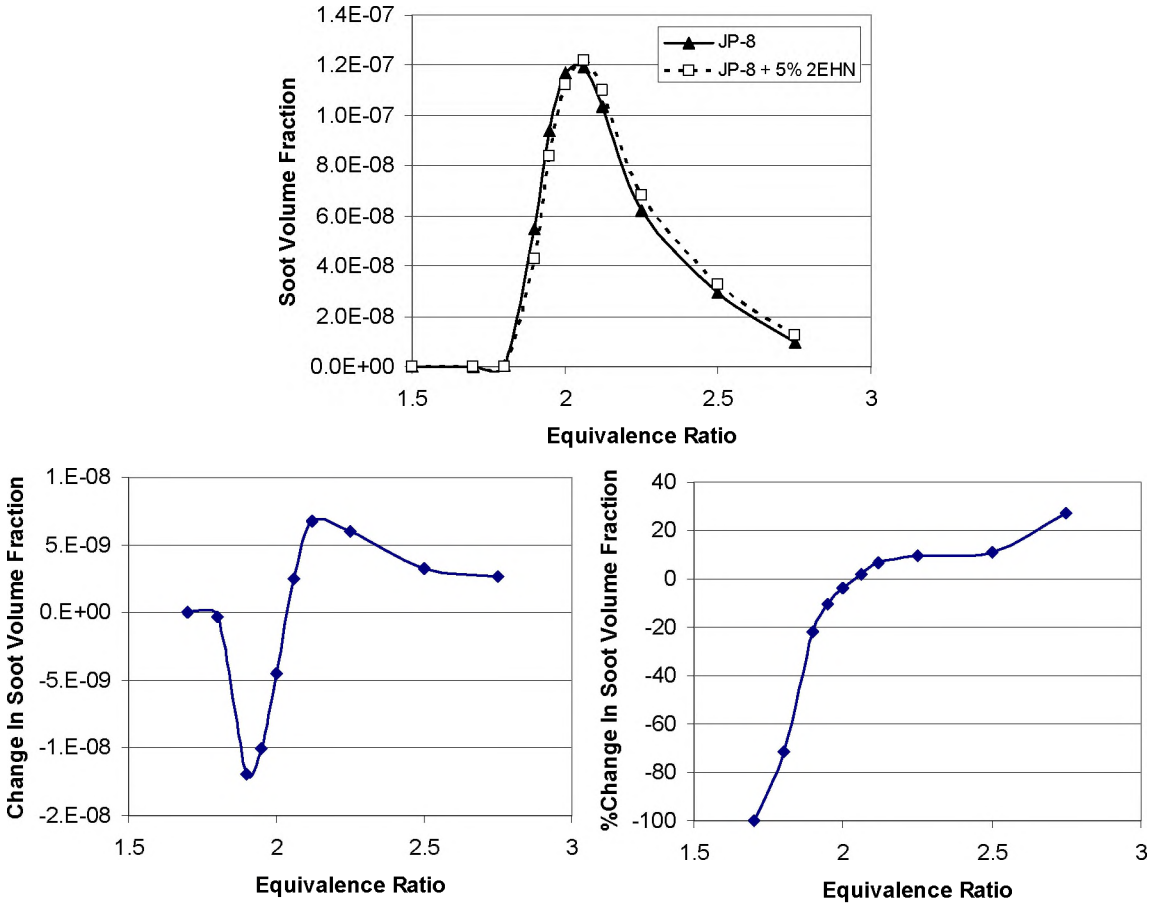

Figure 62. The effect of addition of 5% 2-ethyl-hexyl nitrate (2EHN) to JP-8 on soot production in an adiabatic PSR as a function of equivalence ratio. Inlet temperature = 300 K, residence time = 0.1 s, pressure = 1 atm.

These preliminary calculations of the effects of adding 2EHN to JP-8 fuel showed that a relatively small amount of this additive has a strong ignition enhancing effect, especially for combustible gas fuel-air mixtures near 1000 K. No effect on ignition was seen for temperatures above about 1400-1600 K, depending on the stoichiometry. The PSR calculations showed that 2EHN will reduce soot under many conditions, with

double-digit percentage decreases occurring when little soot is present, but more modest (3-10% for a 5% additive concentration) reductions being found for conditions where the most soot was produced. Exothermic reactions of 2EHN can raise the combustion temperature which may increase or decrease the amount of soot formed, depending on the conditions.

6.4 CFD Modeling

The UNICORN (UNsteady Ignition and Combustion with ReactioNs) CFD code has been run for a number of cases of interest for examining additive effectiveness. The first runs were made with the full Violi et al. (2002) mechanism and with a reduced version of it. Later, the Zhang mechanism, including DTBP kinetics was used. Cases were run simulating a jet flame, the University of Utah drop-tube reactor and the WPAFB swirl-stabilized combustor.

6.4.1 JP-8 Jet Diffusion Flames

The earliest runs were made using two different versions of the Violi et al. (2002) JP-8 mechanism. The detailed mechanism has 266 species and 5032 reactions, while a smaller "skeletal" mechanism has 161 species and 769 reactions. Although the skeletal mechanism gives almost identical results in ignition delay calculations, differences do appear in the temperature and species profiles when the mechanisms are implemented into UNICORN. UNICORN was run to simulate a central fuel-jet composed of the 6-specie JP-8 surrogate. The jet diameter was 10 mm and the jet velocity was 3 cm/s. The fuel jet was surrounded by an annular air jet with a diameter of 200 mm and a velocity of 10 cm/s.

Figure 63 compares temperature contours for the UNICORN jet flame cases with the detailed and skeletal mechanisms. Figure 64 makes a similar comparison for the calculated benzene mole fraction. Figure 65 shows radial profiles of velocity and temperature at an axial location 20 mm from the burner exit. Again, the detailed and skeletal mechanisms are compared. Figure 66 makes a similar comparison for the six components of the JP-8 surrogate blend and the OH radical.

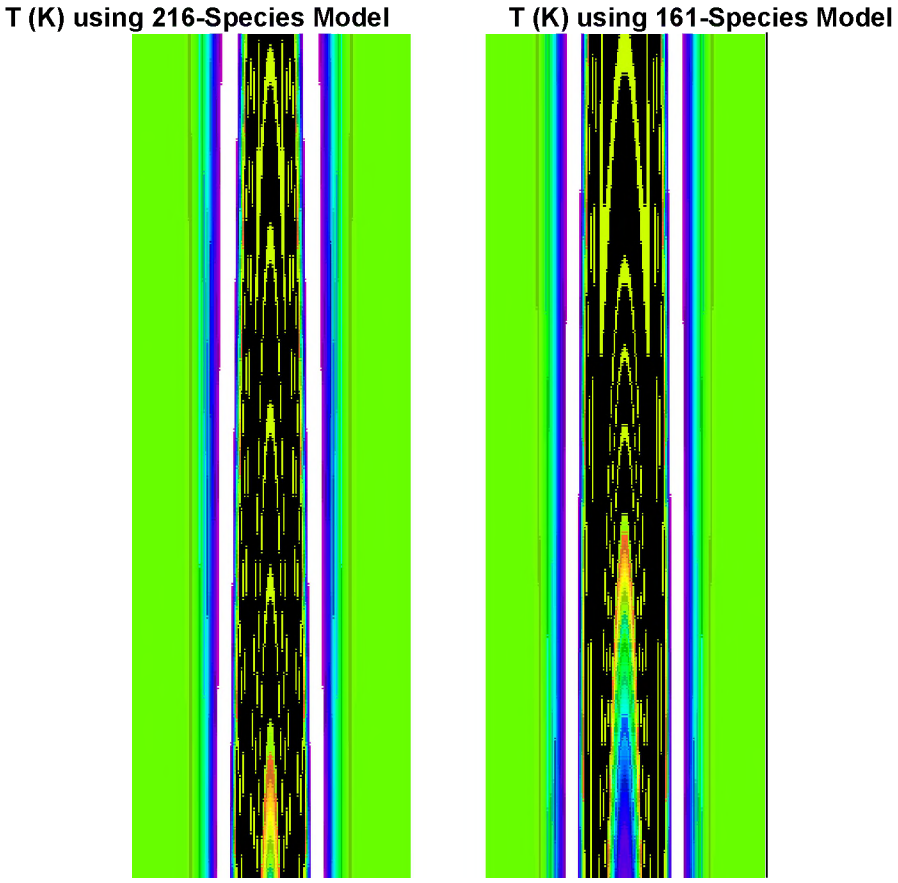

Figure 63. Comparison of calculated jet flame temperatures from the UNICORN CFD code using the full and skeletal versions of the Violi JP-8 mechanism.

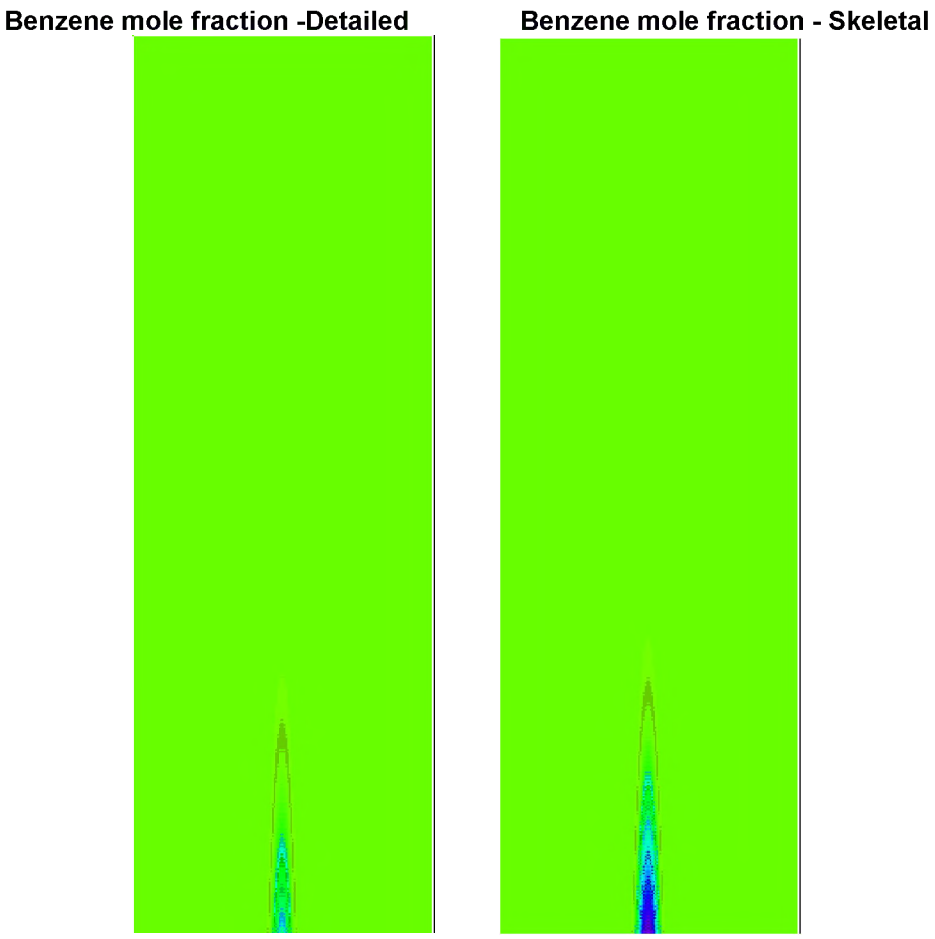

Figure 64. Comparison of calculated jet flame benzene mole fraction contours from the UNICORN CFD code using the full (left) and skeletal (right) versions of the Violi JP-8 mechanism.

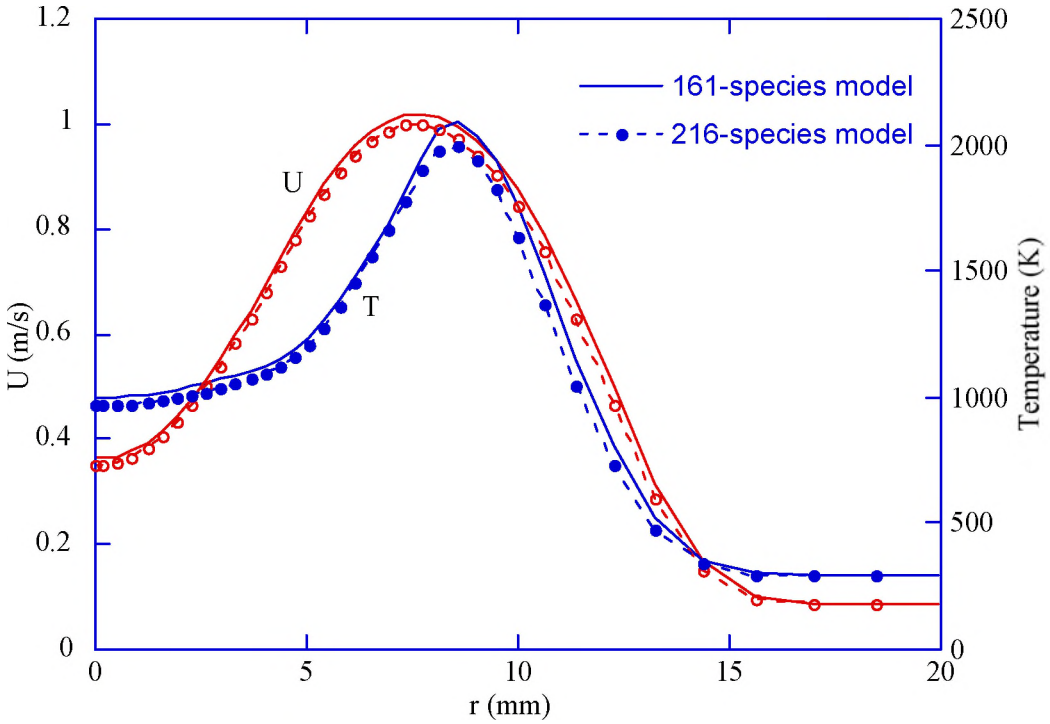

Figure 65. Comparison of radial profiles of temperature (T) and axial velocity (U) 20 mm above the burner for the detailed and skeletal JP-8 mechanisms in a jet flame modeled with UNICORN.

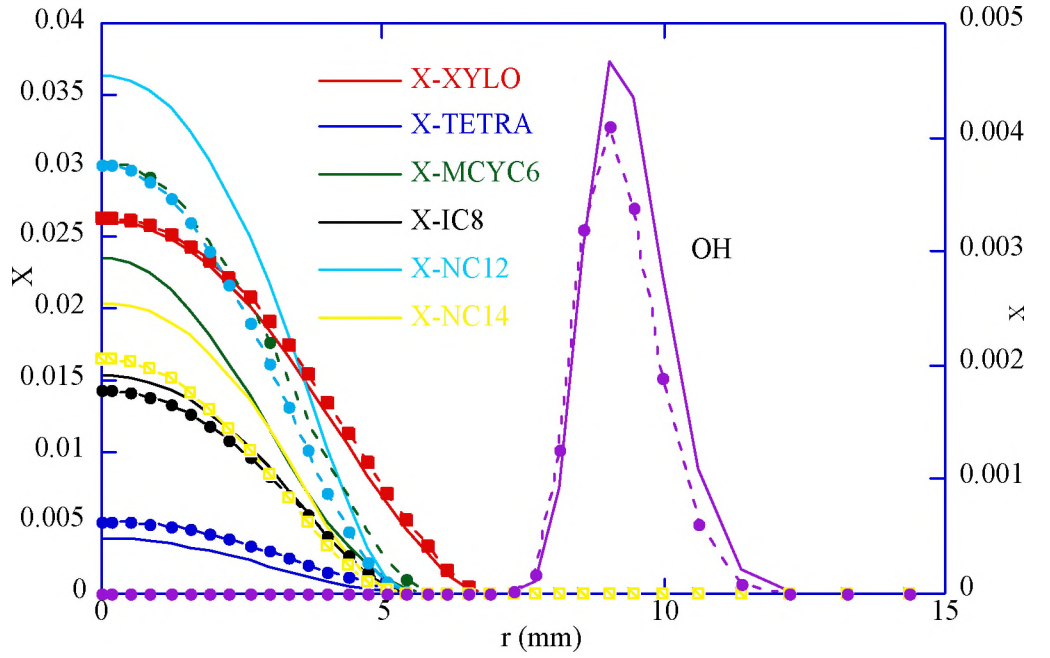

Figure 66. Comparison of radial profiles of fuel component and OH mole fractions 20 mm above the burner for the detailed and skeletal JP-8 mechanisms in a jet flame modeled with UNICORN.

Results comparing diffusion flame and premixed flame results using Violi's (2002) and Zhang's (2005) mechanisms are shown in Figures 67 and 68, respectively. There are some differences, but fairly good agreement between the predictions made by Violi's and Zhang's mechanisms was obtained.

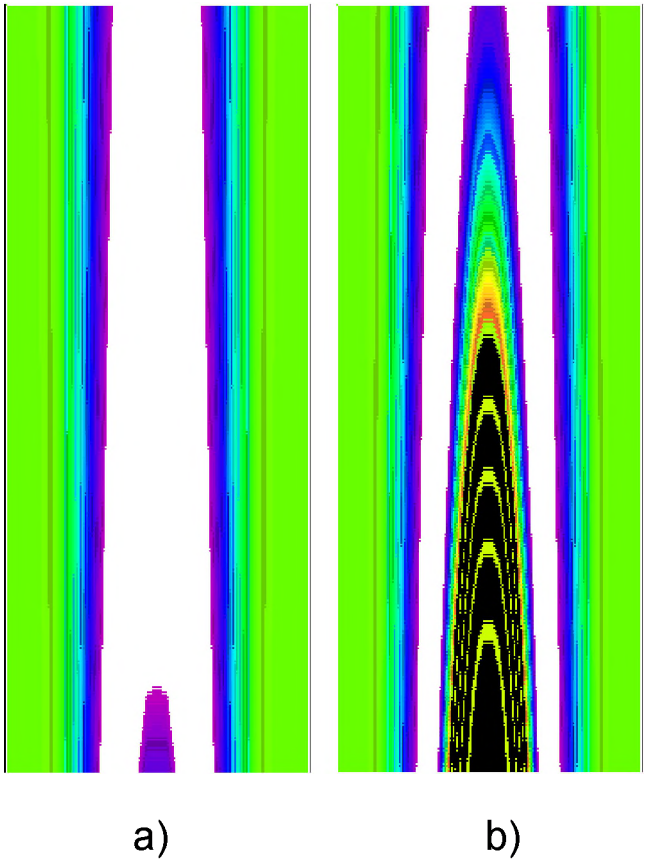

Figure 67. Jet diffusion flame simulation results for temperature using calculated using (a) Violi mechanism and (b) Zhang mechanism.

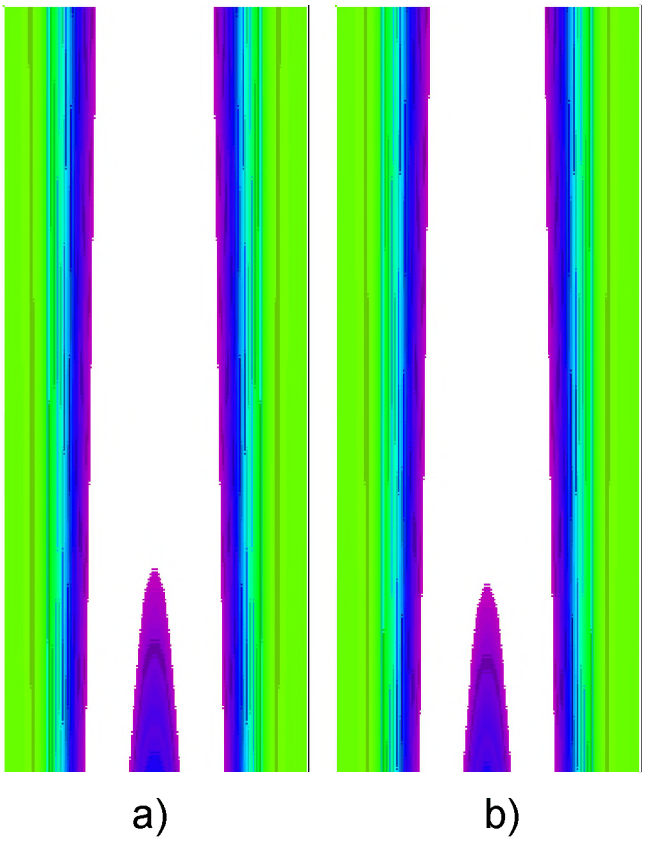

Figure 68. Premixed jet flame simulation results for temperature using calculated using (a) Violi mechanism and (b) Zhang mechanism.

6.4.2 Drop Tube Experiment Modeling

The drop tube experiment at the University of Utah, was modeled using UNICORN. This axisymmetric experiment was modeled as shown in Figure 69. Only the top 80 cm of the reaction chamber was modeled for the sake of reducing the computational time. As there was no entrainment of fluid from the bottom opening of the reaction chamber, omission of the last 30-cm section is not expected to impact the predicted results obtained in the top 80-cm reaction chamber.

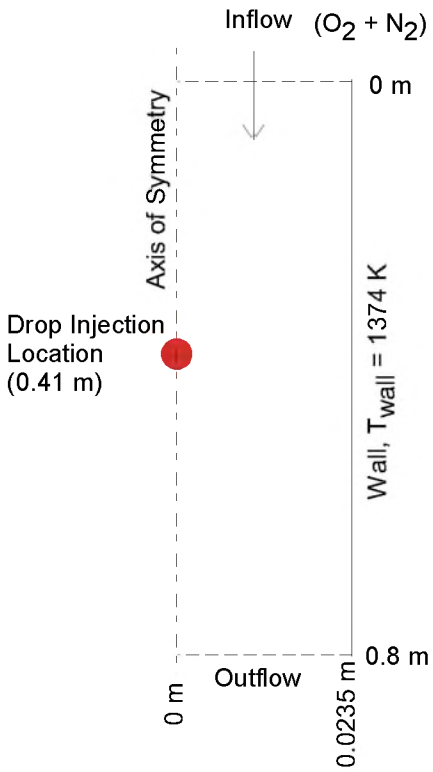

Figure 69. Diagram of the drop tube model used for the UNICORN simulations.

The UNICORN code can simulate gas flow and combustion processes associated with the drop tube using its built-in mathematical models. However, in order to simulate the evaporation of liquid fuel, additional models were incorporated into UNICORN. The fuel droplets injected into the reaction chamber (at h = 41 cm) travel downstream and vaporize gradually. During the descent of a droplet, its velocity changes due to the drag and gravitational forces acting on it. Therefore, instantaneous locations of the droplets must be calculated using Lagrangian approach. The evaporation characteristics of JP-8 droplets were experimentally determined previously. The change in droplet size due to evaporation is given by

$$d^2 = d_0^2 - kt \qquad \text{(Eqn. 5)}$$

Here, d is the droplet diameter, t is time, and k is a constant (2.13 x 10-2 cm^2/s for JP-8) derived from droplet size measurements in a drop tube flame. Subscript 0 represents conditions at $t = 0$. Based on Eqn. 5, the rate of fuel evaporation ($\dot{m}$) is

$$\dot{m} = 0.25 \times 10^{-6} \pi \rho_l k \sqrt{d_0^2 - kt} \qquad \text{(Eqn. 6)}$$

Here, ρ_l is the density of JP-8 in kg/m^3 and $\dot{m}$ is in kg/s. UNICORN was modified by incorporating Lagrangian calculations for droplet trajectories and mass source terms (Eqn. 2) into species conservation equations. Note, as JP-8 fuel was considered as a surrogate mixture of 6 components, portions of $\dot{m}$ appear in the corresponding six species conservation equations.

Calculations for the flame structure in the drop tube were performed for an oxidizer flow rate of 6.9 l/min (velocity of 6.63 cm/s) and the furnace wall temperature of 1100° C. A grid system of 151 x 51 nodes was used for these simulations. Grid points were clustered near the droplet injection location for accurately capturing the ignition process. Results were obtained for two oxidizers: normal air and a mixture of 40% O_2 and 60% N_2 by volume. The shortened version of the Violi mechanism (161 species and 1538 reactions) was used for these calculations.

6.4.2.1 Gravity Effects The drop tube in the experiments was mounted vertically so the droplets flow downward. Consequently, heavy droplets were expected to accelerate while combustion products decelerate. To investigate gravity effects on the ignition characteristics calculations were performed without and with gravitational force acting in the axial direction. Computed temperature distributions for these two cases are shown in Figure 70. Purple color in these figures represents 1373 K while red color

represents the peak value of 2270 K. The temperature distributions between heights 40 and 45 cm are shown in Figure 70. Size and location of the fuel droplets are superimposed over temperature with black color. The droplet's initial size was 300 μm. Only one out of three droplets in the drop tube are shown. Normal air at room temperature was flowing from top to bottom. The uniform purple color (1373 K) at the top of the images suggests that the wall has heated the passing air completely by the time it reached the height of 40 cm.

Fuel vapor released by the droplets burned quickly in both zero-g and normal-g cases. Such rapid burning resulted in nearly zero ignition distance. On the other hand, experiments have indicated a finite ignition distance (~ 4.6 cm) for JP-8 fuel. Later refinement of the input parameters gave very good agreement between measured and calculated flame liftoff distances (see Section 6.4.2.4).

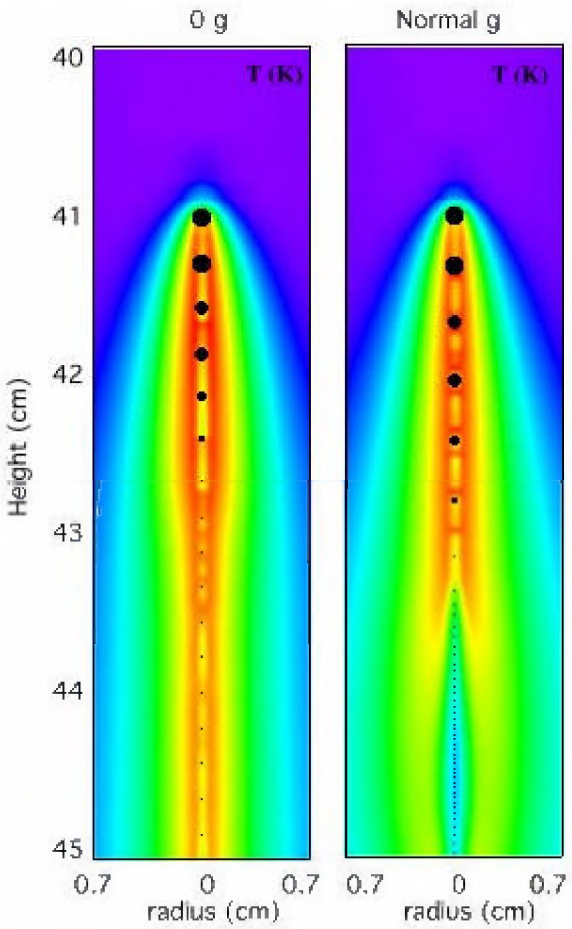

Figure 70. Predicted temperature distributions calculated under zero-g and normal-g conditions for the drop-tube model.

The temperature distributions obtained with zero-g and normal-g are very similar, especially, near the ignition location. Nevertheless, some interesting differences occurred downstream. Droplets were separated more under normal gravity when their size was reasonably large and are clustered when they became small. Droplets were uniformly distributed in the zero-g case. Clustering of small droplets in the normal-g case resulted in high concentration of fuel in the downstream location and the diffusion flame was pushed outward in the radial direction.

6.4.2.2 Effect of Oxygen Concentration on Flame Structure Results obtained with different oxidizers are shown in Figures 71 and 72. Gravity was neglected in these calculations. Distributions of temperature, *m*-xylene (a JP-8 fuel surrogate component) concentration and soot volume fraction are shown for each case. Figure 71 shows the results of the normal-air case and Figure 72 depicts those of the enriched-oxygen case. Soot was calculated using the two-step model of Lindstedt (1994), which is much more amenable for inclusion in a CFD simulation than the Method of Moments model. As expected, oxygen-rich air consumed the fuel more rapidly than normal air. Traces of fuel were evident in the downstream locations of the normal-air case (Figure 71) and the flame structure resembled that of a jet diffusion flame. Interestingly, only a column of soot was formed in both the cases and weak oscillations (wavy patterns) developed in soot distributions.

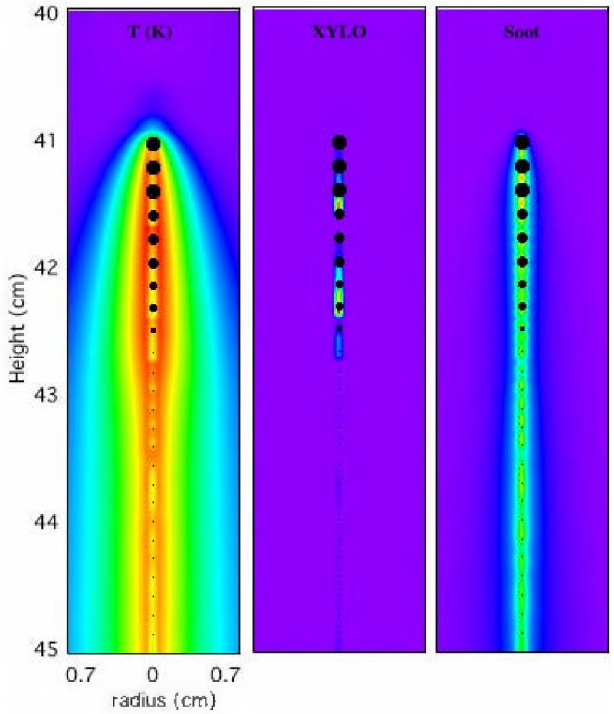

Figure 71. Predicted temperature, *m*-xylene (a fuel fragment, designated XYLO above), and soot distributions using atmospheric air as the oxidizer in the drop-tube model.

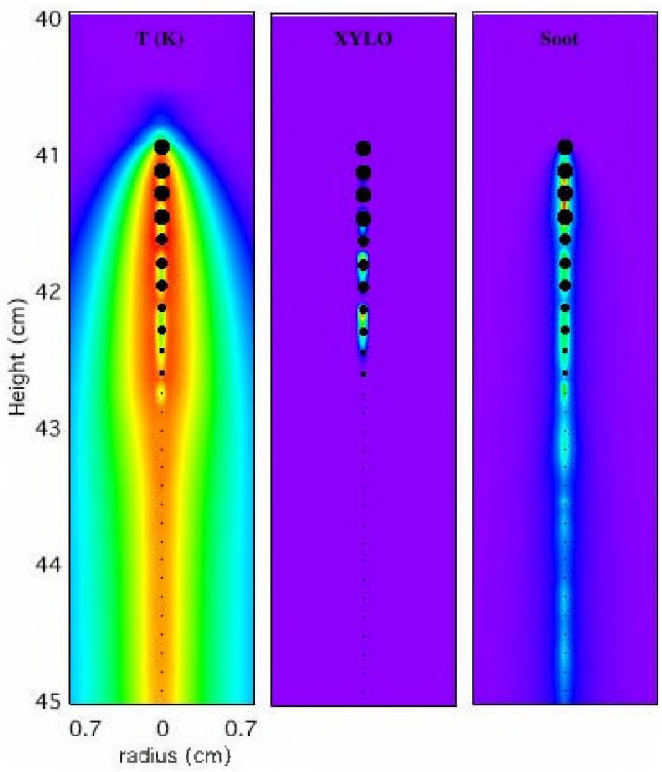

Figure 72. Predicted temperature, xylene (fuel fragment), and soot distributions for enriched-oxygen air flow in the drop-tube model.

6.4.2.3 Re-ignition Phenomena It was interesting to note pockets of fuel developing as the droplets vaporized (Figures 71 and 72). To explain this phenomenon, blown-up views of temperature field for both the oxidizer cases are shown in Figure 73. Here, the same color scheme (rainbow colors between 1373 K and 2680 K) was used for both the images. The oxygen-enriched case gives a peak temperature of 2680 K, which is 18% higher than that obtained with atmospheric air. In both cases, bridges of high-temperature contours established periodically which caused the formation of fuel pockets. Evaporation of fuel from the first (top) droplet mixed with the surrounding oxygen and established a flame when auto-ignition took place. Further evaporation of fuel from the moving droplets cooled the local gases (combustion products). While the radical pool built up, re-ignition took place when the fuel-air mixture reaches auto-ignition conditions.

This effect was seen in the drop-tube experiments for oxygen-enriched coflow gas (see Figure 11).

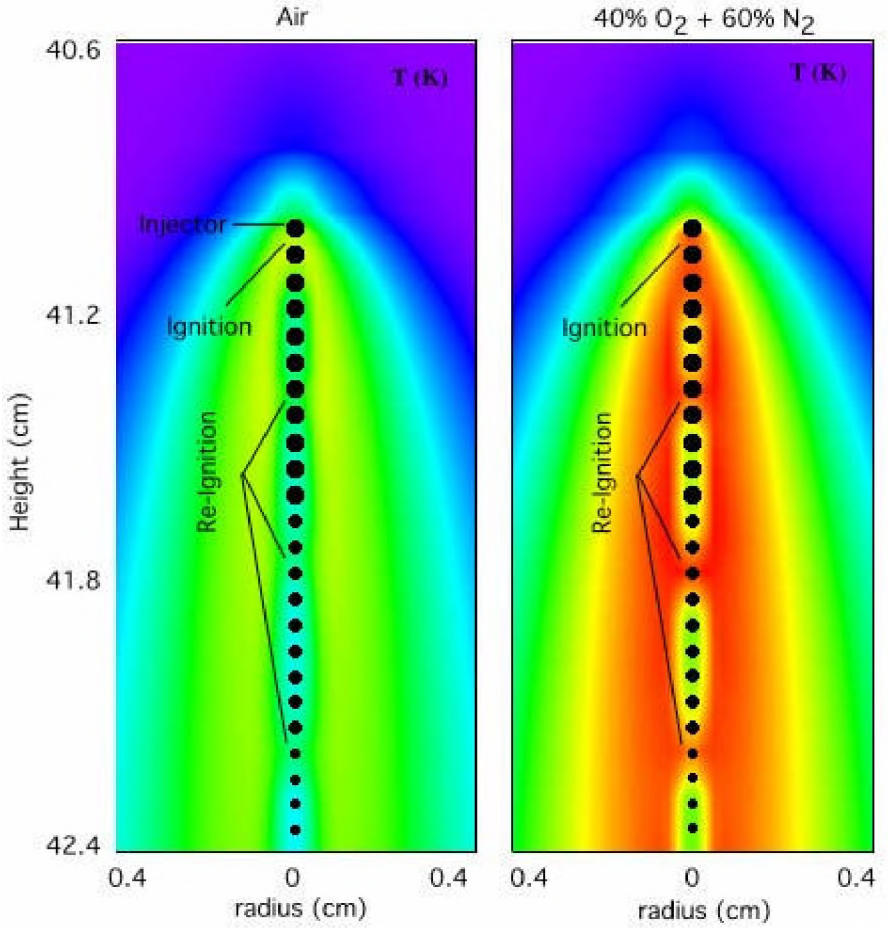

Figure 73. Close-up of the temperature distributions for normal and enriched-oxygen air flow in the drop-tube model.

6.4.2.4 Improved Model Inputs Initial drop tube model calculations yielded very small ignition distances whereas experiments showed ignition distances of 4 to 5 cm. Later calculations for the drop tube experiment were made using the experimental conditions derived from microphotography of the experiment as described in Section 5.1.6. The flame liftoff distance was very close to the experimental value. The distance in the simulations was about 4.8 cm. It fluctuates slightly (~ 2 mm) as the droplets passed

through the flame. Figure 74 shows input conditions and results from this drop-tube simulation.

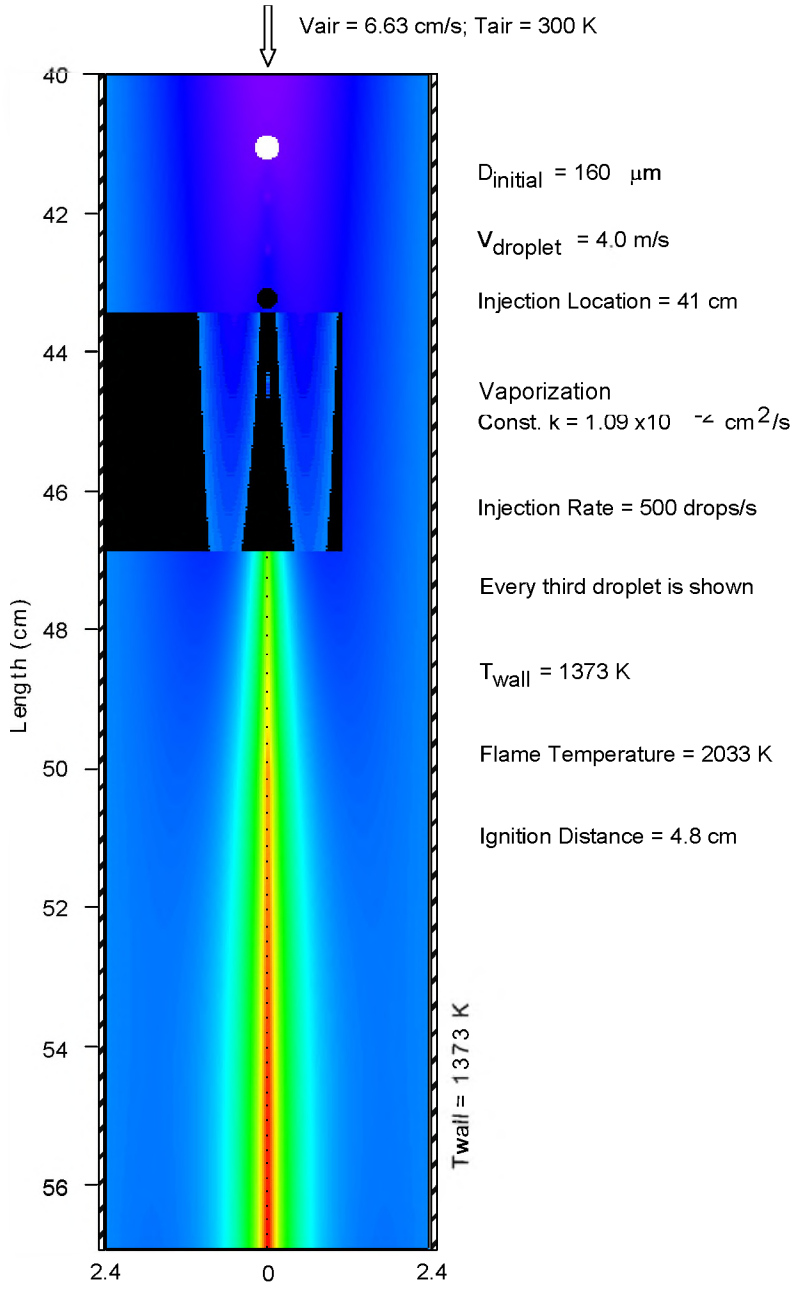

Figure 74. Input conditions and temperature results from the final drop-tube simulation.

6.4.3 Additive Effects

This section reports recent work on CFD simulations of JP-8 jet and swirl-stabilized flames and the effects of the additive DTBP. Performance of di-tert-butyl-peroxide (DTBP) additive in a jet diffusion flame and in a swirl combustor (CFM56) was tested through performing several calculations using UNICORN code. Violi's mechanism for JP-8 fuel and the mechanism for DTBP developed during this project were incorporated into the CFD code. Additive was added to JP-8 fuel using Zhang's mechanism coupled with the new additive kinetics as described in Section 6.2.1.

6.4.3.1 Jet Flame The flame modeled was a diffusion flame formed between gaseous JP-8 fuel and air. The velocity of the fuel injected from a 1.0-mm diameter tube at room temperature was 0.2 m/s, while that of the annulus air was fixed at 0.05 m/s. DTBP additive was added to the fuel jet by replacing the equal amount of JP-8 such that the exit velocity of the fuel jet was not altered. Axisymmetric calculations for this jet diffusion flame were performed for various concentrations of DTBP on a non-uniform grid system of 151x71. The chemistry model was the JP-8 mechanism of Zhang with additive kinetics developed in this program. The soot model of Lindstedt (1994) was used.

Results obtained for the base flame (without adding any DTBP) are shown in Figure 75. The iso-temperature plot in Figure 75(a) suggests that significant preheating of fuel prior to entering into the flame zone took place. The flame, in general, was burning intensely in the shoulder region with a significantly cooler flame tip. The peak temperature was about 2000 K. Distribution of the soot formed in this flame is shown in

Figure75(b). As expected, a significant amount of soot was produced at the flame tip, which was then gradually burned off downstream.

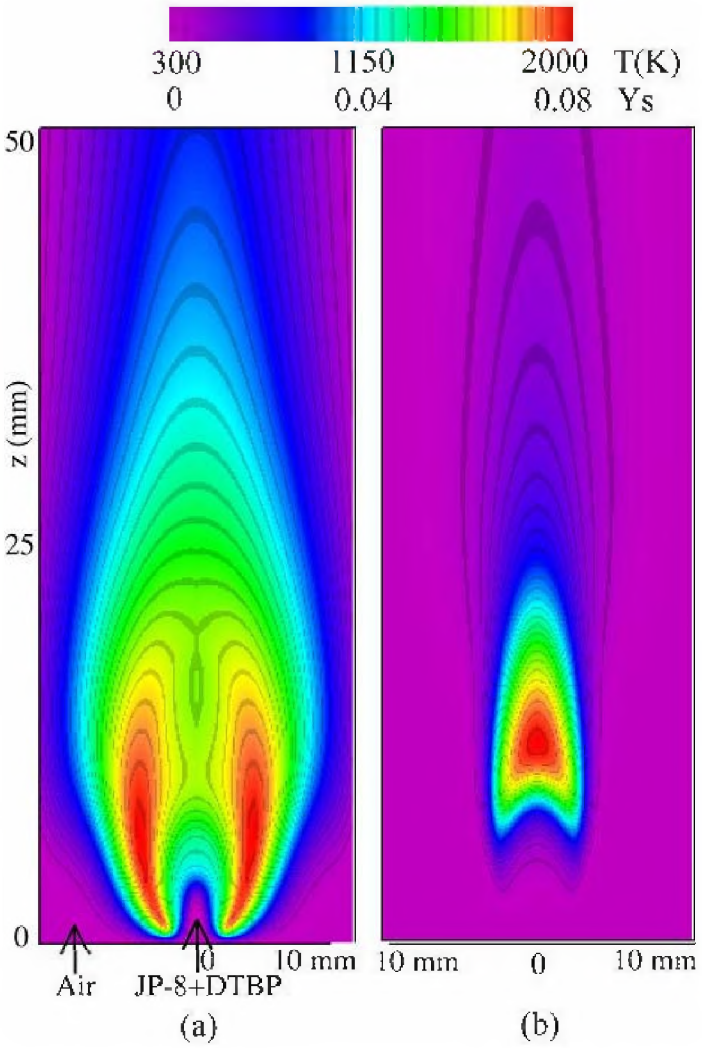

Figure 75. Jet diffusion flame used for the investigation of additive effects on soot formation. (a) Temperature, and (b) soot-mass-fraction (Y_s) distributions of the base flame.

Variations of temperature and soot volume fraction along the centerline (r = 0) at different heights for several concentrations of DTBP are shown in Figure 76. Note that the temperature at the flame tip was only about 1500 K and the peak soot concentration was located slightly downstream of the flame tip. Radiation from soot is causing a dip in the temperature. Addition of DTBP had only marginal effects on this diffusion flame. In

general, the temperature increased and soot was decreased with the addition of DTBP, however, these changes became pronounced only for DTBP concentration of 30%. At this high concentration of DTBP soot in the exhaust gases was reduced by ~50%. It should be recalled that this additive is known for reducing the ignition delay time and its effects on soot reduction are unknown. As expected, ignition along the centerline in the jet diffusion flame was enhanced with the addition of DTBP while the final temperature in the exhaust remained nearly the same.

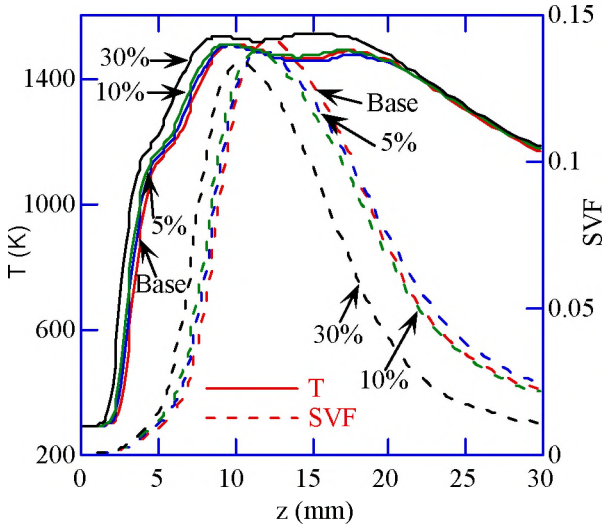

Figure 76. Predicted distributions of temperature and soot volume fraction along the centerline of the jet diffusion flame for different concentrations of DTBP.

Decomposition of DTBP and production of benzene along the centerline are shown in Figure 77. Most of the added additive was consumed in the preheating region of the fuel (i.e., T < 1000 K) prior to the formation of benzene. Figure 77 further suggests that the peak concentration of benzene decreased with the addition of DTBP, which means that the soot reduction observed with this additive occurred through a decrease in formation rate rather than an increase in soot destruction rate.

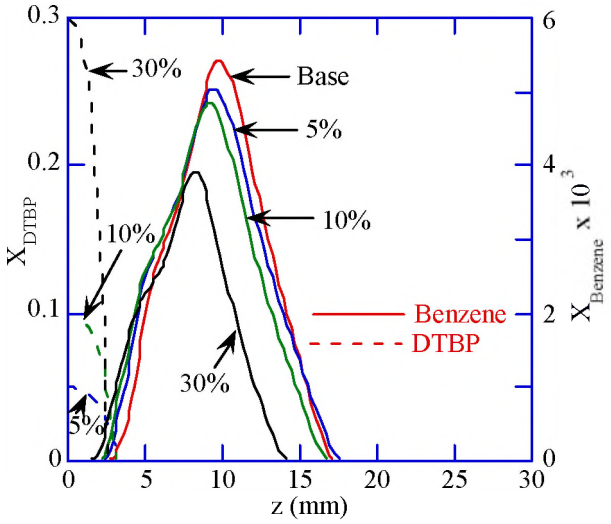

Figure 77. Consumption of DTBP and production of benzene along the centerline of the jet diffusion flame for different additive concentrations.

It was found that this additive had no effect on soot formation in the jet diffusion flame even for concentrations up to 10%, as shown in Figure 78, in which soot mass fraction distributions are plotted for three different concentrations of DTBP.

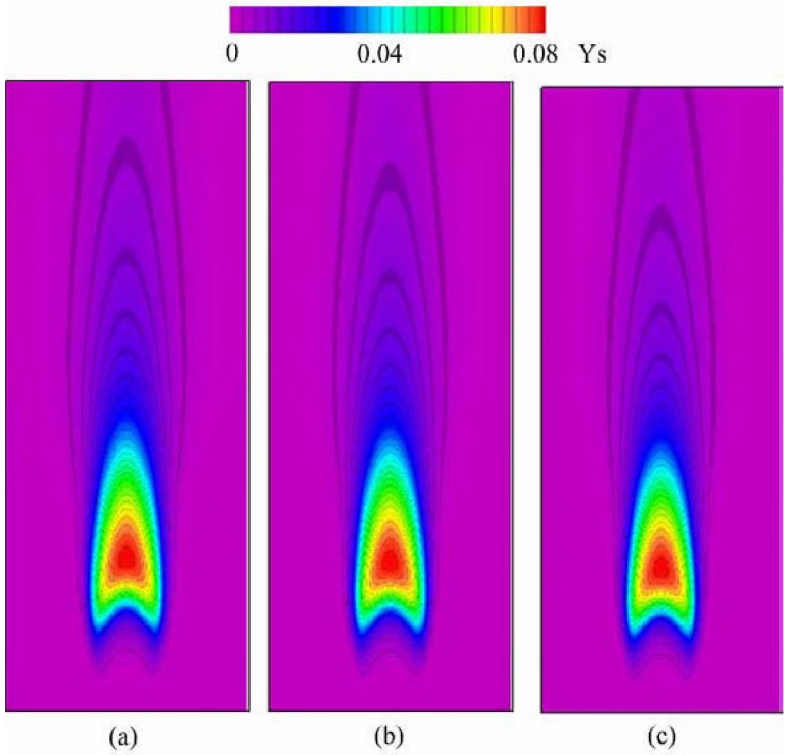

Figure 78. Soot mass fractions in a jet diffusion flame with (JP-8 + DTBP) as fuel. (a) 2%, (b) 5%, and (c) 10% additive.

6.4.3.2 Swirl-Stabilized Combustor The near-field structure of swirl-stabilized flames is highly dependent upon the characteristics of the fuel injector and the geometry of the surrounding flame tube. The injector configuration used in the modeled swirl-stabilized combustor was a generic swirl-cup liquid-fuel injector studied at the Atmospheric-Pressure Combustor-Research Complex of the Air Force Research Laboratory's Propulsion Directorate (Meyer et al. 2004, Roy et al. 2004). It employs pressure atomization and dual-radial, counter-swirling co-flows of air to entrain the fuel, promote droplet break-up, and enhance mixing. The 40-mm-exit-diameter swirl cup is installed at the entrance of a 15.25 cm × 15.25 cm square-cross-section flame tube. After exiting the primary flame zone, the combustion products are allowed to mix thoroughly along the 48-cm long flame tube before entering a 43-cm-long, 5.7-cm exit-diameter exhaust nozzle that is designed to create a uniform exhaust-gas temperature and concentration profiles.

An axisymmetric mathematical model for the swirl-stabilized combustor was constructed using a 17.2-cm diameter, 48-cm long chimney and with thin tubes separating the fuel and air flows at the combustor entrance. Gaseous JP-8 fuel along with DTBP additive was injected at the center while the two outer air jets are forced into the combustor with counter swirling motions. The computational domain was discretized using a non-uniform grid system of 251x126. Comparisons of model soot predictions to laboratory data for the swirl-stabilized combustor can be found in Katta et al. 2005

Calculations for the swirl-stabilized combustor were made for different equivalence ratios and additive concentrations. It was found that the effectiveness of

DTBP in highly fuel-rich conditions was very limited. However, as the equivalence ratio decreased the effectiveness of DTBP increased, in agreement with the drop tube experiment findings. Results for a fuel-rich condition (ϕ = 1.15) are shown in Figure 79. Temperature distributions inside the combustor are plotted in Figures 79(a) and 79(b) for the no additive case and 5% DTBP case, respectively. The nozzle geometry incorporated in the model is also shown in these figures. Gaseous JP-8 (or JP-8+DTBP) was injected from a 4-mm hole at the center with an axial velocity of 40 m/s and swirl angle of 70°. This high swirl angle for the fuel jet was used in order to represent the cone angle of the liquid spray. The fuel jet was immediately surrounded with a 2-mm-thick wall and then a high-speed air jet with axial velocity of 100 m/s and a swirl angle of -30°. A second air jet of 100 m/s issued through the 5 mm annular gap between the nozzle walls at a velocity of 100 m/s and at a swirl angle of 45°. The velocity of the fuel jet was changed for achieving different equivalence-ratio conditions.

The swirling air jets merge and expand radially as they propagate downstream. Such radial expansion of high momentum air jets creates two toroidal recirculation regions- one in the corner and the other one at the center. Typically, flames can establish along either or both of these recirculation zones. The temperature field in Figure 79(a) suggests that the corner recirculation zone was the hottest region for this fuel-rich case. The flame was anchored between the air jets and the corner recirculation zone and no flame was established between the air jets and the central recirculation zone.

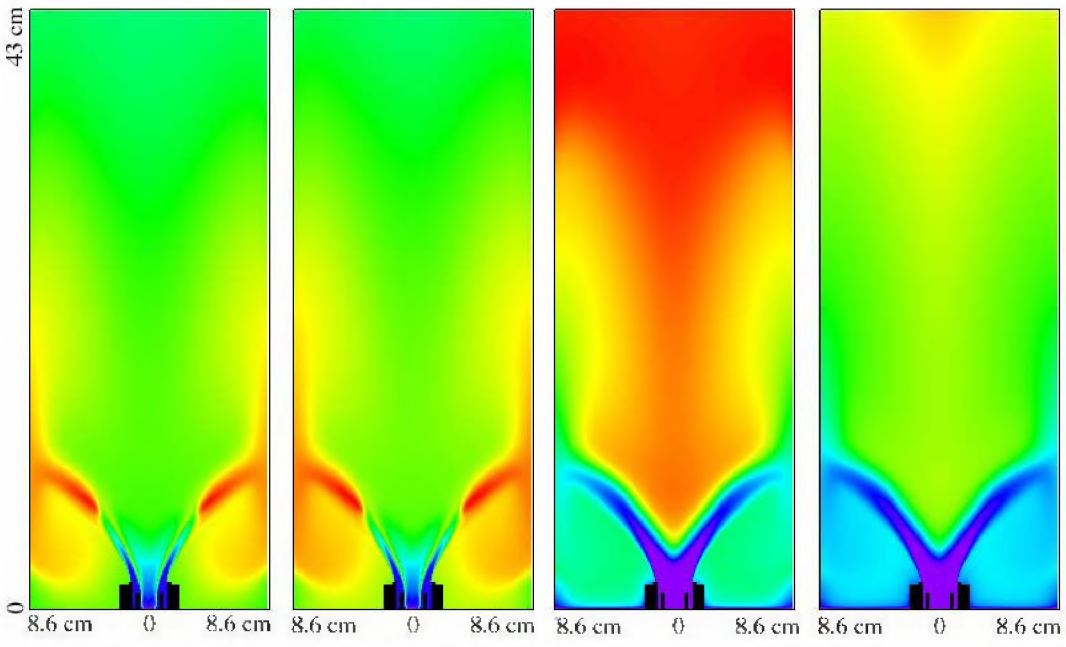

Figure 79. Effect of DTBP in swirl-stabilized combustor operating at ϕ = 1.15. Distributions of (a) temperature and (c) soot mass fraction when no additive was added; (b) and (d) are those when 5% DTBP was added.

Addition of 5% DTBP did not change the temperature significantly. Figure 79(b) indicates a slight increase in temperature in the region where the air jets impinge the combustor wall (z ~ 11 cm). Soot produced in the combustor with and without DTBP is shown in Figures. 79(c) and 79(d). Significant amount of soot was generated under these fuel-rich operating conditions. Even though some soot was found in the corner recirculation zones, most of it was actually generated in the central recirculation zone and carried into the former. Significant soot growth occurred in the region downstream of the central recirculation zone (z > 25 cm).

A comparison of soot distributions obtained with and without DTBP (Figures 79(c) and 79(d)) suggests that 5% addition of DTBP significantly reduced the soot levels. In fact, reduction in soot is evident in all regions of the combustor. Such soot reduction

was not observed either in the jet diffusion flames or in the combustor flows under fuel-rich conditions.

Distributions of temperature and various species along the centerline are shown in Figures. 80(a) and 80(b) for different amounts of DTBP. Similar to the results obtained for a jet diffusion flame, addition of DTBP increased the centerline temperature in the swirl-stabilized combustor also. However, DTBP was more effective in the combustor than in jet diffusion flame. The low concentrations of OH along the centerline suggest that flame was not established. Interestingly, acetylene concentration has increased in certain regions and decreased in others whereas soot was reduced everywhere.

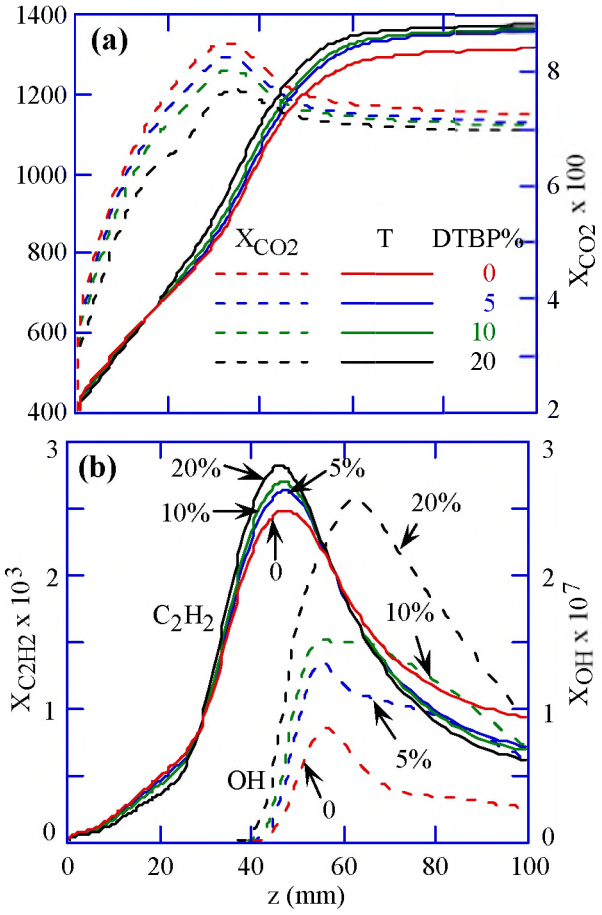

Figure 80. Distributions of temperature and species concentrations along the centerline for various amounts of DTBP added to the swirl-stabilized combustor fuel jet. ϕ = 1.15

The mass integrated soot and various species at different axial locations are shown in Figures 81(a) and 81(b). With the addition of 5% DTBP soot mass decreased by ~23% at z = 30 cm. On the other hand, further increasing DTBP did not cause much reduction in soot. Similarly, aromatic species such as benzene and phenol also decreased with the addition of DTBP.

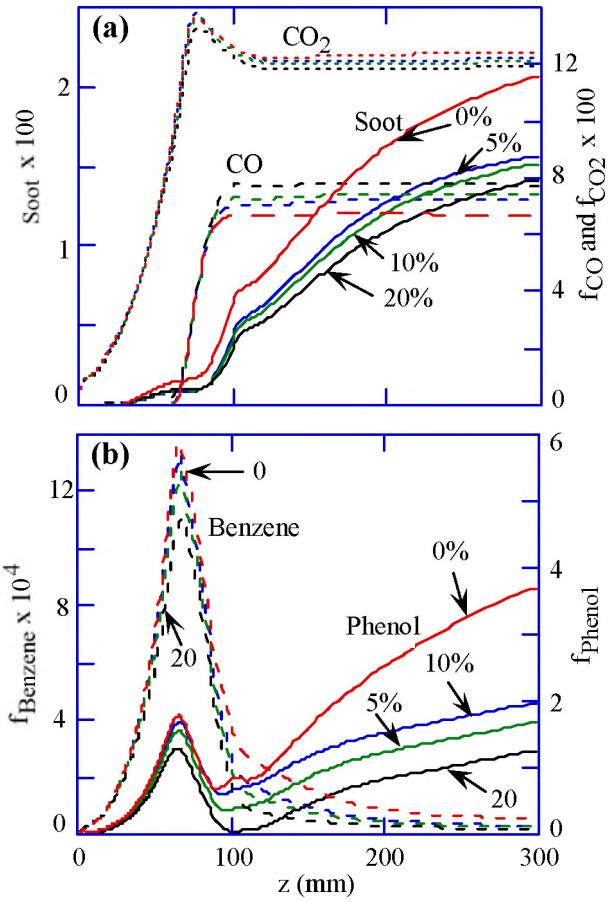

Figure 81. Net mass fractions of soot and other species at different axial locations for various amounts of DTBP added to the swirl-stabilized combustor fuel jet. ϕ = 1.15

The effect of adding 5% DTBP to the swirl-stabilized combustor operating under stoichiometric (ϕ = 1.0) conditions is shown in Figure 82. Fuel jet velocity used for this condition was 30 m/s. Temperature distributions obtained with and without DTBP are shown in Figs. 82(a) and 82(b), respectively. Significant amounts of combustion products

were entrained into the corner recirculation zone, supporting the flame. Addition of DTBP increased the temperature in both the recirculation regions. Soot formed under stoichiometric conditions is shown in Figure 82(c) without the addition of DTBP and in Figure 82 (d) with the addition of 5% DTBP. Significant reduction in soot was obtained in this case.

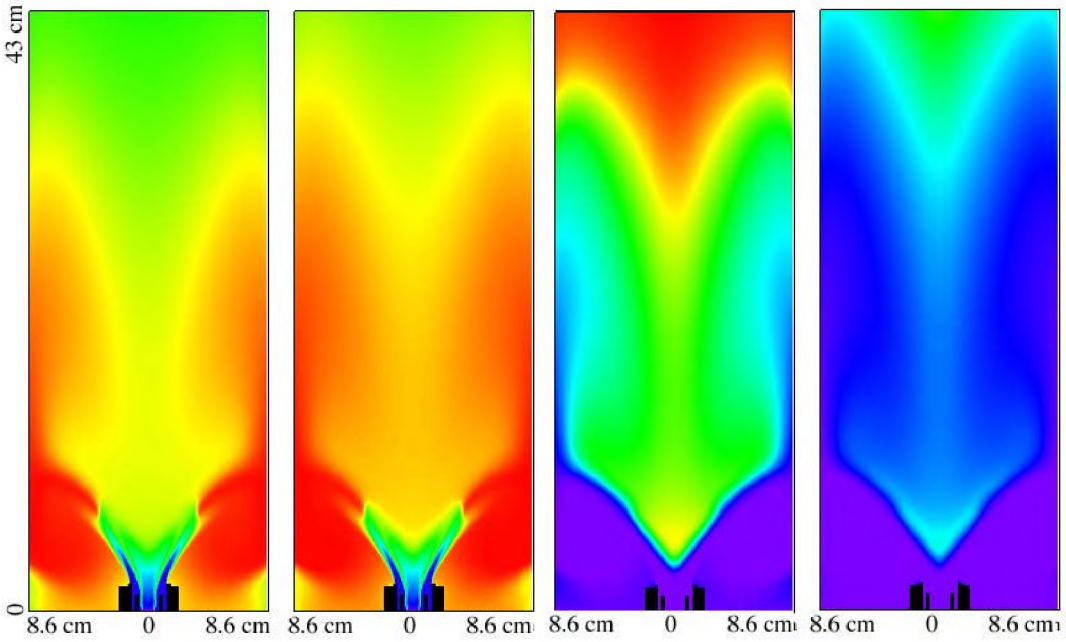

Figure 82. Effect of DTBP in swirl-stabilized combustor operating at ϕ = 1.00. Distributions of (a) temperature and (c) soot mass fraction when no additive was added; (b) and (d) are those when 5% DTBP was added.

Distributions of temperature and species concentrations along the centerline are shown in Figures 83(a) and 83(b). Temperature of the central recirculation zone has increased by ~150 K with the addition of 5% DTBP. More significantly, another flame was established at the upstream tip of the central recirculation zone as evident in OH profile. This suggests that DTBP additive is improved ignition in the swirl-stabilized combustor. Average mass fractions of soot and other species at several cross sections

along the combustor length are plotted in Figures 84 and 85. Soot mass under stoichiometric conditions decreased by ~70% with the addition of 5% DTBP. Interestingly, benzene and phenol concentrations did not change much with the addition of DTBP. This was, in part, due to the rapid burn-off of these species in high-temperature combustion products in the central recirculation zone.

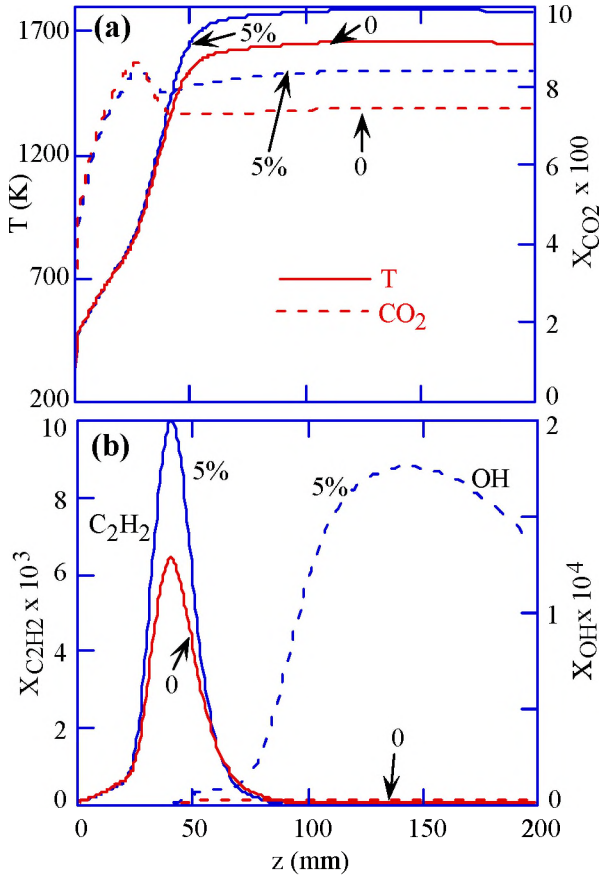

Figure 83. Distributions of temperature and species concentrations along the centerline for various amounts of DTBP added to the swirl-stabilized combustor fuel jet. $\phi = 1.0$

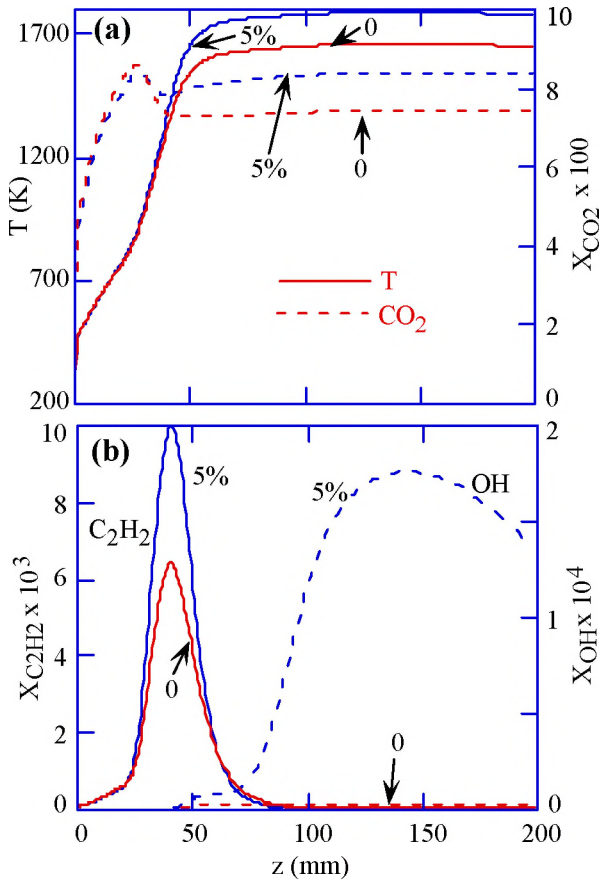

Figure 84. Distributions of temperature and species concentrations along the centerline for various amounts of DTBP added to the swirl-stabilized combustor fuel jet. $\phi = 1.0$

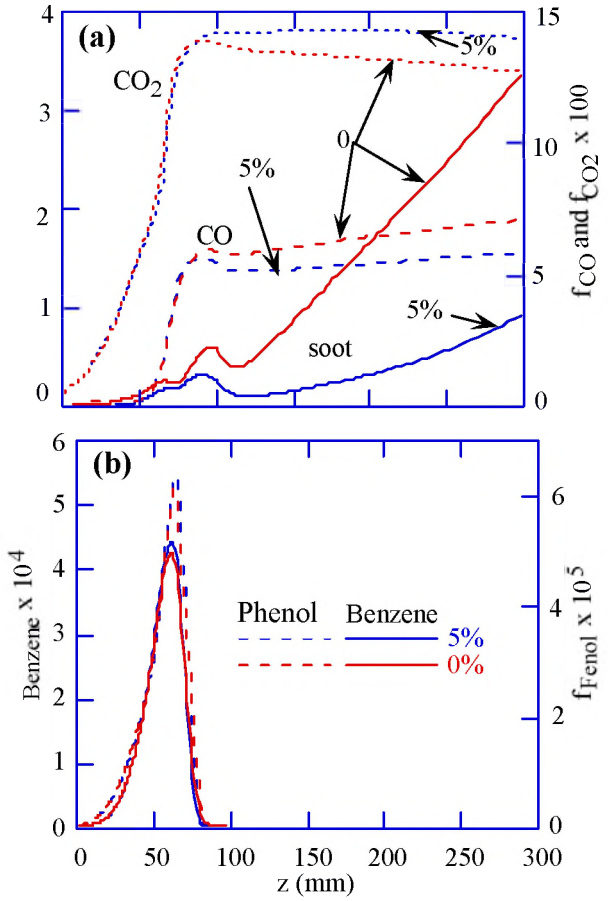

Figure 85. Net mass fractions of soot and other species at different axial locations for various amounts of DTBP added to the swirl-stabilized combustor fuel jet. $\phi = 1.0$

7. Validation

Several striking comparisons were found between the modeling work done in this project and experiments, either published or performed as part of this project. The major validations are listed below:

- The qualitative agreement between model and published data predictions for the sootiness of various fuels as shown in Section 6.1, Figure 49.
- The qualitatively correct effect of the new additive kinetics for DTBP and 2EHN on both ignition delay and soot production in simple reactor calculations (Section 6.3).
- The demonstration that for a time vs. temperature and stoichiometry resembling the average values found in a gas turbine combustor, the additive DTBP could reduce soot up to 65% (Section 6.3.1.3, Figure 56.). While we do not have gas turbine data for DTBP, similar reductions were found for DTBP addition in the drop tube (Figure 12) for enriched oxygen concentrations. These conditions in the drop tube have shown correspondence to gas turbine results for other additives, such as PA-5.
- The excellent agreement found for liftoff distance in the drop tube model when more precisely used input parameters were used (Section 6.4.2.4, Figure 73.)
- The prediction of flame undulations observed in the drop tube by the UNICORN CFD code simulations (Section 5.1.3, Figure 12 and Section 6.4.2.3, Figure 71.

- The agreement with the drop tube experiments and the swirl-stabilized combustor results that DTBP significantly reduces soot under lean conditions but gives almost no result under rich conditions (Section 5.1.3, Figure 13 and Section 6.5.3, Figures 79 and 82.

Aspects of the experimental results also validate our experimental screening procedures, most notably the considerable agreement between the drop tube results with a 40% oxygen coflow stream with WPAFB gas turbine engine (T-63) results (Corporan et al. 2002). See Section 5.1.4, Figure 16.

- PA-5 1000 ppm: soot reduction on the order of 40 – 50%.
- +100 Additive at 256 ppm: no soot reduction.

8. Technology Transfer

In addition to the required project reporting, project results were transferred to research and industrial organizations through papers and presentations at technical conferences. The presentations made during the project are listed below.

Montgomery, C., "REI SBIR Overview," presentation at SERDP Review Meeting, WPAFB, OH, Sept. 20-21, 2004.

Montgomery, C., and Sarofim, A., "Evaluation of Soot Reducing Fuel Additives in a Drop Tube Furnace," presentation at SERDP Review Meeting, WPAFB, OH, Feb. 24, 2005.

Katta, V., and Montgomery, C., "Studies on Soot Formation in JP-8 Diffusion Flames," Sixth International Symposium on Special Topics in Chemical Propulsion, Santiago, Chile, Mar. 8-11, 2005.

Montgomery, C. J., Sarofim, A. F., Preciado, I., Marsh, N. D., Eddings, E. G., and Bozzelli, J. W., "Experimental and Numerical Investigation of Soot-Reducing Fuel Additives," AIAA Paper 2005-4472, 41st AIAA/ASME/SAE/ASEE Joint Propulsion Conference, Tucson, AZ, July 10-13, 2005.

Katta, V.R., Meyer, T.R., Montgomery, C., and Roquemore, W.M., "Studies on Soot Formation in a Model Gas Turbine Combustor," AIAA Paper 2005-3777, 41st AIAA/ASME/SAE/ASEE Joint Propulsion Conference, Tucson, AZ, July 10-13, 2005.

Eddings, E.G., Yan, S. Zhang, H., Marsh, N.B., Sarofim, A.F., Montgomery, C.J., and Katta, V., "Methodology for the Simulation of Complex Hydrocarbon Mixtures," American Society of Chemical Engineers National Meeting, Cincinnati, OH, Oct. 30-Nov. 4, 2005.

Katta, V., Mawid, M., Sekar, B., Corporan, E., Zelina, J., and Montgomery, C., "Comparison of Chemical-Kinetics Models for JP-8 Fuel in Predicting Premixed and Diffusion Flames," AIAA-2006-4745, accepted, 42nd AIAA/ASME/SAE/ASEE Joint Propulsion Conference & Exhibit, Sacramento, CA July 9-12, 2006.

Several discussions were also held with additives experts to discuss the feasibility of commercializing an additive technology identified during the program. The most in-depth of these were confidential conversations with Dr. Dan Daly of the University of Alabama about the reverse micelle concept. He felt the idea was novel, but may be too

expensive to be commercially competitive. Commercial options for this technology are still being considered.

9. Conclusions

This project has addressed limitations regarding the ability to identify and screen appropriate soot suppression additives for JP-8 fuel in jet aircraft engines. This required improved fundamental understanding of the action of soot-reducing additives under a variety of combustion conditions in order to develop the ability to predict additive effectiveness in engines using screening tools, specifically laboratory tests and numerical computations. Key results from the program were as follows:

- The experimental program demonstrated that a laminar drop tube furnace at the University of Utah (the U) could effectively screen a large number of additives relatively rapidly and inexpensively as a function of furnace temperature, injection orifice size, injection pressure, and oxygen concentration. Additives were found to be most effective under highly oxidizing conditions. Soot reductions of over 90 percent were observed for metal-containing additives, known ignition enhancers, a range of proprietary additives provided by Afton Chemicals, and additives produced at the U using a novel micellar synthesis technique particularly suited for the production of multifunctional additives.
- Limited experimental results were obtained at the U on the effects of additives on soot oxidation kinetics using a two-stage burner, providing data that confirmed that both metallic additives and organic ignition enhancers were effective under oxidizing conditions, but that metal additives produced aerosol residues that would be a deterrent to their acceptance.

- An AMT-400 small scale turbine at the U showed limited applicability in determining the effects of additives. The large amounts of unburned fuel, resulting from the use of fuel as a lubricant, masked the effect of additives on soot formation and suppression.
- Modeling capabilities for assessing the effectiveness of additives were also developed. Soot models using the method of moments and sectional methods were combined with detailed kinetics models for surrogates of JP-8. The models were validated with experimental data in the literature for a number of simple fuels.
- Detailed kinetic mechanisms were developed at NJIT for two of the organic ignition enhancers in the study, di-tertiary butyl peroxide (DTBP) and 2-ethyl-hexyl-nitrate. These kinetics were used to augment the mechanism for the JP-8 surrogate providing, for the first time, a theoretical method for evaluating the effect of soot additives.
- The kinetic model was used in a simple reactor model of a gas turbine combustor. As in the experiments, the reactor model showed that the additives were effective only in a certain range of conditions, those in which the change in time to ignition influenced the soot burnout.
- Finally the kinetic models were incorporated in the UNICORN CFD code by ISSI to evaluate diffusion flames representative of both the drop tube experiments at the University of Utah and a swirl-stabilized combustor. The computations for one of the laboratory flames showed the reproduction by the model of many of the features of the flame, including a previously unexplained undulation in the flame width. But the model greatly under-predicted the effects of additives on soot emission. The

UNICORN model of a swirl stabilized flame, however, showed that the addition of DTBP to the flame can significantly reduce soot in the flame.

In conclusion, this research has demonstrated the design and application of experimental and numerical screening tools for assessing aircraft engine soot suppression additives. The screening techniques, both experimental and computational, have shown that the effect of additives on soot formation is very sensitive to experimental conditions, explaining the highly variable results that have been observed with additives in the field. The additives tested in this study were most effective in the oxidation regime. If an additive can be found that is effective under fuel-rich conditions then the micellar synthesis technique developed in this study could be used to synthesize a multi-functional additive that could be valuable over a wider range of operating conditions. The new fundamental understanding and screening capabilities developed in this program provide a method for the U.S. Air Force to more efficiently and cost-effectively identify candidate fuel additives for comprehensive testing in jet engine combustion applications.

10. Bibliography

Appel, J., Bockhorn, H., and Frenklach, M., "Kinetic Modeling of Soot Formation with Detailed Chemistry and Physics: Premixed Flames of C_2 Hydrocarbons," *Combustion and Flame* 121: 122-136, 2000.

Corporan, E., DeWitt, M., and Wagner, M., "Evaluation of Soot Particulate Mitigation Additives in a T63 Engine," Proceedings of the International Conference on Air Quality III, Washington D.C., Sept. 10-12, 2002.

Edwards, T. and Harrison, B., "Update on the Development of JP-8+100," AIAA Paper 2004-3886, 2004.

Feitelberg, A. S., Longwell, J. P., and Sarofim, A. F., "Metal Enhanced Soot and PAH Formation," *Combustion and Flame* 92:241-253, 1993.

Frenklach, M., and Wang, H., "Detailed Modeling of Soot Particle Nucleation and Growth," Twenty-Third Symposium (International) on Combustion, pp. 1559-1566, 1990.

Fuchs, N.A., *The Mechanics of Aerosols*, Pergamon, New York, pp. 291-294, 1964.

Hall, R.J., Smooke, M.D., and Colket, M.B., Predictions of soot dynamics in opposed jet diffusion flames, in *Physical and Chemical Aspects of Combustion: A Tribute to Irvin Glassman*, R.F. Sawyer and F.L. Dryer, eds, Combustion Science and Technology Book Series, Gordon & Breach, Langhorne, PA, pp.189-230, 1997.

Howard, J. B. and Kausch, W. J., *Progress in Energy and Combustion Science*, 6:263-276, 1980.

Jiang, P, "Modeling of Aerosol Dynamics in Flames and Exhaust Plume," Ph.D. Thesis, University of Utah, 2003.

Katta, V.R., Meyer, T.R., Montgomery, C., and Roquemore, W.M., "Studies on Soot Formation in a Model Gas Turbine Combustor," AIAA Paper 2005-3777, 41st AIAA/ASME/SAE/ASEE Joint Propulsion Conference, Tucson, AZ, July 10-13, 2005.

Lighty, J. S. Veranth, J. M. and Sarofim, A. F. "2000 Critical Review-Combustion Aerosols: Factors Governing Their Size and Composition and Implications to Human Health", *Journal Air Waste*, 50(9):1565-1622, 2000.

Lindstedt, P. R., in *Soot Formation in Combustion* (H. Bockhorn, Ed.), Springer Verlag, Heidelberg, 1994, p. 417.

Meyer, T.R., Roy, S., Sivaram P. Gogineni, S.P., Vincent M. Belovich, V.M., Corporan, E. and Gord, J.R., "OH PLIF and soot volume fraction imaging in the reaction zone of a liquid-fueled model gas-turbine combustor," GT2004-54318, Proceedings of ASME Turbo Expo, Vienna, Austria. June 14-17, 2004.

Nagle, J. and Strickland-Constable, R.F., , *Proceedings of the Fifth Carbon Conference*, Vol. 1, Pergamon, p.154., 1963

Neoh, K.G., Howard, J.B., and Sarofim, A.F., *Particle Carbon: Formation during Combustion,* D.C. Seigla, and G.W. Smith, eds., Plenum, NY. p. 261, 1981.

Rah, S. C., Sarofim, A. F., and Beer, J. M., "Ignition and Combustion of Fuel Droplets," *Combustion Science and Technology* 48:273-284, 1986.

Roy, S., Meyer, T.R., Lucht, R.P., Belovich, V.M., Corporan, E., and Gord, J.R., "Temperature and CO_2 concentration measurements in the exhaust stream of a liquid-fueled combustor using dual-pump coherent anti-Stokes Raman scattering (CARS) spectroscopy," *Combustion and Flame* 138: 273-284, 2004.

Sangiovanni, J.J., and Liscinsky, D.S., "Soot Formation Characteristics of Well-Defined Spray Flames", *Twentieth Symposium (International) on Combustion,* pp 1063-1073, 1985.

Violi, A., Yan, S., Eddings, E. G., Sarofim, A. F., Gratata, S., Faravelli, T., and Ranzi, E., "Experimental Formulation and Kinetic Model for JP-8 Surrogate Mixtures," *Combustion Science and Technology,* 174:339-417, 2002.

Wright, F. J., "The Formation of Carbon Under Well-Stirred Conditions," *Twelfth Symposium (International) on Combustion*, pp. 867-875, 1968.

Zhang, H., Ph.D. Thesis, Department of Chemical Engineering, University of Utah, 2005.

List of Acronyms

2EHN	2-ethylhexylnitrate
CFD	Computational Fluid Dynamics
$Co(AOT)_2$	Cobalt bis(2-ethylhexylsulfosuccinate)
CVODE	Variable-order Ordinary Differential Equations in C
DoD	Department of Defense
DTBP	di-tertbutyl peroxide
$Fe(AOT)_3$	Iron bis(2-ethylhexylsulfosuccinate)
HACA	Hydrogen Abstraction C_2H_2 Addition
MMT	methylcyclopentadienylmanganese tricarbonyl
MoM	Method of Moments
MPC	monolayer-protected cluster
PFR	Plug Flow Reactor
PM	particulate matter
PM 2.5	PM with a diameter $\leq$ 2.5 nm
PM 10	PM with a diameter $\leq$ 10 nm
ppm	parts per million
PSD	Particle size distribution
PSR	Perfectly Stirred Reactor
REI	Reaction Engineering International
NaAOT	Sodium bis(2-ethylhexylsulfosuccinate)
PAH	Polycyclic aromatic hydrocarbons
REKS	Reaction Engineering Kinetics Solver
SMPS	scanning mobility particle sizer
UNICORN	UNsteady Ignition and Combustion with ReactioNs